The Ministry of Science and Higher Education
of the Republic of Kazakhstan

Karaganda University of the name of Academician E.A. Buketov

This work was performed within the grant funding of young scientists on scientific and (or) scientific-technical projects of the Ministry of Science and Higher Education of the Republic of Kazakhstan, grant No. AP09058188

Zh.T. Kambarova

DESIGN OF ELECTROSTATIC ENERGY ANALYZERS

Monograph

Karaganda
2023

Recommended for publication by the Scientific Council of
Karaganda University of the name of Academician E.A.Buketov

UDC 537.533.34
LBC 22.33
K18

Kambarova Zh.T. **Design of electrostatic energy analyzers**: monograph. - Karaganda: Polygraphist, 2023. - 123 p.

ISBN 978-601-362-164-7

The monograph focuses on the computation and simulation of electrostatic energy analyzers used in the energy-angle analysis of matter.

The monograph is intended for scientists and engineers specializing in electron spectroscopy, corpuscular optics, and analytical instrumentation and can serve as a textbook useful for master students and doctoral students in the corresponding physics and technology, and natural science disciplines.

Reviewers:
Kazhikenova S.Sh., Doctor of Technical Sciences, Associate Professor, Head of the Department "Higher Mathematics", NLC "Abylkas Saginov Karaganda Technical University".
Agelmenev M.E., Doctor of Chemical Sciences, Candidate of Physical and Mathematical Sciences, Professor, NLC «Karaganda University of the name of Academician E.A. Buketov».

ISBN 978-601-362-164-7

Contents

Symbols and abbreviations

The following notations and abbreviations are used in this work:
AES - Auger-Electron Spectroscopy
BEM - Boundary Element Method
CM - Cylindrical mirror
CMA - Cylindrical mirror analyzer
ES - Electron Spectroscopy
FDM - Finite Difference Method
FEM - Finite Element Method
HCP - Hexapole-cylindrical field
HM - Hyperbolic mirror
MCF - Multipole-cylindrical field
OCF - Octupole-cylindrical field
PCMA - Parallel cylindrical mirror analyzer
SM - Spherical mirror
TCCMA – Two-cascade cylindrical mirror analyzer

Introduction

Surface physics deals with the investigation of the elemental composition and atomic arrangement on the surfaces of solids. Theoretical and experimental studies of the mechanical, chemical and other properties of surfaces are also conducted. Like in the study of bulk solids, the main objective is to establish the relationship between the properties, composition and structure of surfaces. Hence, an accurate determination of the elemental composition of a surface or a surface layer with a certain thickness is crucial for the correct interpretation of experiments in surface physics [1].

There is a vast and continuously expanding range of methods available for investigating surfaces. Currently, there are over seventy techniques specifically designed for surface analysis, many of which have multiple variations with different capabilities. These methods are based on the interaction between charged particle beams and solid surfaces, and therefore require a high vacuum during experimentation. Surface analysis techniques provide data on the type of particles emitted from the surface of a material, their spatial and energy distribution, as well as their quantity. This information can be used to understand the surface properties and dynamics during measurement.

Modern technologies, particularly nanotechnologies, are heavily influenced by surface phenomena. With the growing interest in nanomaterials and nanoscale structures, surface properties have become increasingly important. The study of solid state surfaces is a rapidly developing field of knowledge that is of great significance for the physics of nanoscale and molecular structures, modern material science, nano- and microelectronics, nanotechnology, condensed matter and thin film physics, chemistry, and other related areas.

Most surface analysis methods share common properties, including high surface sensitivity. This is due to the fact that electrons with energies in the range of 5-2000 eV have a high probability of undergoing inelastic scattering. Therefore, if the energy of the detected electrons does not change during their interaction with the surface of a solid body, it can be assumed that the electrons only passed through a very thin surface layer, making the method surface-sensitive. In addition, since most of these methods rely on measuring

electron energy, energy analyzers are required in the experimental setup of most methods [2].

In the field of nanoelectronics, there is a growing need for research methods that can accurately determine the structure and composition of nanosystems and nanomaterials. Electron spectroscopy (ES) methods offer promising solutions for this type of diagnostic work, as they are capable of providing nanometer-scale resolution in the depth of a solid body. ES methods typically allow for analysis of a surface layer with a depth ranging from 0.5 to 2 nanometers.

The method of electron spectroscopy is one of the widely used and actively developed methods for studying the physicochemical properties of solids in the near-surface region. This method was developed on the basis of the works of K. Siegban [3] and is currently a powerful tool for determining the composition and electronic structure of solids. ES-methods are based on the analysis of energy of electrons emitted by the surface of the studied substance under the influence of external radiation. The electron spectrometer isolates from the incoming particles the particles whose energies are in a certain narrow region, and the main analyzing element of the spectrometer is the energy analyzer.

Axially symmetric energy analyzers are well-suited for surface Auger spectroscopy due to their high luminosity and resolving power, making them one of the most effective physical methods for insitu analysis of the formation processes of micro- and nanostructures.

Most electron and ion optics use focusing elements that create axially symmetric electrostatic and/or magnetic fields which can be described by scalar potentials [4]. The main challenge in electronic devices is the formation, focusing, and deflection of electron beams by electric and magnetic fields. This problem is tackled by corpuscular optics which deals with families of trajectories and their properties [5]. The principles of corpuscular optics underpin the field of physical electronics and its subfields such as electron spectroscopy, mass analysis, and nanotechnology.

An analysis of existing devices revealed that the cylindrical mirror developed by Professor V.V. Zashkvara was the best analyzer in terms of resolution and sensitivity. This was particularly true when the cylindrical mirror was used in the second-order focusing mode

with the sample and detector positioned on the symmetry axis at the meridional angle θ [6]. Even today, the use of cylindrical mirrors remains relevant.

The advancement of modern technology and nanotechnology heavily relies on the state of diagnostic tools available. Therefore, further progress in energy analysis of charged particle beams requires continued development and improvement of existing corpuscular-optical systems, as well as the development of new systems through theoretical advancements.

1 Energy Analyzers for Charged Particle Beams

1.1 Overview of Charged Particle Beam Energy Analyzers

The task of surface analysis is to determine the qualitative as well as quantitative composition of the surface or surface layer of a certain thickness. As a rule, surface is understood as a part of a material volume with thickness of ~ 1-10 atomic layers [1, p.6].

Particular attention to the thin near-surface layer of solids is one of the characteristic features of modern materials science. This is because the surface composition and structure determine many physical and chemical properties of solids and play a major role in many processes and phenomena, often of great technological importance. In addition, our time is often referred to as the beginning of the nanotechnology revolution. One of the characteristic features of nanoscopic objects as compared to ordinary macroscopic bodies is the sharp increase in the relative proportion of atoms lying on the surface as compared to the total number of atoms in the system [7].

The energy analyzer is a critical component of the experimental scheme, as it enables the determination of the current density of charged particles within a specific energy range from E to $E+\Delta E$. By examining the energy distribution of the charged particles in the flux, the energy analyzer provides valuable insight into their behavior [8]. Principle scheme is presented in Fig. 1.1.

There are now many methods available for surface analysis. New techniques and instruments are constantly being created to meet the technological needs. Electrostatic devices with the field geometry outlined below are utilized for energy analysis:

- spherical field;
- cylindrical field,
- hyperbolic field,
- uniform field, etc. [9].

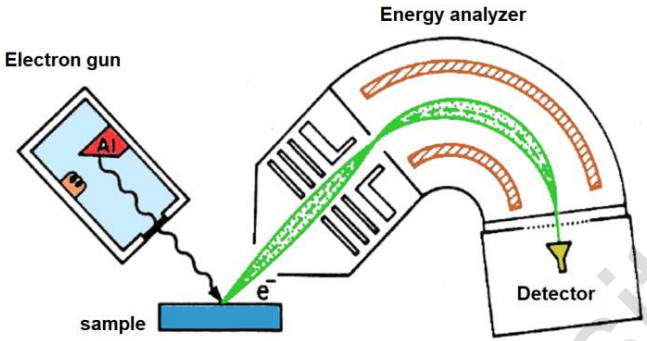

Fig. 1.1. Experimental scheme with the energy analyzer

The energy analyzer with a uniform field, i.e. a plane mirror, performs focusing in one direction. The main reason for its wide use in energy analysis of charged particle fluxes is the simplicity of its design. The energy analyzer operates on the principle of utilizing the dispersion properties of a uniform electric field.

A new modification of the analyzer with second-order focusing in a planar configuration for an arbitrary input angle was developed in work [10]. The proposed analyzer with a small input angle has an advantage at low voltage values. The analyzer is very useful for energy analysis in the MeV range. In works [11,12] a 45° plane electrostatic energy analyzer designed specifically for low-energy electron spectroscopy was proposed (Fig. 1.2).

A unique device, a two-cascade plane mirror that simultaneously measures different energies and angles of charged particles formed in the same beam, was described in work [13]. The ability to isolate and register particles with opposite polarity allows one to measure them simultaneously. Equations for the particle trajectories were derived and discussed in detail. Expressions for the corresponding particle detection resolution were presented.

An electrostatic system designed to produce a monoenergetic electron beam was proposed by Fishkova T.Ya. [14]. The system comprises a primary energy filter designed in the form of a planar mirror with enclosed ends and the additional plane capacitor compensating the initial energy dispersion. The analytical formula for the relation between the intensities of these fields was obtained.

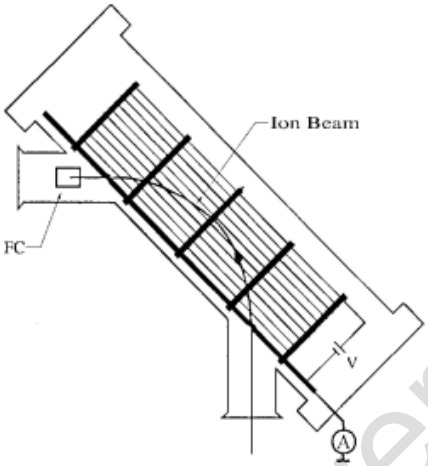

Fig. 1.2. Schematic diagram of the 45° plane electrostatic energy analyzer

The cylindrical mirror (CM) type analyzer is widely used. The analyzer has high electron-optical characteristics and is relatively simple in design.

In work [15] parameters of CM with end electrodes, when scanning the sample surface by a thin primary beam, were determined. The problem was solved numerically by using programs for calculating two-dimensional problems of electron optics.

In [16], Trubitsyn A.A. introduced the electron-optical scheme of the energy analyzer, which is a combination of the simplest (and technological) figures - cylinders and rings. The analyzer provides second-order angular focusing at α_0=90°. This focusing angle makes it possible to build an effective diagram of angular measurements, and the second-order focusing means a significant reduction in controversy contained in the requirement of simultaneously high values of luminosity and resolution, compared with the case of the first order focusing.

The design of a cylindrical mirror analyzer (CMA), which has two modes of angular focusing, was calculated in work [17] for Auger spectroscopy. Due to this, two methods can be applied in Auger-analysis of the sample surface in the study.

The focus of [18] was on creating a small-sized cylindrical reflecting mirror analyzer for low-energy ion scattering spectrometer used in vacuum deposition systems of thin film. The energy analyzer's configuration: an electrostatic reflecting mirror of cylindrical sector type with an average curvature radius of 4.0 cm and a sector angle of 70°, a high energy filter and two slits.

The article [19] describes the design of a parallel cylindrical mirror analyzer (PCMA) with an axis-axis configuration. The analyzer covers a wide range of energies in the parallel collection mode. A second-order focusing mode exists in the region of a limited range of energies with high energy resolution. The PCMA operates between the parallel collection and second-order focusing modes.

The objective of [20] was to create a compact energy analyzer that utilizes a high-resolution reflecting field for measuring the energy spread of electron beams with a volumetric charge. The energy analyzer were evaluated using electron beams with an energy of 2.5 kiloelectronvolts and a current of 60 milliamperes. The authors compared the measured energy spread of the electron beams analyzed by the energy analyzer with the results of theoretical calculations that considered the two main sources of energy spread namely the Bersh effect and longitudinal attenuation.

The calculation of the electron-optical properties of the modified CMA was presented in work [21]. The analyzer consists of two concentric cylinders with conical ends whose incomplete angles are between 30° and 90°. It was shown that the CMA with conical ends has second-order focusing properties with high dispersion. The analyzer expands the applications of cylindrical mirrors in atomic physics and surface physics because the conical ends provide more favorable geometric conditions for sample irradiation as well as for electron detection.

In [22], a device that filters charged particle beams by energy was proposed and theoretically investigated. The device is composed of cylindrical electrodes, with a plane grounded electrode located in the meridional plane, and grounded diaphragms located at the ends, serving as the input and output of the beam. Parameters were calculated for two cases, namely double focusing of the beam on the

flat electrode and parallel beam transfer, over a wide range of changes in the system geometry.

The study of the properties of the 127° CMA by using the SIMION 3D program version 6.0 was carried out in [23]. The analyzer is intended for use in low-energy ion scattering experiments. The optical properties of the analyzer can be fully described by the dependence of the obtaining solid angle Ω on the relative particle energy ε and the coordinates (x,y) on the target plane.

An ion energy loss spectrometer was designed in work [24]. The energy analyzer consists of 180°cylinder capacitor equipped with Matsuda plates. Its advantage is that focusing can be achieved by changing the electrical potential on the Matsuda plates which are located at both ends of the cylindrical capacitor. With this method, the energy analyzer becomes equivalent to an ordinary spherical capacitor, and eliminates the edge field.

In work [25], it was confirmed experimentally that the 210° drift-space CMA provides second-order focusing. The properties of the analyzer strongly depend on the edge field near the entrance and exit of the cylinders.

In order to avoid rotation of large electron sources and detectors in experiments on quantum particle scattering in work [26] was developed a device in which the rotation of the electron beam was achieved by combining three small CMA in a sequence. The first analyzer is stationary, while the other two rotate together around the output axis of the first cylinder.

The features of the cylindrical type electrostatic energy analyzer were described in order to measure the finite ion losses [27]. The analyzer provides information on the density of ion distribution in the cone region of the velocity space.

Work [28] is devoted to the description of the electrostatic energy analyzer scheme which allows simultaneously register the energy spectrum of charged particles in a wide energy range and in the whole range of azimuthal directions. The analyzer is similar to the CMA with the exception that linear changes in the potential are applied in the axial direction of the outer cylinder. The analyzer can be used in second-order focusing mode to analyze a narrow range of energies with high energy resolution.

Work [29] describes the development of a cylindrical sector energy analyzer that can operate with electrons having kinetic energies of up to 15 keV and high voltage.

Many multi-cascade energy analyzers have been developed based on CM, whose corpuscular-optical parameters exceed single CM. Work [30] presents an electrostatic electron spectrometer that allows for simultaneous measurements of energy and angular distributions of electrons over the full range of scattering angles (0°-180°), while maintaining high energy resolution. The first and second stages of the analyzer consist of three parts with cylindrical symmetry. The analyzer body and inner cylinder are under ground potential, the outer cylinder with conical ends under negative potential. The first stage of the electron spectrometer focuses electrons emitted near 90° from a point source on the axis to the point of focus. Such an entrance angle is not feasible in a conventional CMA. Electrons then pass through a second stage, focusing into a ring. Fig. 1.3 shows a schematic of the longitudinal section of a two-stage electrostatic analyzer.

An article [31] describes the design of a two-cascade CMA. This electron energy analyzer with a diameter of less than 1.5 inches (30 mm) outperforms a single-cascade CMA with a similar diameter.

Two-stage CMA for spin-polarized Auger-electron spectroscopy was presented in [32]. The analyzer has high transmission, small angular emission of electrons, and a large focal length. The combination of the analyzer with the compact classical Mott detector provides the Auger spectrometer with a very high efficiency.

Work [33] focuses on the development of a miniature two-cascade cylindrical mirror electronic energy analyzer (TCCMA) with an outer diameter of 26 mm. TCCMA consists of a screen for the electric field, inner and outer cylinders, two micro holes with diameters of 2.0 mm, and an electron multiplier. TCCMA is assembled into an axially - symmetric mirror electron analyzer designed for Auger-Photoelectron coincidence spectroscopy analysis. The electron-energy resolution of the TCCMA is $E/\Delta E=20$. This value is higher than that of the miniature single-cascade CMA ($E/\Delta E=12$), which was used in the previous Auger-photoelectron coincidence spectroscopy analyzer.

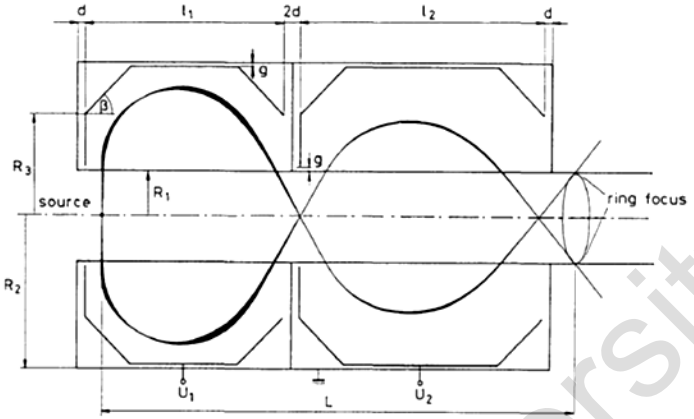

Fig. 1.3. Schematic of the longitudinal section of a two-cascade CMA with several electron trajectories near the 90° entrance angle

A new type of electron energy analyzer for Auger-Electron Spectroscopy (AES) was described in work [34]. It consists of three coaxial cylindrical electrodes to separate secondary electrons emitted from an excited substrate. The basics were briefly described, including the electron trajectories inside the analyzer, and details of the calculations of the geometric parameters of the design were presented. The sample-to-image distance is 200 mm, the analyzer constant is 2, the theoretical energy resolution is 0.03%, and the analyzer entrance angle is 33°55'±6°. Using the constructed analyzer combined with a scanning electron gun with a sliding slope of 15°, the C-272 eV carbon Auger peak for the chemically etched Si (1 1 1) substrate was recorded in E from N(E) mode and then numerically differentiated EdN(E)/deE to test the possibility of constructing an Auger spectrometer.

The scheme and design of an electron energy analyzer for studying electron processes in atoms and molecules of solids were described in work [35]. The analyzer consists of an 180° hemispherical deflector and five input optical elements. The focusing characteristics of the analyzer were investigated by means of the "SIMION" electron trajectory simulation program. The input lens system into the hemispherical deflector was designed to provide a

high collecting capacity for low-energy electrons. The lens system consists of three lenses, an accelerating or decelerating lens, an entrance and an exit slits. The entrance and exit slits of the lens system have fixed diameters of 2 mm to reduce aberrations in the field.

The spherical mirror (SM) refers to corpuscular-optical systems providing focusing in two directions. Due to its high parameters this type of analyzer has been widely used in various fields of research. A number of companies produce electron spectrometers in which the analyzer is a SM.

The time-of-flight characteristics of the electrostatic SM-type energy analyzer for charged particle fluxes of the under the conditions of ideal angular spatial focusing for a point source located on the symmetry axis of the spectrometer were studied in work [36]. It has been shown that the time of motion of the particle from the source to the ideal focus, also located on the axis, in the first approximation does not depend on the direction of flight near the normal to the axis. Thus, the time-of-flight focusing mode will make it possible to effectively use SM in electron spectroscopy methods (ESM) in which each act of emission is registered separately.

A new type of hemispherical electron energy analyzer for angular and spin-resolving photoelectron spectroscopy was developed in work [37]. The analyzer allows obtaining spectra with angular resolution by recording with a two-dimensional detector, and in parallel using a mini Mott polarimeter determining the particle spin. General scheme considerations and technical solutions were discussed. The results of tests from the Au surface were presented.

The article [38] presents a scheme of an original device for X-ray photoelectron diffraction and X-ray photoelectron holography measurements. The compact electron spectrometer is characterized by high sensitivity, high energy and spatial resolutions. The design is based on a combination of an axially-symmetric 90°-sector spherical deflector with second-order spatial focusing and a hollow conical moderating immersion lens. The energy range of photoelectrons varies from 0 to several thousand electron-volts, thus the analyzer can be used for studies of valence and ground electron levels. Fig. 1.4 presents scheme of the energy analyzer based on a combination of an

axially-symmetric 90°-sector spherical deflector with second-order spatial focusing and a hollow immersion retarding conical lens. The energy resolution of the analyzer is $\frac{\Delta E}{E} = 10^{-4}$. This resolution can be achieved in experiments with an angular resolution of 0.25° for electrons emitted from an extended sample area up to 4 mm^2 or more, over a range of initial polar or azimuth angles up to 60°. In addition, resolution can be achieved in spectromicroscopic mode with a solid angle of 0.5 steradian.

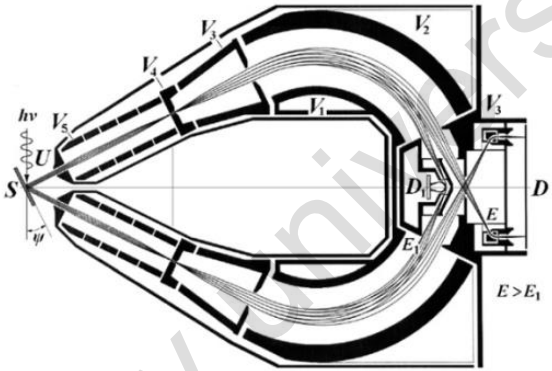

V_1, V_2 are potentials of the spherical deflector, V_5, V_4, V_3 are potentials of the retarding system

Fig.1.4. The energy analyzer scheme based on a combination of an axially-symmetric 90° sector spherical deflector with spatial second-order focusing and a hollow immersion decelerating conic lens

The characteristics of an analyzer consisting of two 180° hemispherical deflecting analyzers arranged in series and equipped with a multichannel detector were investigated in work [39]. The energy resolution and pass times for nonrelativistic electrons were calculated by using numerical methods. The optimal size and shape of the entrance slit with respect to the multichannel detector were calculated. The electron energy spectra were simulated with a multidetector with 100 discrete channels to show the possibility of a "fast counting" of an analyzer. Fig. 1.5 shows a scheme of the two-cascade analyzer. Here V_1 and V_2 are the potentials of the inner and

outer hemispheres, respectively, with an average radius R_0. Regions I and IV are free fields, while in regions II and III the $1/r^2$ field is supported by potentials. The electrons enter through the entrance slit with width W and are collected by the detector after deflection through the hemispherical sectors.

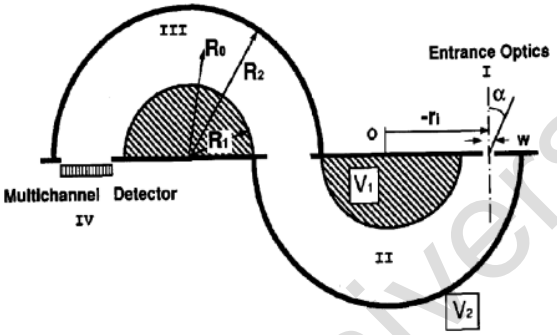

Fig. 1.5. Scheme of a two-cascade hemispherical analyzer

Hyperbolic mirror (HM) also belongs to the number of electrostatic mirrors with high luminousity, the focusing schemes of which were considered by Zashkvara V.V. et al. in work [40].

A hyperboloidal mass spectrometer with an analyzer on a three-dimensional ion trap bounded by the z=0 plane was proposed in [41]. Based on the numerical simulation of the electric field and the process of sorting of charged particles the mass peaks for different regimes of operation of the mass-spectrometer were plotted. The results are the basis for the creation of a hyperboloidal mass spectrometer with a simple electrode system and high resolution capability.

A new type of electrostatic charged particle analyzer, capable of parallel detection of a large range of kinetic energies, was described in work [42]. The main purpose was the simultaneous detection of electrons scattered from the surface and having energies from several tens of eV to 2000 eV. A prototype approximating a hyperbolic reflecting field was constructed. The energy resolution is a few eV and the collection efficiency was 0.05 % of 2π steradian. Significant improvements in the time of spectra acquisition give many possibilities for Auger and photoelectron spectroscopy.

Second-order focusing is a property of a dispersive-type electron energy analyzer, since it has a large angular acceptance or, on the contrary, a high energy resolution [43]. Second-order focusing conditions were obtained for the hyperbolic analyzer, which allows collecting a large range of energies in parallel, making it suitable for surface analysis, for example, in Auger spectroscopy.

A comparatively new type of electrostatic energy analyzers with angular resolution forms an analyzer consisting of a conical electrostatic prism and a position-sensitive detector for photoelectron spectroscopy [44]. The analyzer performance was validated by measuring the Ar photoelectron spectra using a helium discharge lamp. The analyzer was able to achieve an angular resolution of 3 degrees at an energy of 5.6 electron volts. The best energy resolution was equal to $\Delta E/E = 0.043$ at $E = 1.4$ eV.

A scheme of a parallel electromagnetic box analyzer in which the detection energy varies from 50 eV to 2500 eV was presented in work [45]. The analyzer has a second-order (or higher) focusing. The analyzer is small enough to function as an adjunct inside the sample chamber of scanning Auger-electron and electron microscopes. The dimensions of the analyzer circuit are 90 mm in length and 40 mm in height.

The article [46] describes the scheme of an original electrostatic "double toroidal" electron energy analyzer with high transmission. With the double toroidal analyzer, it is possible to measure both the kinetic energy and angular distribution of electrons at the same time with high resolution and high luminosity by means of a two-dimensional position-sensitive detector. The exact shape of the electrodes is derived analytically as well as by numerical calculations of electron trajectories.

The toroidal electrostatic analyzer described in work [47] has been designed for the scattering of medium-energy ions for structural analysis of surfaces. This analyzer has a wide interelectrode distance of 16 mm and an energy range of 10% of the transmission energy at a constant voltage value. The analyzer is mounted horizontally on a turntable and accepts ions scattered at well-defined angles. To obtain good energy resolution, a photon counting system (PIAS, Hamamatsu Photonics) with a spatial resolution of 40-50 mm, combined with a

three-stage microchannel plate, is used. The electric fields in the toroidal spectrometer, and including the scattered field, were calculated by the finite element method. The electron trajectories through the analyzer were calculated by using the Monte Carlo method. Thus, the optimal conditions for the geometry and dimensions of the entrance and exit slits were determined.

A new mirror axially symmetric electrostatic energy analyzer with an outer toroidal electrode was proposed in work [48]. Due to its toroidal geometry, this analyzer has excellent focusing properties, allowing for high angular reception and high energy resolution to be achieved simultaneously. Fig. 1.6 shows the second-order focusing of the axis-axis and axis-ring type in the toroidal mirror analyzer.

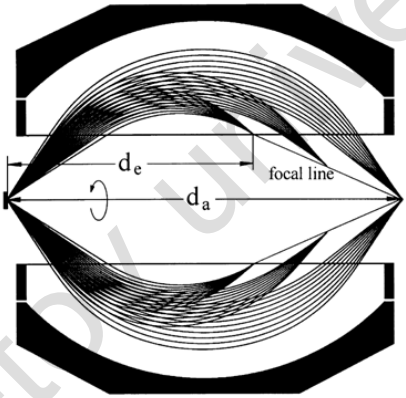

Fig. 1.6. Second-order focusing of the axis-axis and axis-ring type in a toroidal mirror analyzer

The toroidal energy-angle photoemission spectrometer was described in work [49]. The device has multi-detection by energy and angle, facilitating rapid measurement of photoemission over the entire hemisphere. The device is ideally suited for studies of the band structure and Fermi surface mapping by using photoemission spectroscopy with angular resolution.

Designs and simulations of ion-optical systems with intermediate focusing and parallel ion flux output intended for joint use with a

quadrupole mass filter to improve its analytical characteristics were proposed in [50].

An electrostatic lens has found application in electron optics, any combination of electrodes which forms an electrostatic field with rotational symmetry and thus allows charged particles to move in the field along the symmetry axis.

Taking into account the integration into a double toroidal electron energy analyzer for Auger-electron and ion coincidence measurements, a four-element conical electron lens was developed in work [51]. Calculation of the lens design by using numerical simulation of electron trajectories was fully conducted in terms of high-resolution electron analysis in the multi-coincidence mode. The design, construction and experimental characterization steps of this electron-optical system were described. Particular attention was paid to the importance of third-generation synchrotron radiation sources in such multicollision experiments.

In [52], computer simulations of energy-analyzing systems were presented, which combined hollow electrostatic lenses with various configurations of axially symmetric sector spherical deflectors. The deflectors had spatial second order focusing and formed systems of "axis-axis," "axis-ring," "ring-axis," and "ring-ring" forms. On the basis of the investigated systems it is possible to build compact high-luminosity spectrometers with energy resolving power in the range from several hundred to tens of thousands of eV.

In order to increase the intensity of the charged particle beam, an electrostatic lens of three coaxial cylinders, which focuses the near-axis beams (due to the axially-symmetric lens) as well as the beams away from the axis (due to the coaxial cylindrical lens) at one point, was theoretically studied [53]. The parameters of such a combined lens were calculated numerically. The gain in beam intensity over the commonly used single axially-symmetric lens was determined.

Work [54] concerns the calculation of the time-of-flight characteristics of a system composed of mirrors with two-dimensional electrostatic fields arranged sequentially and sharing a common symmetry plane. The time-of-flight focusing conditions for the divergence angle of the charged particle beam and the energy spread are found.

Paper presents a new time-of-flight photoelectron energy analyzer which uses an electrostatic field to reflect and focus electrons. Using a high-quality ellipsoidal grid, photoelectrons can be collected with high efficiency and focused on the detector. The problems of spatial charge and extended electron sources in an ellipsoidal mirror analyzer have been discussed. The proposed spectrometer analyzes single- and multiphoton ionization processes and operates in a wide range of energies. Experimental data indicate a high collection efficiency. Spectra were obtained at vacuum less than 10^{-7} Torr.

Designs of time-of-flight mass spectrometers for studying the elemental composition of gas flows, dust particles, and micrometeoroids are described were work [56]. Calculation of the mass spectrometer parameters is based on determining the law of potential distribution on the electrodes forming the electric field.

A tandem of two time-of-flight analyzers in a new "nested time" mode was proposed in [57]. The tandem allows parallel analysis of fragment spectra for ions within one separation cycle in the first "slow" analyzer. a new type of "slow" time-of-flight analyzer was proposed, which combines transverse confinement of the low-energy ion beam in periodic lenses with multiple ion reflections between planar mirrors without a grating.

For increase the rate and sensitivity of tandem mass spectrometric analysis, [57] proposed using a tandem of two time-of-flight analyzers in a fundamentally new mode of "nested times," allowing parallel analysis of fragment spectra for ions within one cycle of separation in the first "slow" analyzer. A new type of "slow" time-of-flight analyzer combining transverse confinement of a low-energy ion beam in periodic lenses with multiple ion reflection between planar gridless mirrors was proposed to implement the method.

A time-of-flight electron energy analyzer operating at a repetition rate of 80 MHz was proposed in work [58]. The analyzer has an energy resolution of 40 meV for electrons with an energy of 3 eV. The energy resolution limit depends on the detector response time or time resolution. Currently, a detector with 100 ps temporal resolution has

an energy resolution of less than 1 MeV for 200 MeV electrons. It provides a high repetition rate of the time-of-flight energy analyzer.

In work [59], the model of an electrostatic spectrograph for energetic analysis of charged particles is proposed. The basic element of device is a five-cascade cylindrical mirror analyzer. The obtained test results agree with the electron-optical parameters of the spectrograph calculated earlier.

An optimal mode of operation of a plane magnetic mirror with a uniform field was found in work [60] in which the luminosity of the device increases due to second-order focusing. In this case, in contrast to the known mass spectrometer with semicircular focusing, the source and receiver are outside the field.

In [60] an optimal mode of operation of a plane magnetic mirror with a uniform field was found. The luminosity of the analyzer increases due to focusing of the second - order. In this case the source and receiver are outside the field. To work in the spectrograph mode, the coordinates of the focus line where the detectors should be placed, are determined.

Second-order focusing conditions in conic systems were investigated numerically in work [61]. Second-order angular focusing as a dependence of the position of the point source on the symmetry axis on the half angle of the cone for systems with parallel formations was presented. The possibility of achieving second-order focusing in finite-dimensional cone systems is discussed. Electron-optical schemes for these devices were given.

Work [62] is devoted to the calculation of an electrostatic spectrograph based on a truncated cylinder-type energy analyzer in a wide range of changes in its parameters. The position of the focus line was found for energy dispersion in the beam that differs by an order of magnitude. Linear and specific energy dispersions were determined. A comparison was made with a widely used spectrograph of two plane electrodes.

Work [63] presents a new scheme for an electrostatic electron analyzer that has high energy resolution and can efficiently collect photoelectrons from submicron regions. The analyzer described in [63] uses a unique electrostatic mirror that has a low aberration value to efficiently collect photoelectrons from submicron regions. In

addition, it incorporates retarded hollow cylindrical lenses and a hemispherical energy analyzer to achieve high energy resolution. Possible modifications of the analyzer have been discussed. The energy analyzer scheme is presented in Fig. 1.7. The beam exits the deflector along the forming surface of the cylinder, then it is retarded by four electrodes of a hollow lens consisting of conical and cylindrical coaxial electrodes, between which a retarded longitudinal electrostatic field is created. This lens performs two actions. First, it retards the beam so that the transmission energy in the hemispherical analyzer remains small, its energy resolution high. Second, it reduces the angular spread in the beam. Indeed, the deflector assembly is reduced to some degree of angular spread in the beam in the polar direction (from 22° at the entrance, 13° at the exit). This spread is still too large for a hemispherical deflector to achieve high energy resolution. The immersion lens further reduces this spread by 8°, resulting in a reduction of up to 80 times the kinetic energy of the electrons. The inevitable consequence of these two actions is a linear increase of up to ten times the image at the lens exit. However, this increase is irrelevant because the width of the ring image at the lens entrance is small compared to the focusing properties of the deflector. In this case, the radial width of the image at the lens exit is determined by the angular aberration of the lens.

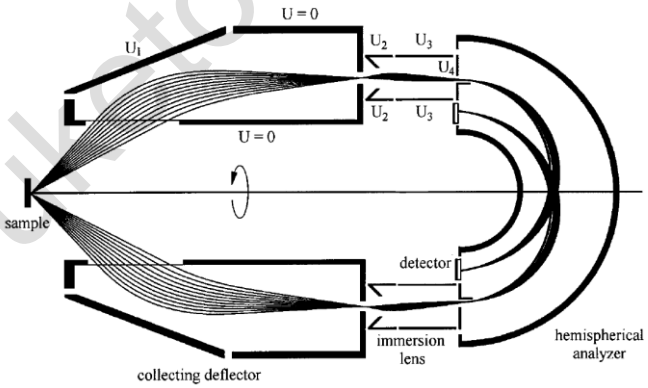

Fig. 1.7. Configuration of the high-transmission energy analyzer consisting of hollow coaxial cylindrical lenses and a hemispherical deflector

However, this magnification is irrelevant because the width of the ring image at the lens entrance is small compared to the focusing properties of the deflector. In this case, the radial image width at the lens exit is determined by the angular aberration of the lens.

In applications not requiring very high energy resolution, the basic hemispherical deflector can be replaced by the simpler mirror analyzer shown in Fig. 1.8 [63, p.1654].

Analyzers operating in multichannel particle registration mode are attractive because of their ability to use energy much more efficiently than analyzers with sequential (in time) dispersion. They operate on the principle of simultaneous measurement of several spectra, which allows them to be used for express simultaneous multi-element analysis.

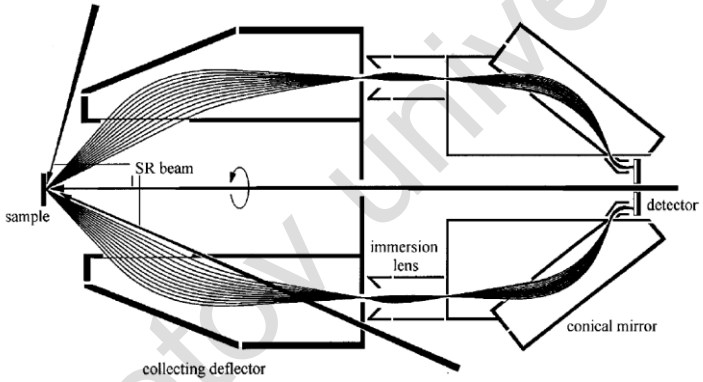

Fig. 1.8. The high-transmission energy analyzer consisting of hollow coaxial cylindrical lenses and a main conical mirror analyzer

A new parallel charged particle analyzer with multichannel energy and angle detection was described in work [64]. Simultaneous multichannel detection of both of these variables was achieved by using a two-dimensional position-sensitive detector. The device was arranged so that the angle information was derived from the azimuthal coordinate and the energy from the radial coordinate of each particle being detected. The device was based on the original circuit "Bessel box" developed by Allen and her colleagues.

The design, modeling and testing results of a new dispersive multichannel analyzer for secondary electrons were presented in work [65]. Due to the experimental resolution of 50 mV and the spectrometer constant, this analyzer is very suitable for voltage measurements in integrated circuits. The analyzer can also be used for complete separation of secondary and reflected electrons in image mode. Parallel detection of the 20 eV wide secondary electron spectrum band can be used in the future to obtain material characterization data at low energies <2 keV of the primary electrons.

A multichannel cylindrical reflecting electron energy analyzer designed to measure weak characteristic signals from electron energy loss spectra was described in work [66]. The analyzer's edge field was nearly ideal. The dependence of the radial coordinate of the particles at the detector on the coordinate of entrance, angle and energy was determined numerically and can be approximated by second-order polynomials.

In [67], an electrostatic multichannel deflector with energy filtering of charged particles was proposed. The deflector was formed by a cylinder with closed ends, and a filament electrode is placed along its longitudinal axis. The potential distribution of such a system in analytical form was found. The parameters of the system at the entrance and exit of the beam through its grounded ends were calculated.

The article [68] describes an energy analyzer with a cylindrical symmetric electrostatic field, for Auger analysis. The device was designed and manufactured. The optimal parameters of the analyzer were estimated and then experimentally verified.

A new type of electron energy analyzer for fast obtaining X-ray photoelectron spectroscopy spectra and designed for operation at a pressure of 10^{-5} Torr was proposed in work [69]. The proposed analyzer uses spherical retarding grids combined with a post-monochromator to achieve bandgap transmittance while maintaining the high transmission of the retarding grid of a conventional analyzer. The purpose of the simulation was to study the interaction between the retarding grids and the post-monochromator. It was determined that the key factors in the performance of the analyzer are the scattering of electrons on the retarding grid and on the edge electric fields. Based

on the simulation results, an electron energy analyzer was constructed and tested using gold samples and polystyrene thin films. A 20-eV width scan over 100-200 with a resolution of 1.0 eV was carried out.

Usually the use of physical limiters (e.g., slits and apertures) on the entrance and exit planes of the deflector type electrostatic electron energy analyzer often introduces undesirable distortions in the "ideal" equipotential distribution and reduces the deflection angle. The effect of physical limiters and Iosta plates on the scattered field in a standard hemispherical energy analyzer by program "SIMION" for electron beam trajectories has been investigated in work [70]. On balancing the edge field effect due to physical confineers with the Iosta plates, the correction of the scheme proposed earlier by Iosta has been continued. This correction scheme has the advantages of simplicity in design.

Work [71] proposed an electron energy analyzer capable of analyzing a broad range of energies simultaneously. In this analyzer, the electrons are introduced through a highly transmissive slit into a magnetic field with relatively uniform strength, causing them to follow helical trajectories. They are subsequently directed through a second slit and focused on the detector. The energies of the electrons are correlated with their azimuthal rotation in the magnetic field, which can be detected by the detector. This example demonstrates that a wide range of energies, varying by a factor of 20, can be analyzed simultaneously with an energy resolution of approximately 1% of the initial energy. Another example showed that the scheme was capable of collecting electrons with energies of 500 eV from small sources and resolving them to 0.6 eV.

An electron energy analyzer with angular resolution and a newly designed entrance lens system was developed in work [72]. In this lens system, angular resolution was achieved by using a plane diffraction slit. Using this system, high angular resolution and high transmission in measurements for photoelectron diffraction were easily achieved. In addition, the angular resolution was easily determined by the size of the planar diffraction slit. In order to evaluate this analyzer, X-ray photoelectron diffraction patterns with MgO (001) and CAF2 (111) were measured.

In work [73], it has been conducted a theoretical investigation on an electrostatic analyzer that includes two electrodes: one is inclined,

and the other is straight with respect to the beam axis. This type of analyzer can be used to study the charge distribution in the beam, with a resolution better than the conventional parallel plate geometry.

The article [74] describes a universal setup for measuring static parameters of high-intensity electron beams. The setup is based on the registration of transient radiation that arises when ribbon and axially symmetric beams fall on a metal target. The principle of operation has been explained in detail in the article. The radiation registration schemes are presented, the peculiarities of the measurement methods depending on the beam configuration are described, and for the first time, the design of a ribbon beam electron analyzer is presented in the work. The effectiveness of the setup is validated through both experimental data and computational simulations.

In [75], a new electrostatic analyzer was introduced for detecting low-energy charged particles known as a segmentoidal analyzer. The paper discussed the determination of the field strength between the plates and analyzed the fundamental features of a spectrometric module built using the segmentoidal analyzer and a VEU-7 secondary electron multiplier detector. Transmission curves for energy and entrance angles, as well as the energy geometric coefficient, were among the key characteristics evaluated in the study. The experimentally obtained value of the energy-geometric coefficient during calibration agreed well with the calculated value of the module.

1.2 Computational Approaches for Energy Analysis Systems in Charged Particle Beams

The improvement of the characteristics of modern electron spectrometers is limited by the limiting parameters of the corpuscular-optical systems used in them. The improvement of the latter is possible by upgrading existing corpuscular-optical systems with additional elements of corpuscular optics; development of new systems with improved electron-optical characteristics, etc.

The most effective approach for the synthesis of corpuscular-optical systems is the approach that implements the formulation and solution of inverse problems of corpuscular optics. This approach requires the use of analytical or semi-analytical methods for

calculating corpuscular-optical systems, including the method of optimal matching of elements. In [76, 77] it was possible to solve the inverse problem of optics: to describe the fields forming this beam using the given electron-optical parameters of a beam of charged particles.

The continuously growing requirements of modern experiments to devices and means of energy analysis stimulate the creation and development of calculation methods, parameter studies, and proposals for new classes of corpuscular-optical systems for application in practice.

In a number of studies led by V.V. Zashkvara, electrostatic axially symmetric multipoles were applied to solve the problem of synthesizing an analyzer with a deflecting field [78-80]. New schemes of analyzers with improved characteristics were proposed. The shapes of deflecting electrodes were calculated. The operator separation method for solving the wave equation was applied in works [81-83]. Solutions describing the evolution of fields with a circular multipole structure in a cylindrical coordinate system were obtained. In work [84] a non-Laplace circular multipole was constructed and the principal possibility of its correcting effect on the angular focusing of the deflector type electrostatic analyzer was considered. In [85], an external boundary Dirichlet problem based on circular multipoles in cylindrical coordinates was solved. A number of multipole-cylindrical fields have been calculated. A method for calculating multipole-cylindrical fields based on the solution of the Dirichlet problem in a cylindrical coordinate system was proposed in [86].

A method using potential decomposition by irreducible representations of the symmetry group of the system's field elements was proposed in [87]. The boundary problem for multipole systems with plane plate electrodes for the case of the C_{nv} symmetry group was solved. A quadrature expression for the field potential of such systems was obtained. The conditions imposed on the potentials of the electrodes, under which such a solution was possible, were found. The results of the calculation of the potential distribution in some specific systems were given.

Approximate-analytical method for calculation of charged particles trajectories in an axially-symmetric mirror with a multipole-

cylindrical field was proposed in [88, 89]. This approach makes it possible to determine the electron-optical characteristics of the high resolution mirror analyzers.

A new class of axially-symmetric Laplace potentials with ring singularity described by elementary functions was proposed in work [90]. Here the possibilities of application of this class in the problems of synthesis of energy analyzing systems and lenses were discussed. Equipotential portraits of electric fields with ring features were presented. General formulas for the reconstruction of two-dimensional Laplace fields according to the given characteristics of focusing and dispersion in the symmetry plane were derived in [91]. The electrode configuration of an energy analyzer with ideal fan-shaped beam focusing was determined, and the plane trajectories parameters, their shape, and energy dispersion were determined.

The synthesis of field structures with conic equipotentials based on the analytical representation of Donkin was considered in [92]. A hierarchy of such structures is established, examples of equipotential portraits were given, and the Cauchy problem for symmetric fields was solved. The electron-optical properties of several systems have been studied in [93].

New approach for the determination of optimal electron-optical scheme for construction the electron (ion) spectrograph can be effectively implemented has been developed in [94]. It is based on electrostatic fields with a Laplace potential subject to the Euler uniformity condition. The principle of operation of spectrographs with such fields is related to the special property of similarity of isoenergetic families of trajectories with different energies under the uniformity condition. A new method of analytical representation has been proposed for constructing the fields to be sought, in which the Donkin complex representation apparatus for cone-shaped fields is the basic one. The developed algorithms allow constructing in the elementary form the uniform potentials in a wide class in which the classical ball and spherical functions are only special cases. On this basis the Cauchy problem for the uniform potentials with the symmetry plane has been put and solved in the general form in the closed analytical form. A number of concrete structures of this series have been given.

New analytical relations between axially-symmetric and planar Laplace potentials were considered and on their basis efficient and compact algorithms for solving the Cauchy problem for axially-symmetric electric fields in regions containing the symmetry axis were constructed in [95]. Accuracy estimates of the obtained approximations were given. A new analytical way of constructing broad classes of three-dimensional Laplace potentials that admit a closed representation in elementary functions has been developed in [96]. These classes are especially useful in problems of synthesis of electron-optical devices on the basis of inverse problems of particle dynamics, when there is an incorrect Cauchy problem for the Laplace equation related to the procedure of analytical continuation of the potential from the plane into space. New classes of multipole electric and magnetic field structures, on the basis of which an effective synthesis of new corpuscular-optical elements is possible, have been given in [97].

A potential model for describing the electric field of a cylindrical mirror analyzer with a one-dimensional grid along the aperture cuts was proposed in [98]. The influence of the boundary field near the grids on the charged particle trajectories was studied. The formulas for the transmission and angular aberration were obtained and some estimates were given. It was shown that the resolution of the analyzer with one-dimensional grids can be even better than without the the boundary field effect.

In [99], analytical expressions for the main parameters of a cylindrical analyzer with planar electrodes and an inner cylinder potential at its ends were derived. The one- and two-period modes of operation of a cylindrical analyzer with first-order angle focusing were calculated. The study found that as the distance between the object and the front end of the analyzer increases, the luminosity of the object decreases. The results obtained from numerical calculations using a two-dimensional charged particle optics program were compared to those obtained from analytical formulas, and it was found that the difference between them was not greater than 10%.

In [100] the calculation of focusing conditions and the angle of slope of the focal line for a beam of charged particles with energy-angle correlation when it passes through systems with transverse

dispersion was carried out. Formulas for the image position in a number of electrostatic and magnetic energy analyzers were given. The parameters for a cylindrical deflector were calculated in detail. In [101], the condition for focusing beams with energy-angle correlation when the source and detector were located on the bottom plate of a plane capacitor was found. Expressions for the second-order spherical aberration and dispersion were given.

In [102], an approach for solving corpuscular-optical problems, such as the correction of geometric aberrations in two cascade systems of electron spectrometers and temporal aberrations in new systems of mass spectrometers, was proposed. The proposed class of electrostatic devices has a high transfer coefficient for transporting fluxes with large phase volume over a given distance.

The article [103] is devoted to the main aspects of the evolution of a new class of electrostatic energy analyzers for electron and ion flows called "quasi-conical" by the authors. It considers the genesis of the main physical and mathematical ideas, constructs an accurate mathematical theory for calculating such systems, describes real designs, presents experimental results, and discusses the prospects for the development of this direction.

In [104], second-order aberration transfer matrices were developed for the electron-optical systems of the monochromator and energy analyzer. Both of these devices have two magnetic circular lenses and a retarding filter. The filter consists of a deceleration lens, a Wien filter and an acceleration lens. Optimal excitation of the circular lenses provides a parallel output of electrons from the accelerating lens. Excitation in the Wien filter regulates the focus of the beam on the slit. The calculation results are useful for finding optimal operating conditions and for explaining the experimental results of the high-resolution electron energy loss spectrometer.

A new geometrical criterion for optimization of a high-resolution electron energy loss spectrometer based on spherical 180°- and cylindrical 127°- deflectors has been proposed in [105]. This criterion is related to the relative geometric configuration of the electrodes and its application improves the energy resolution of the tandem monochromator-analyzer spectrometer used in high-resolution electron energy loss spectroscopy for surface studies. Calculations of

electron trajectories for spherical and cylindrical fields have shown that there is a tandem configuration in which electrons are well refocused in position and energy at the analyzer exit. The usual tandem configuration gives a poorly defined image due to optical aberrations of the deflectors. Correcting for these aberrations is possible by applying a modification to the conventional configuration. The new geometry can be achieved by simply rotating both analyzers and the monochromator 90° with respect to the beam axis, or by rotating the monochromator 180° from the conventional configuration. It has been also shown that the adoption of these geometrical configurations is consistent with the principle of dispersion compensation if the monochromator output aperture and the analyzer input aperture are increased, respectively.

In the paper [106] the properties of the time-of-flight focusing in a two-dimensional electrostatic field with a median plane were investigated. Simple analytical relations linking the expansion coefficients of the particle's time-of-flight and its coordinates in series on small parameters were obtained. Conditions for elimination of various kinds of time-of-flight aberrations were found.

The problem of numerical analysis of the electrostatic field of individual elements of complex three-dimensional electron-optical systems was considered in work [107].

In [108], a method for analyzing the spatial and time-of-flight characteristics of polar toroidal analyzers for charged particles was presented. The method involves the calculation of aberration integrals. The method effectiveness was illustrated by comparing the results of calculations based on it with the results of numerical simulations and experimental measurements.

In [109], the amplitudes of spatial field harmonics were calculated for given displacements of the quadrupole mass filter electrodes with respect to the optimum position. The cases of radial and angular displacements of the electrodes, asymmetry of electrode feeding, and non-identity of the rod diameters have been considered. The data obtained are necessary for calculating the real shape of the mass peak and will be useful in the design of the mass filter.

The calculation of the image position depending on the position of the object (hollow beam) for an electrostatic system in the form of

two coaxial cylinders and an end diaphragm with an ring slit was given in [110].

A static mass-based charged particle analyzer with an nonuniform magnetic field was proposed in [111]. An expression for the magnetic potential distribution was obtained analytically, on the basis of which formulas for the main parameters in the dispersion plane were found in the presence of first-order angular focusing. The conditions of spatial focusing were also obtained for the source and receiver to be located outside the magnetic field. Operating modes were found in which the trajectory had three rotations, i.e. a long path of charged particles. This led to a significant increase in mass dispersion.

In [112] the distribution of the electrostatic potential is obtained, and the basic parameters of the energy analyzer of simple design are found. The mode of its operation with the maximum possible dispersion in a wide range of angular sizes of the field charge electrode was found.

In [113] the rules of electron motion in spherical coordinates were used to consider irregular, nonspherical boundaries in "Herzog fields" on output and input planes of hemispherical energy analyzers. Comparisons and verification for improvements of some classical schemes, i.e., the sudden reduction of the "ideal field" approximation, real apertures in the 180° plane, the Herzog correction, the Jost correction, and reduced spheres, were made. Focusing, maximum trajectory width, basic resolution, and banana asymmetry for the circular recommended path were investigated. Design equations were presented.

In [114] the distribution of the transit times of electrons passing through a high resolution hemispherical energy analyzer was determined. A comparison of measurement results with analytical expressions, showed that the different transit times between electrons with the same kinetic energies grow on the Kepler orbit, in which the electrons move around the hemispheres. To facilitate measurements, a position-sensitive electron detector capable of triggering a single event within the spectrometer was installed. This instrument was based on anode delay lines.

Based on the analysis of the charged particle motion in dispersive analyzers in [115] the equations relating the signal at the analyzer output and the energy distribution function of the charged particles falling into it were obtained and solved. The influence of corrections on the recovery of the energy distribution as compared to the standard procedure was considered.

An equation connecting the signal at the exit of the electrostatic dispersion analyzer and the energy distribution function of the charged particles falling into it, taking into account potential fluctuations at the deflecting electrodes, was obtained in [116]. Solutions to this equation were obtained. The effect of noise on the hardware functions of the analyzers was considered.

Work [117] is devoted to the study of the influence of electron beam input parameters on the shape of the hardware function of a cylindrical energy analyzer. It was shown that the choice of the electron beam entry angles into the energy analyzer can significantly reduce the "tails" of the peaks.

In [118], an algorithm is introduced to tackle the axis problem encountered when solving the axial Laplace equation. The approach involves converting the integral equation into a matrix equation using the collocation method and the method of analytical substitution. Analytical integration is then applied to derive an algorithm capable of calculating the potential and its derivatives on the axis up to the fourth order.

An algorithm for calculating the hardware function of axial electrostatic energy analyzers based on the numerical solution of the equations of motion and the processing of the results of calculations was presented in [119].

The use of perturbation theory has been discussed in [120] as a means to solve a range of important problems in computational optics of charged particles. These include the calculation of electric and magnetic field perturbations due to minor deviations in electrode or magnetic pole symmetry, as well as edge effects. The paper also addresses the general tensor form of aberration analysis for charged particle beams. Methods of perturbation theory in combination with other numerical approaches, such as the tau-variation method and the generalized method of varying initial parameters, prove to be effective

in the problems of calculating mechanical tolerances, as well as modeling Coulomb rearrangement and scattering of particles on grids.

In [121], numerical investigations into second-order focusing conditions in conic systems were carried out. The study focused on second-order angular focusing. Corresponding dependencies for different values of the half angle of the inner cone were presented. Second-order angular focusing as a dependence of the position of a point source on the symmetry axis on the half angle of the cone for systems with parallel formations is presented. The electron-optical schemes for these devices were given.

In [122], a numerical method was proposed to determine the order of angular focusing, which was one of the crucial parameters in electron-optical systems. The method was based on determination of the mutual correlation magnitude of the power function and the angle-of-flight function of charged particles formed during trajectory analysis. The method was tested on systems admitting analytical solutions.

The articles [123,124] present a method for numerical simulation of electron- and ion-optical systems; algorithms and methods for high accuracy in calculating the potential distribution function by the boundary element method were proposed; a method for finding high order angular and spatial focusing conditions was developed. On the basis of these methods, software for trajectory analysis of corpuscular optics systems was created, calculation errors were studied, and detailed testing on model schemes was carried out.

The mathematical apparatus for solving the Dirichlet planar external problem was developed and formulas for calculating boundary integrals, including those with singular kernels, were obtained in [125]. On the basis of the proposed apparatus the software for modeling of electron-optical systems was created, the study of calculation errors and testing on model schemes were carried out.

A numerical method to estimate one of the most important parameters of electron-optical systems, the order of spatial focusing, was proposed in work [126]. The approach relies on evaluating the mutual correlation between the power function and a specific function derived from the initial coordinate of a charged particle during the

trajectory analysis. The effectiveness of the method was verified through experimentation on systems that possess analytical solutions.

A method for eliminating the defocusing of charged particle beams in the dispersion plane in the edge fields of a sector deflector was proposed in [127]. The method is based on modification of the geometry of the edge region of the deflector, a nonmonotonic distribution of the intensity of the deflecting electrostatic field on the optical axis.

The article [128] is devoted to further progress in the theoretical synthesis and practical implementation of electrostatic energy analyzers with record parameters in terms of luminosity and resolution. The search for optimal solutions is based on a computer strategy using the most advanced software packages, in particular "SIMION". In this case it is about deep smooth deformation of quasi-conical systems in order to improve the manufacturability of the design and increase the energy analyzing characteristics.

The authors of [129] have derived differential equations that describe the deviations of charged particle trajectories from the axial trajectory in curvilinear coordinates related to the beam axial trajectory. The resulting equations are suitable for numerical calculations of charged particle beam dynamics, including relativistic effects. These equations are also written in the linear approximation.

The article [130] describes the results of using numerical methods, specifically the boundary element method and the finite difference method, to optimize the scattered field of a hemispherical deflector analyzer.

The peculiarities of applying the finite element method to calculate the trajectories of particles in high-current electron beams taking into account their spatial charge were considered in work [131]. The nonphysical effects arising on an irregular finite-element grid associated with the calculation of the electric field strength using a shape function were shown and ways to eliminate them were proposed.

The electron-optical characteristics of two-dimensional electric fields with a complex potential of the form $\Omega=i(x+iy)^n$, where n was a real number, was studied in [132]. The particle dynamics was studied in the symmetry plane and its vicinity in order to construct an

effective spectrograph of electron fluxes. It was shown that in the range of $0< n<1$ in the system the spatial focusing by angles of arrival of conic beams, having II order in the symmetry plane and, at least, I order across it, was realized.

A method for obtaining electrostatic fields of a given shape in an implicitly-electrode cylindrical system was considered in [133]. "Distributed" electrodes allowed to solve the inverse boundary problem - to set such azimuthal distribution of electric potential along the cylinder perimeter in order to obtain the desired field inside, while ensuring a larger working area as compared to the explicit-electrode system.

2 INVESTIGATION INTO THE FEASIBILITY OF DEVELOPING A HIGH-PERFORMANCE ENERGY ANALYZER ON MULTIPOLE ELECTRODE

2.1 Investigation into the feasibility of developing a high-performance energy analyzer based on octupole-cylindrical field

Based on a brief review of the most notable and recent works in corpuscular optics, it appears that novel and efficient energy analyzers are predominantly constructed through modifications and combinations of individual electrostatic mirrors, as well as by utilizing newly synthesized fields of non-traditional types.

Therefore, it is important to continue exploring and discovering new axially symmetric fields that have wider analytical capabilities and can facilitate high-resolution luminosity energy analysis.

The consideration of using multipole fields in the synthesis of analyzing systems is both reasonable and necessary for the development of highly sensitive methods for analyzing corpuscular particle fluxes. This discussion may lead to the creation of high luminosity devices that are essential for achieving such analytical capabilities.

The multipole approach to the synthesis of electrostatic fields is particularly interesting in the theory of corpuscular-optical system calculations. Multipole fields are characterized by the presence of N equally spaced symmetry or antisymmetry planes. Their name is a consequence of the fact that such fields can always be constructed using a set of electrodes and poles. They are usually used as focusing, deflecting and correcting elements in electron and ion optics. The potential in the cylindrical coordinate system for a multipole field containing N planes of symmetry can be expressed as follows:

$$u(r,\alpha,z)=\sum_{n=0}^{\infty}A_{n,N}(r,z)r^{nN}\cos nN\alpha$$

The component of the field that corresponds to n=0 characterizes the axially symmetric component. The potentials for the remaining terms can be expressed in the following way.

$$u(r,\alpha,z)\big|_{nN=m=const} = A_m(r,z)r^m \cos m\alpha$$

When m=1, the equation can be written as $u(x,y)=A_1x$, which represents the potential distribution of an infinite planar capacitor, also known as a dipole. When m=2, the equation takes the form $u(x,y)=A_2(x^2-y^2)$, which characterizes the potential distribution caused by an ideal quadrupole. This quadrupole consists of four identical hyperbolic surfaces of infinite size with alternating positive and negative potentials. Further similarly, *m=3* corresponds to a hexapole, *m=4* to an octupole, and *m=5* to a decapole.

The multipoles are symmetric with respect to the plane y=0. To make them antisymmetric with respect to this plane, it is sufficient, using the property of rotation symmetry of planar multipoles, to rotate the x,y coordinate system with respect to the origin by an angle $\pi/2m$, where *m* is the multipole index.

Among the known potential fields satisfying the Laplace equation, a special place belongs to multipoles containing nodal points or lines where zero-point equipotential surfaces converge, dividing the field into regions with potentials of the opposite sign. The simplest multipole structure is a planar multipole of 2 order, in the general case, containing *n* symmetry planes and as many antisymmetry planes that intersect the multipole axis and are equidistant along the polar angle. For example, the sextupole *n*=3 contains three symmetry and antisymmetry planes each and is realized in a region surrounded by six symmetrically arranged hyperbolic profile electrodes with potentials alternating in sign. Formulas describing planar multipoles in the Cartesian coordinate system *x,y,* in which they are uniform polynomials of two variables [134] are presented below:

$$U_2 = x^2 - y^2 \text{ - quadrupole,} \quad (2.1)$$

$$U_3 = x^3 - 3xy^2 \text{ - sextupole,} \quad (2.2)$$

$$U_4 = x^4 - 6x^2y^2 + y^4 \text{ - octupole,} \quad (2.3)$$

$$U_5 = x\ -10x^3y^2 + 5xy^4 \text{ - decapole.} \quad (2.4)$$

Multifields with a curvilinear axis, in particular circular multipoles whose center line is a circle of some radius, are more complex in structure. These fields have no symmetry elements with respect to the centerline due to its curvature.

By combining multipole components of various orders (quadrupole, hexapole, sextupole, etc.) with a fundamental cylindrical field, a diverse range of axially-symmetric fields can be synthesized, which includes variations of mirror analyzer configurations with enhanced angular focusing capabilities.

In [135, 136] a new approach to solution of the Laplace equation for analytical representation of circular multipoles has been proposed. This new class of axially-symmetric Laplace fields is based on the superposition of a cylindrical type field and components of new harmonic functions - circular multipoles. It is both reasonable and necessary to explore the potential application of this field class in the synthesis of analysis systems. Such exploration could result in the development of high-luminosity devices, which are essential for achieving highly sensitive energy analysis.

A diverse range of potential fields has been developed using the multipole approach, which are practical for investigating the mirror effect on charged particle beams. Mirror energy analyzers have been extensively studied using electrostatic quadrupole-cylindrical [137-139], hexapole-cylindrical [140-142], and decapole-cylindrical fields [143-146]. Several monographs [147-149] have been dedicated to exploring their electron-optical characteristics and potential, as well as searching for optimal electron-optical configurations with high energy resolution and focusing quality.

In [150] the was suggested an energy analyzer for space research utilizing the electrode system of an axially-symmetric electrostatic decapole-cylindrical field. The calculations reveal that the energy specific dispersion, which determines the resolving power of the decapole-cylindrical field, is twice as high as that of the classical cylindrical mirror analyzer, when calculated for particles with an initial angular dispersion of 12°. This instrument enables the detection of elementary particle fluxes from outer space and the acquisition of various high-resolution spectra.

The proposed approach for constructing an energy analyzer field, as outlined in [135], involves combining a base field with a series of coaxial circular multipoles. Specifically, in the case of an electrostatic deflecting field, the construction takes the following form:

$$g(R,\xi) = \ln R + qU_q(R,\xi) + sU_S(R,\xi) + \omega U_{oct}(R,\xi) + \\ + dU_{dec}(R,\xi) + ..., \tag{2.5}$$

where $\ln R$ is basic cylindrical field, $U_q, U_S, U_{oct}, U_{dec}$ are circular multipoles (quadrupole, hexapole, octupole, decapole, etc.), q, s, ω, d, are weight coefficients of multipoles, $R = r/r_0$, $\xi = z/z_0$ are relative radial and axial coordinates, r_0 is radius of the axial circular trajectory of the analyzed charged particle beam (Fig. 2.1).

The electrostatic multipole-cylindrical field is created within the area between two coaxial axially-symmetric electrodes. The inner electrode (2) has a cylindrical shape with a radius of r_0 and is maintained at zero potential. The outer electrode (3) has a curvilinear profile that replicates the equipotential of the multipole-cylindrical field and is applied with the deflecting potential .

The shape of the outer electrode is of interest. It has a profile that follows one of the equipotential surfaces of the cylindrical multipole, as shown in Fig. 2.1. Aperture windows are provided in the cylindrical electrode to allow the charged particle beam to enter and exit the mirror field region.

The special feature of the multipole-cylindrical field (5) is its uniqueness as circular multipoles of different orders have distinct impacts on the electron-optical properties of the energy analyzer [20]:

– The first-order angular focusing conditions, such as linear energy dispersion and magnification, are determined by the quadrupole component in (5);

– The second-order angular aberrations are affected by the hexapole component in addition to the quadrupole component;

– The characteristics starting from the third order are influenced by the octupole component and so on.

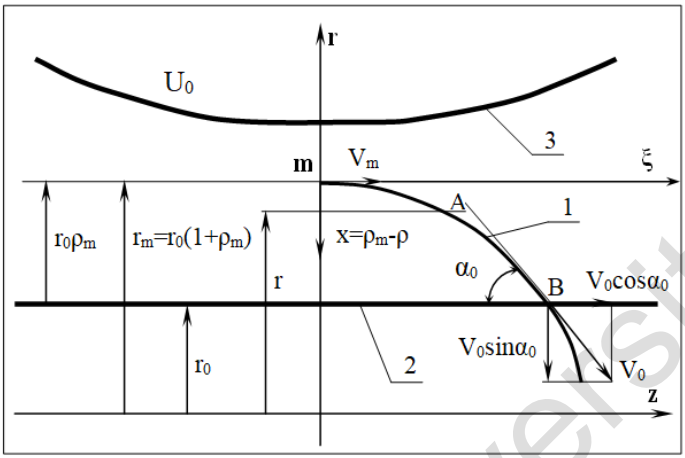

1 – The trajectory of charged particles, 2 - cylindrical electrode under zero potential, 3 – outer deflecting electrode

Fig. 2.1. Electron-optical scheme of an energy analyzer based on MCF

The multipole approach solves the problem of synthesizing an analyzing field with a circular basic orbit very simply: first, the electron-optical characteristics of various orders are specified, then the weight coefficients *q, s, w,* etc. are calculated, then the multipole-cylindrical field (5), which determines the required potential distribution in the entire space, is synthesized. Calculation of the field equipotentials and finding the profile of deflecting electrodes on the basis of the multipole-cylindrical field is reduced to solving an algebraic equation.

2.2 Calculation and analysis of equipotential portraits of the electrostatic octupole-cylindrical fields to determining the electrode configuration of the mirror-type energy analyzer

The calculation and analysis of equipotential portraits are an important step in determining the electrode configuration of an electrostatic octupole-cylindrical field, which can be used as a mirror analyzer for charged particles. By analyzing the equipotential

portraits, one can determine the optimal shape of the electrodes and adjust the parameters of the field to achieve the desired electron-optical characteristics.

The equipotential portraits of an octupole-cylindrical field can be calculated using numerical simulation techniques such as finite element analysis or boundary element method. The resulting equipotential portraits provide a visual representation of the electric field distribution in the space between the electrodes and can be used to identify regions of high and low potential gradients.

Based on the equipotential portraits, the electrode configuration of the mirror analyzer can be optimized to achieve high energy resolution and angular focusing quality. The octupole component of the field can be used to correct higher-order angular aberrations, while the quadrupole component provides first-order angular focusing. By adjusting the strengths of these components, the electron-optical characteristics of the mirror analyzer can be optimized for a particular application.

The primary focus of the study is an electrostatic energy analyzer with axial symmetry, which utilizes a circular octupole.

The potential of the cylindrical octupole field can be expressed in the r, z coordinate system using the following equation:

$$U(r,z) = \mu \ln r + \omega U_{oct}(r,z) \qquad (2.6)$$

where *lnr* is the cylindrical field potential,

μ is the coefficient specifying the weight contribution of the cylindrical field *lnr (*this coefficient determines the relative contribution of the cylindrical field to the overall potential of the octupole-cylindrical field),

U_{oct} is the circular octupole potential of the first type,

ω is the weight contribution of the circular octupole.

Below are the distribution functions of the circular octupole $U_{oct}(\rho,\xi)$ constructed using the summation symmetry rule:

$$U_{oct}(\rho,\xi)=\frac{1}{4!}\xi^4+\frac{1}{2}\xi^2\left\{\frac{1}{4}\left[1-(1+\rho)^2\right]+\frac{1}{2}\ln(1+\rho)\right\}+$$
$$+\frac{1}{64}(1+\rho)^4+\frac{1}{16}(1+\rho)^2-\frac{1}{8}\ln(1+\rho)\left[\frac{1}{2}+(1+\rho)^2\right]-\frac{5}{64} \quad (2.7)$$

$$U'_{oct}(\rho,\xi)=\frac{1}{5!}\xi^5+\frac{1}{3!}\xi^3\left\{\frac{1}{4}\left[1-(1+\rho)^2\right]+\frac{1}{2}\ln(1+\rho)\right\}+$$
$$+\frac{1}{64}\xi\left\{(1+\rho)^4+4(1+\rho)^2-8\ln(1+\rho)\left[\frac{1}{2}+(1+\rho)^2\right]-5\right\} \quad (2.8)$$

The field expressed in equation (7) is referred to as a component of a circular octupole with cylindrical symmetry plane. For this field $U_{oct}(\rho,-\xi)=U_{oct}(\rho,\xi)$. The field (8) is referred to as the component of a cylindrical circular octupole with an antisymmetry plane. This field fulfills the antisymmetry condition in relation to the plane $\xi=0$:

$$U'_{oct}(\rho,-\xi)=-U'_{oct}(\rho,\xi).$$

By expanding equations (7) and (8) as series in powers of ρ and ξ around the axial circle $\rho=0$, $\xi=0$ and selecting the terms with the lowest powers, we obtain:

$$U_{oct}(\rho,\xi)\sim\xi^4-6\xi^2\rho^2+\rho^4 \quad (2.9)$$

$$U'_{oct}(\rho,\xi)\sim\xi\left(\frac{1}{5}\xi^4-2\xi^2\rho^2+\rho^4\right) \quad (2.10)$$

Function (9) can be considered as an octupole in a symmetric representation, which is an analogue of a planar multipole with a straight axis. On the other hand, function (10) can be seen as a component of a planar multipole with a straight axis, but in an antisymmetric representation.

The equipotential family of an axially-symmetric electrostatic octupole-cylindrical field has been calculated and the equipotentials of the and fields are shown in Figure 2.2.

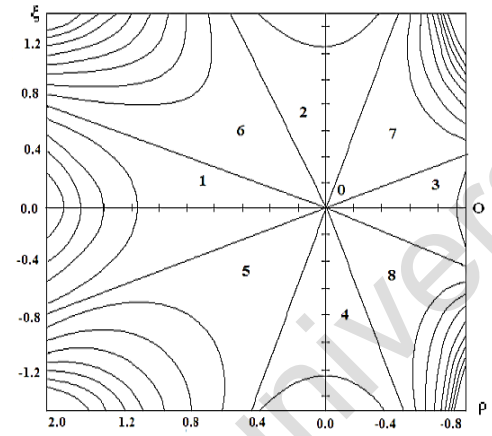

a

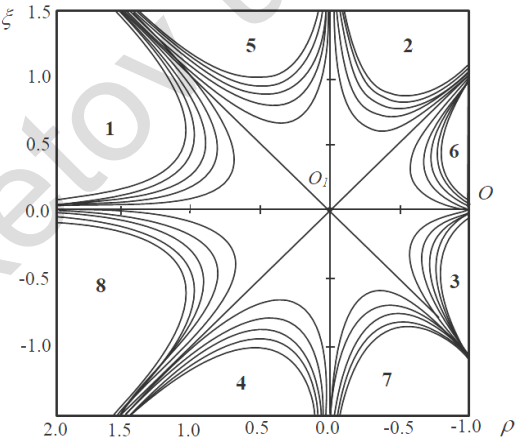

b

Fig. 2.2. Family of equipotentials of a cylindrical octupole with a symmetry plane (a) and an antisymmetry plane(b)

The coordinates $\rho = \xi = \frac{z}{r_0}$ are linear and are counted in the direction of the symmetry axis. In the cross section by the plane ρ, ξ, each of the fields is divided into alternating regions in which the potentials are opposite in sign. These regions are separated by zero-potential lines which are close to rectilinear and converge at the nodal point O ($\rho = \xi = 0$). It follows from Fig. 2.2 a and b that for each type of symmetry with respect to the plane $\xi = 0$, the presented fields are formed by octupole sets of electrodes carrying a sign-variable potential. In Fig. 2.2, regions 1,3,5,7 and 2,4,6,8 are regions with potentials of the opposite sign.

To understand the structure of the octupole and electrostatic cylindrical field superposition, we need to consider how these fields are combined. The central circumference of the octupole is at zero equipotential in the logarithmic field when the fields are added. By analyzing different combinations of the μ and ω coefficients, we can determine which scheme is most promising. This analysis will help in predicting the suitability of different field superpositions [151].

We will focus only on examining the structures of the octupole-cylindrical field that exhibit symmetry with respect to the symmetry plane. Subsequently, we will provide an algorithm for determining the equipotential lines in such fields:

$$U_{oct}(\rho,\xi) = U_0 \left[\begin{array}{l} \frac{1}{4!}\xi^4 + \frac{1}{2}\xi^2 \left\{ \frac{1}{4}\left[1-(1+\rho)^2\right] + \frac{1}{2}\ln(1+\rho) \right\} + \frac{1}{64}(1+\rho)^4 + \\ \frac{1}{16}(1+\rho)^2 - \frac{1}{8}\ln(1+\rho)\left[\frac{1}{2} + (1+\rho)^2\right] - \frac{5}{64} \end{array} \right] = U_0 f_{oct},$$

$$U = U_0 \left[\mu \ln r + f_{oct}\right],$$

$$\frac{U}{U_0} = \mu \ln r + f_{oct},$$

$$-\frac{U}{U_0} + \mu \ln(1+\rho) + f_{oct} = 0,$$

1) $\frac{U}{U_0}$ =0; 0.1; 0.2;...1.

2) We set the values of ρ from 0 ..... 1;

3) We obtain the values of ξ at $R(\xi)=0$;

$$R(\xi)=\frac{-U}{U_0}+\mu\ln(1+\rho)+f_{oct}$$

Given

$R(\xi)=0$

$Find(\xi)\rightarrow$

The figures in 2.3-2.6 show different families of equipotential lines resulting from the superposition of the cylindrical field and circular octupole:

$$U=\mu U_{cyl}+\omega U_{oct} \tag{2.11}$$

where $U_{cyl}=U_0\ln r=U_0\ln(1+\rho)$ is distribution of the cylindrical field;

$$U_{oct}(\rho,\xi)=\frac{1}{4!}\xi^4+\frac{1}{2}\xi^2\left\{\frac{1}{4}\left[1-(1+\rho)^2\right]+\frac{1}{2}\ln(1+\rho)\right\}+$$

$$+\frac{1}{64}(1+\rho)^4+\frac{1}{16}(1+\rho)^2-\frac{1}{8}\ln(1+\rho)\left[\frac{1}{2}+(1+\rho)^2\right]-\frac{5}{64}$$

is octupole distribution.

For the series of Fig. 2.3 (a-f), the values of the coefficient setting the weight contribution of the cylindrical field μ = 0.01; 0.1; 0.25; 0.5; 1; 2 with the weight contribution of the circular octupole ω = 1 being constant. From Figure 2.3, we can observe the gradual changes in the field structure as the coefficient μ, which determines the weight contribution of the cylindrical field, increases. When μ > 0, the vertices are removed along the ρ and ξ axes, leading to the merging of regions 1 and 3, and displacement of regions 5, 6, 7, and 8. As μ increases, the field space is filled with equipotentials similar to those of the logarithmic field lnr. Thus, the field structure transforms

from an octupole to a field that resembles a cylindrical field as the value of μ increases.

The series of figures presented in Fig. 2.4 (a-f) display equipotential fields resulting from the superposition of the cylindrical field and the circular octupole, where the weight contribution of the circular octupole remains constant at a value of ω = 1, but with negative values of the coefficient that specifies the weight contribution of the cylindrical field, i.e., μ = -0.01, -0.1, -0.25, -0.5, -1, and -2.5. When $\mu < 0$, vertices are removed along the ξ axis, which leads to the displacement of regions 2, 4, 5, 6, 7, 8 as the coefficient μ increases. This eventually results in the rearrangement of the equipotential field lines into lines characteristic of a cylindrical field.

The series of Fig. 2.5 (a-f) presents families of equipotentials of the cylindrical field and cylindrical octupole superposition. For this series, the weight contribution of the circular octupole is varied while the weight contribution of the cylindrical field is kept constant at μ = 1. The values of ω are 0.001, 0.1, 0.25, 0.5, 1, and 2.5. As the value of ω decreases, the equipotential lines gradually transform from the characteristic lines of the cylindrical octupole to the symmetric lines typical of the cylindrical field described by the potential lnr.

In the series of Fig. 2.6 (a-f), the equipotential fields are based on the superposition of the cylindrical field and circular octupole with negative values of the weight contribution of the circular octupole ω = - 0.001; - 0.1; - 0.25; - 0.5; - 1; - 2.5 and a constant value of the weight contribution of the cylindrical field μ = 1. As the weight contribution of the circular octupole ω increases, the equipotential lines of the logarithmic field gradually disappear and vertices appear in all regions 1-8.

By analyzing the equipotential portraits of the fields $U(\rho,\xi) = \omega U_{oct}(\rho,\xi) + \mu \ln(1+\rho)$, it has been established that changes in the weight contributions of the cylindrical field and the circular octupole can cause significant transformations in the field.

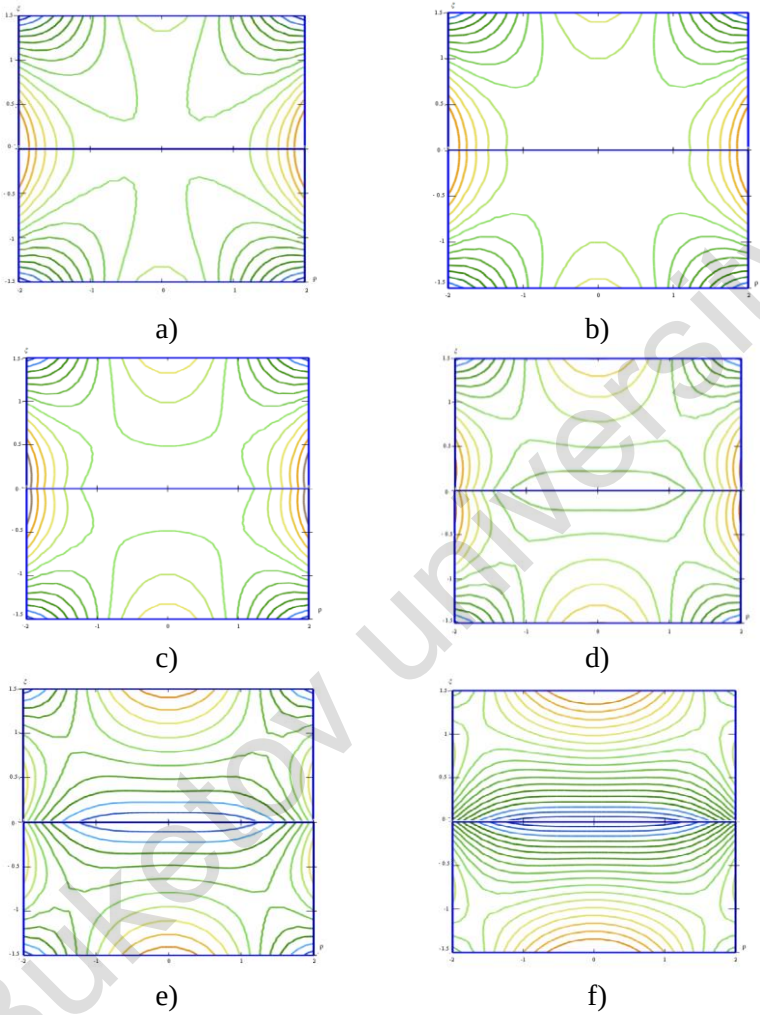

Fig. 2.3. Equipotential fields $U(\rho,\xi)=\omega U_{oct}(\rho,\xi)+\mu\ln(1+\rho)$ at $\omega=1$:

a) μ = 0,01; b) μ=0,1; c) μ=0,25; d) μ = 0,5; e) μ = 1; f) μ = 2

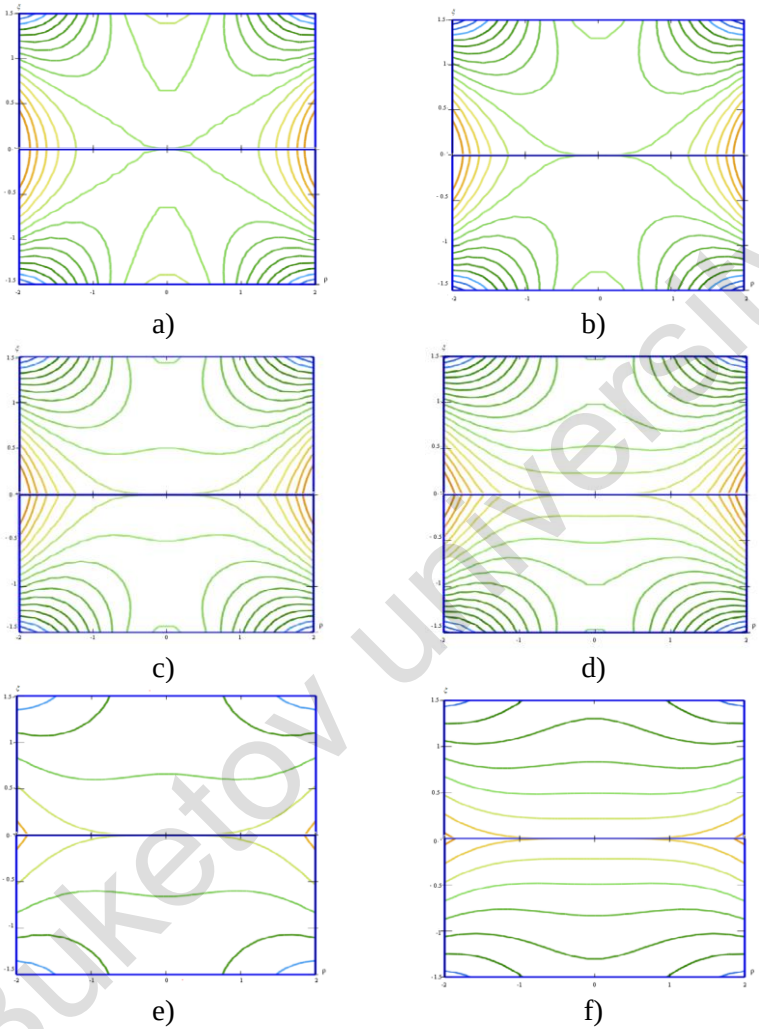

Fig. 2.4. Equipotential fields $U(\rho,\xi)=\omega U_{oct}(\rho,\xi)+\mu\ln(1+\rho)$ at $\omega=1$:
a) μ = - 0,01; b) μ = - 0,1; c) μ = - 0,25; d) μ = - 0,5;
e) μ = - 1; f) μ = - 2,5

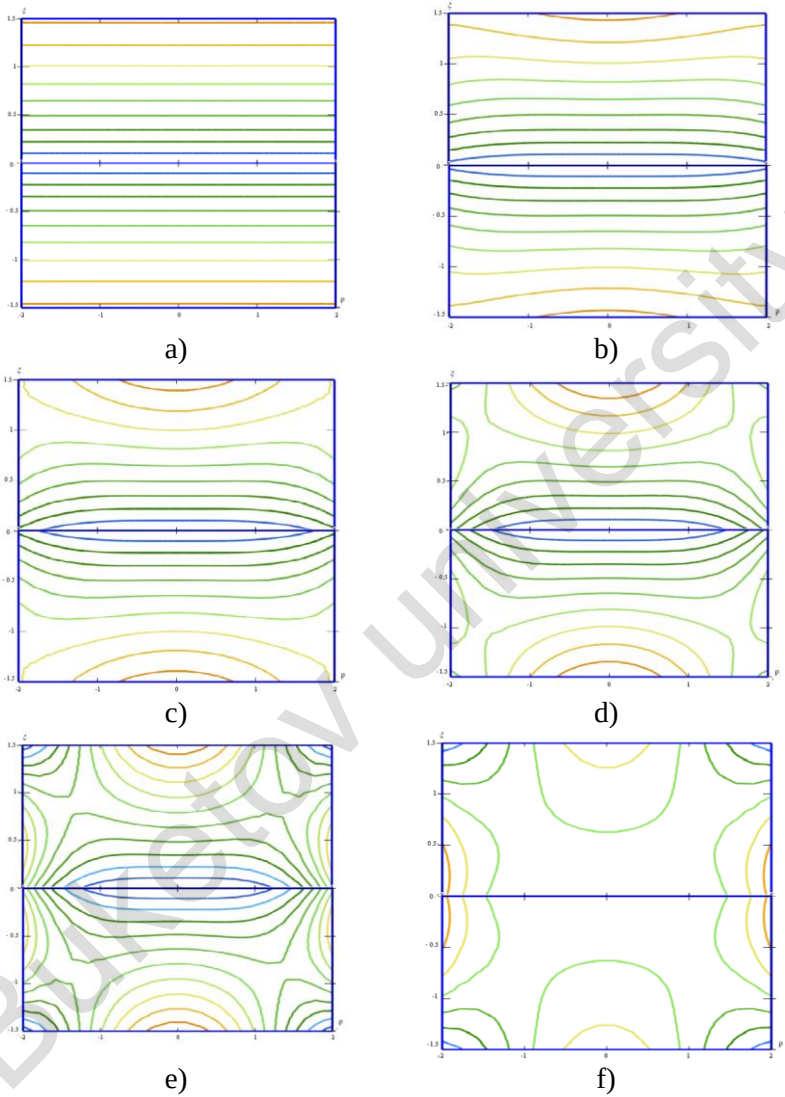

Fig. 2.5. Equipotential fields

$U(\rho,\xi) = \omega U_{oct}(\rho,\xi) + \mu \ln(1+\rho)$ at $\mu = 1$:

a) ω= 0,001; b) ω= 0,1 ; c) ω =0,25; d) ω =0,5; e) ω= 1; f) ω =2,5.

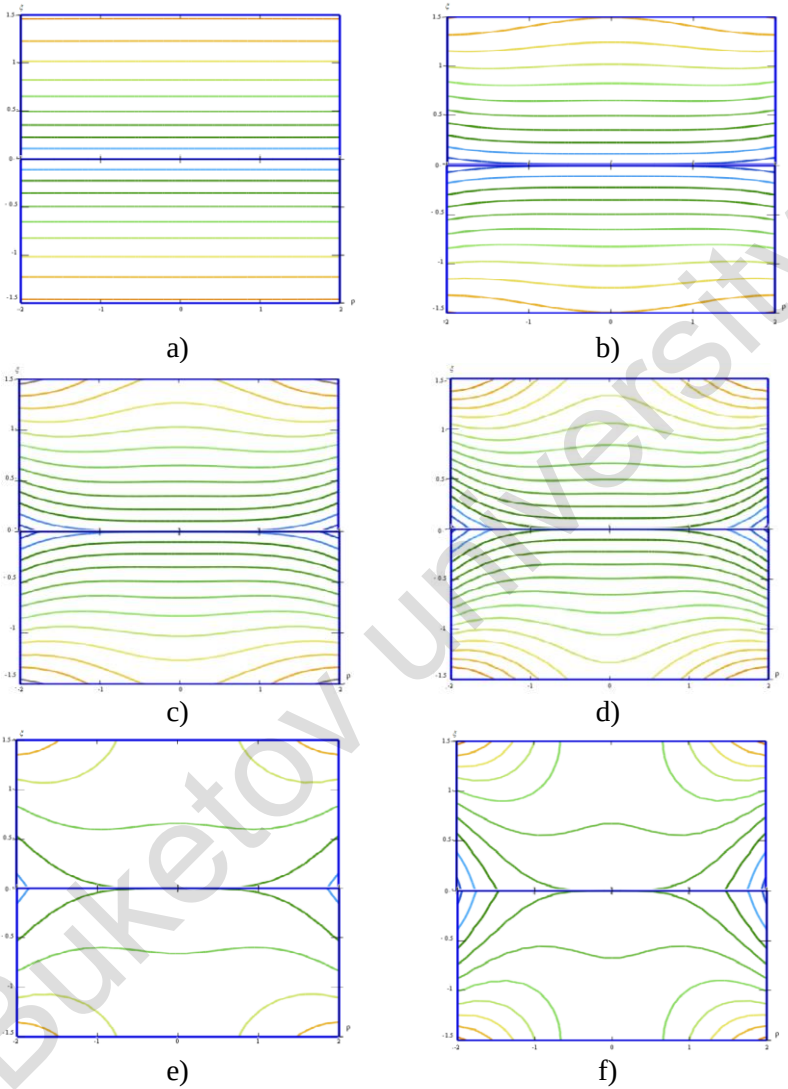

Fig. 2.6. Equipotential fields $U(\rho,\xi)=\omega U_{oct}(\rho,\xi)+\mu\ln(1+\rho)$ at μ = 1:
a) ω= - 0,001; b) ω = - 0,1; c) ω = - 0,25; d) ω =- 0,5; e) ω = - 1; f) ω = - 2,5

The combination of the cylindrical field and circular octupole has practical applications in constructing an electrostatic mirror with axial symmetry. The mirror comprises a cylindrical electrode at zero potential and a deflecting electrode with axial symmetry that coincides with one of the field equipotentials $U(\rho,\xi)=\omega U_{oct}(\rho,\xi)+\mu\ln(1+\rho)$. By creating appropriate aperture windows in the cylindrical electrode, a charged particle beam can be introduced and extracted from the mirror field region. The design of the deflecting electrode is determined by calculating the equipotential lines in the octupole-cylindrical field.

Fig. 2.7 presents an example of the picture of the equipotential field in the three-dimensional Surface Plot coordinate system with the values ω = - 1.5, μ=1.

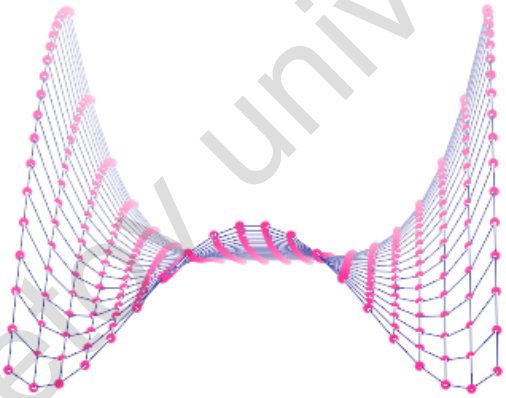

Fig. 2.7. Picture of the equipotential field in the three-dimensional coordinate system at ω = - 1.5, μ=1

3 CALCULATION OF TRAJECTORIES OF CHARGED PARTICLES IN AN AXIALLY-SYMMETRIC ELECTROSTATIC FIELD

3.1 Equations of motion of charged particles in an axially - symmetric electrostatic octupole-cylindrical field

This section proposes a calculation of charged particle trajectories in the electrostatic octupole-cylindrical field (OCF) obtained through the superposition of the fields of a cylindrical mirror and a circular octupole:

$$U(r,z) = \mu \ln r + \omega U_{oct}(r,z) \tag{3.1}$$

where

$$U_{oct}(r,z) = \frac{1}{4!}z^4 + \frac{1}{2}z^2\left\{\frac{1}{4}\left(1-r^2\right)+\frac{1}{2}\ln r\right\}+ \\ +\frac{1}{64}r^4+\frac{1}{16}r^2-\frac{1}{8}\ln r\left[\frac{1}{2}+r^2\right]-\frac{5}{64} \tag{3.2}$$

is circular octupole, μ is the coefficient specifying the weight contribution of the cylindrical field , ω is the weight component of the circular octupole.

When analyzing the motion of a charged particle in an octupole-cylindrical field, it is necessary to calculate its trajectory. To perform this calculation, the reference point of the trajectory is shifted to the vertex **m**, and the origin of coordinates *x, ξ* is placed at the same point (as shown in Figure 1). All linear dimensions are then expressed in terms of the radius r_o of the inner cylindrical electrode.

$$\frac{r}{r_0} = \frac{r_0 + r_0\,\rho}{r_0} = 1+\rho, \qquad x = \frac{r_m - r}{r_0} = \rho_m - \rho, \qquad \xi = \frac{z}{r_0} \tag{3.3}$$

The expression for the distribution of the octupole-cylindrical field (3.1) in the transformed coordinates **x,ξ** (for any μ and ω) is given by equation (3.4).

$$U(x,\xi)=U_0 g(x,\xi)=U_0 g_x \tag{3.4}$$

where

$$g(x,\xi)=g_x=\mu\ln(R-x)+\omega\left[\frac{1}{4!}\xi^4+\frac{1}{2}\xi^2\left\{\frac{1}{4}\left[1-(R-x)^2\right]+\frac{1}{2}\ln(R-x)\right\}+\right.$$
$$\left.+\frac{1}{64}(R-x)^4+\frac{1}{16}(R-x)^2-\frac{1}{8}\ln(R-x)\left[\frac{1}{2}+(R-x)^2\right]-\frac{5}{64}\right], \tag{3.5}$$
$$R=1+\rho_m$$

Let us examine the trajectory of a charged particle in an octupole-cylindrical field for the specific values of the cylindrical field and octupole weight contributions, namely μ = 1 and ω = 1. In this case, the potential can be expressed in the coordinate system as follows:

$$U(x,\xi)=U_0 g(x,\xi)=U_0 g_x \tag{3.6}$$

where

$$g(x,\xi)=g_x=\ln(R-x)-\frac{1}{4!}\xi^4-\frac{1}{2}\xi^2\left\{\frac{1}{4}\left[1-(R-x)^2\right]+\frac{1}{2}\ln(R-x)\right\}+$$
$$-\frac{1}{64}(R-x)^4-\frac{1}{16}(R-x)^2+\frac{1}{8}\ln(R-x)\left[\frac{1}{2}+(R-x)^2\right]+\frac{5}{64}, \tag{3.7}$$

The system of equations that describes the motion of a charged particle in the axially-symmetric octupole-cylindrical field (3.6) is as follows:

$$m\ddot{x}=qU_0\varepsilon_1,\qquad \varepsilon_1=-\frac{\partial g(x,\xi)}{\partial x}, \tag{3.8a}$$

$$m\ddot{\xi}=qU_0\varepsilon_2,\qquad \varepsilon_2=-\frac{\partial g(x,\xi)}{\partial \xi}. \tag{3.8b}$$

The conservation of energy law in the static potential field states that the variation of the kinetic energy of a charged particle is equivalent to the potential difference it undergoes. By integrating

equations (3.8a) and (2.8b) along the particle's trajectory from the vertex **m** to any arbitrary point, we obtain the conservation of energy law for a charged particle moving in the electrostatic octupole-cylindrical field, which relates the kinetic energy variation to the potential difference:

$$\frac{m\upsilon_m^2}{2}-\frac{m}{2}\left(\dot{x}^2+\dot{\xi}^2\right)=-q\left(U_m-U\left(x,\xi\right)\right)=-qU_0\left(g_0-g_x\right) \qquad (3.9)$$

where $U_m=U_0g\left(x_m,\xi_m\right)=U_0g_0$ is the field potential at point **m**, with $x_m=\xi_m=0$, $g_x=g\left(x,\xi\left(x\right)\right)$; $g_0=g\left(x,\xi\right)\big|_{\substack{x=0\\ \xi=0}}$.

We determine the value from equation (3.8b) by integrating it within the range from **m** to an arbitrary point of the trajectory, taking into account that $\upsilon_m^2=\dot{\xi}_m^2+\dot{x}_m^2=\dot{\xi}_m^2$, since at the top of the trajectory $\dot{x}_m=0$, and using the relation $\dot{\xi}=\frac{d\xi}{dt}=\frac{d\xi}{dx}\frac{dx}{dt}=\xi'\dot{x}$, we obtain

$$\frac{m\upsilon_m^2}{2}-\frac{m\dot{\xi}^2}{2}=qU_0\int_x^{x_m}\frac{\partial g\left(x,\xi\right)}{\partial\xi}\frac{d\xi}{dx}dx=qU_0\int_0^{x}\frac{\partial g\left(x,\xi\right)}{\partial\xi}\xi'dx \quad . (3.10)$$

According to Fig. 2.1, when $x=\rho_m$, $\frac{m\dot{\xi}^2}{2}=\frac{m\upsilon_0^2}{2}=W\cos^2\alpha_0$, therefore equation (3.10) can be rewritten relative to $\frac{m\upsilon_m^2}{2}$ the following:

$$\frac{m\upsilon_m^2}{2}=W\cos^2\alpha_0+qU_0f_m, \qquad (3.11)$$

where

$$f_m=\int_0^{\rho_m}\frac{\partial g\left(x,\xi\right)}{\partial\xi}\xi'd\xi. \qquad (3.123)$$

3.2 The integro-differential equation of trajectories in an electrostatic octupole-cylindrical field

Substituting equations (3.11) and (3.12) into equation (3.10), we obtain an integro-differential equation of motion of a charged particle in an octupole-cylindrical field (3.6):

$$\left(\xi'\right)^2\left[g_0 - g_x + f_x\right] = P^2\mathrm{ctg}^2\alpha_0 + f_m - f_x\,, \tag{3.13}$$

$$\left(\xi'\right)^2 = \frac{P^2\mathrm{ctg}^2\alpha_0 + f_m - f_x}{g_0 - g_x + f_x}\,, \tag{3.14}$$

where

$$f_x = \int_0^x \frac{\partial g\left(x,\xi\right)}{\partial \xi}\xi' dx \tag{3.15}$$

and $P_0^2 = \dfrac{W}{qU_0}\sin^2\alpha_0$ is the reflection parameter that relates the geometric properties and energy parameters of the octupole-cylindrical field.

The solution of the integro-differential equation (3.13) is found by using a power series expansion with unknown coefficients. These coefficients are calculated by substituting the power series into equation (3.13). However, it should be noted that equation (3.13) has a singular point at *x=0* since the multiplier $\left(\xi'\right)^2$ is zero in this case. To overcome this, the method of decomposing the solution of the equation for ξ into a fractional power series is used for integration.

$$\xi = \sqrt{x}\sum_{n=0}^{\infty} C_n x^n\,. \tag{3.16}$$

or

$$\xi = \sqrt{x}\left(C_0 + C_1 x + C_2 x^2 + C_3 x^3 + C_4 x^4 + C_5 x^5 + C_6 x^6 + ...\right)\,. \tag{3.17}$$

Let us decompose all the functions in equation (3.13) into power series using the expression ξ and its derivative.

$$\xi' = \frac{d\xi}{dx} = \frac{1}{2}x^{-1/2}\sum_{n=0}^{\infty} C_n x^n + \sqrt{x}\sum_{n=1}^{\infty} nC_n x^{n-1}. \qquad (3.18)$$

Find

$$\frac{d\xi}{dx} = \frac{C_0 + C_1 x + C_2 x^2 + C_3 x^3 + C_4 x^4 + C_5 x^5 + C_6 x^6}{2\sqrt{x}} + \\ + \sqrt{x}\left(C_1 + 2C_2 x + 3C_3 x^2 + 4C_4 x^3 + 5C_5 x^4 + 6C_6 x^5\right) \qquad (3.19)$$

Calculate

$$\left(\frac{d\xi}{dx}\right)^2 = \frac{1}{4x}\left(\sum_{n=0}^{\infty} C_n x^n\right)^2 + \left(\sum_{n=0}^{\infty} C_n x^n\right)\left(\sum_{n=1}^{\infty} nC_n x^{n-1}\right) + \left(\sum_{n=1}^{\infty} nC_n x^{n-1}\right)^2 \qquad (3.20)$$

$$\left(\frac{d\xi}{dx}\right)^2 = \frac{C_0^2}{4} + \left(\frac{3C_0C_1}{2}\right)x + \left(\frac{9C_1^2}{4} + \frac{5C_0C_2}{2}\right)x^2 + \left(\frac{7C_0C_3}{2} + \frac{15C_1C_2}{2}\right)x^3 + \\ + \left(\frac{25C_2^2}{4} + \frac{9C_0C_4}{2} + \frac{21C_1C_3}{2}\right)x^4 + \left(\frac{11C_0C_5}{2} + \frac{27C_1C_4}{2} + \frac{35C_2C_3}{2}\right)x^5 + \\ + \left(\frac{49C_3^2}{4} + \frac{13C_0C_6}{2} + \frac{33C_1C_5}{2} + \frac{45C_2C_4}{2}\right)x^6 \qquad (3.21)$$

$$\left(\frac{d\xi}{dx}\right)^2 = h_0 + h_1 x + h_2 x^2 + h_3 x^3 + h_4 x^4 + h_5 x^5 + h_6 x^6 \qquad (3.21a)$$

The radial component of the turning point $R = 1 + \rho_m$ of the trajectory, which is required to calculate the value of ξ, can be obtained by using the trajectory integral-differential equation (3.8) for the point $x = \rho_m$. In this case:

$$(\xi')^2 = \operatorname{ctg}^2\alpha_0, \quad g_{x=\rho_m} = 0$$

and

$$g_0 + f_m = P^2,$$

Substituting from equation (3.3) into (3.16) we arrive at the expression

$$\ln R = \frac{8\left(P^2 - f_m\right) + \frac{1}{8}R^4 + \frac{1}{2}R^2 - \frac{5}{8}}{\left(\frac{17}{2} + R^2\right)}.$$

The method of successive approximations is used to determine the value of R from the this equation, where the previous approximation is used to calculate the next approximation. As the initial approximation, the parameters of CMA are used.

$$R_0 = \exp\left(P^2\right) = 1 + P^2 + \frac{1}{2}P^4 + \frac{1}{6}P^6 + \frac{1}{24}P^8 + \ldots \quad \text{and} \quad f_{m_0} = 0.$$

Thus, the equation for determining ρ_m:

$$\rho_m = \exp\left[\frac{8\left(P^2 - f_m\right) + \frac{1}{8}R^4 + \frac{1}{2}R^2 - \frac{5}{8}}{\left(\frac{17}{2} + R^2\right)} - 1\right],$$

If you decompose $lnR = \ln\left(1 + \rho_m\right)$ in series by ρ_m, you can use another equation:

$$\ln R = \ln\left(1 + \rho_m\right) = \rho_m - \frac{\rho_m^2}{2} + \frac{\rho_m^3}{3} - \frac{\rho_m^4}{4} + \frac{\rho_m^5}{5} - \frac{\rho_m^6}{6} \ldots$$

Calculation scheme: using zero approximation, we determine the coefficients C_n, then we find the radial coordinate of the trajectory rotation point R_1 in the first approximation from equation (3.16) by successive approximations, then we determine the coefficients C_n and f_m the value R_2 in the first approximation using the first approximation data, and so on.

Let us write down some expansions necessary for further calculations:

$$\xi^2 = \left(\sqrt{x}\sum_{n=0}^{\infty} C_n x^n\right)^2 = C_0^2 x + 2C_0C_1x^2 + \left(C_1^2 + 2C_0C_2\right)x^3 + 2\left(C_0C_3 + C_1C_2\right)x^4 + \\ + \left(C_2^2 + 2C_0C_4 + 2C_1C_3\right)x^5 + 2\left(C_0C_5 + C_1C_4 + C_2C_3\right)x^6 + \ldots \quad (3.22)$$

$$\xi^4 = \left(\sqrt{x}\sum_{n=0}^{\infty} C_n x^n\right)^4 = C_0^4 x^2 + \\ + \left(4C_0^3C_1\right)x^3 + \left(6C_0^2C_1^2 + 4C_0^3C_2\right)x^4 + \\ + \left(4C_0C_1^3 + 4C_0^3C_3 + 12C_0^2C_1C_2\right)x^5 + \\ + \left(C_1^4 + 6C_0^2C_2^2 + 4C_0^3C_4 + 12C_0C_1^2C_2 + 12C_0^2C_1C_3\right)x^6 + \ldots \quad , \quad (3.23)$$

$$\rho = \rho_m - x \ , \quad \rho + \frac{\rho^2}{2} = \rho_m\left(1 + \frac{\rho_m}{2}\right) - \left(1 + \rho_m\right)x + \frac{x^2}{2} \ , \quad (3.24)$$

$$\ln\left(1+\rho\right) = \ln\left(1+\rho_m\right) + \ln\left(1 - \frac{x}{1+\rho_m}\right) = \ln\left(1+\rho_m\right) - \frac{x}{1+\rho_m} - \frac{x^2}{2\left(1+\rho_m\right)^2} - \\ - \frac{x^3}{3\left(1+\rho_m\right)^3} - \frac{x^4}{4\left(1+\rho_m\right)^4} - \frac{x^5}{5\left(1+\rho_m\right)^5} - \frac{x^6}{6\left(1+\rho_m\right)^6} - \ldots \quad . \quad (3.25)$$

Convert expression (3.7) using R=1+ρ:

$$g\left(x,\xi\right) = g_x = \ln\left(1+\rho\right) - \frac{1}{4!}\xi^4 - \frac{1}{2}\xi^2\left\{\frac{1}{4}\left[1 - \left(1+\rho\right)^2\right] + \frac{1}{2}\ln\left(1+\rho\right)\right\} - \\ - \frac{1}{64}\left(1+\rho\right)^4 - \frac{1}{16}\left(1+\rho\right)^2 + \frac{1}{8}\ln\left(1+\rho\right)\left[\frac{1}{2} + \left(1+\rho\right)^2\right] + \frac{5}{64} \quad (3.26)$$

Using formulas (3.23), (3.24), and (3.25), transform the bracketed expression in formula (3.26) to the following form

$$\xi^2\left\{\frac{1}{4}\left[1-(1+\rho)^2\right]\right\}=\xi^2\left\{-\frac{1}{2}\left[\rho+\frac{\rho^2}{2}\right]\right\}=\left(-\frac{1}{4}{\rho_m}^2C_0^2-\rho_mC_0^2\right)x+$$
$$+\left(\frac{1}{2}C_0^2+\frac{1}{2}\rho_mC_0^2-\frac{1}{2}{\rho_m}^2C_0C_1-\rho_mC_0C_1\right)x^2+$$
$$+\left(-\frac{1}{4}C_0^2-\frac{1}{2}\rho_mC_1^2+C_0C_1-\frac{1}{4}{\rho_m}^2C_1^2-\frac{1}{2}{\rho_m}^2C_0C_2+C_0C_1\rho_m-\rho_mC_0C_2\right)x^3+$$
$$+\left(\frac{1}{2}C_1^2+\frac{1}{2}\rho_mC_1^2-\frac{1}{2}C_0C_1+C_0C_2-\frac{1}{2}{\rho_m}^2C_0C_3-\frac{1}{2}{\rho_m}^2C_1C_2-\rho_mC_0C_2-\rho_mC_0C_3-C_1C_2\rho_m\right)x^4+$$
$$\left(\begin{array}{l}-\frac{1}{2}C_0C_2-\frac{1}{4}C_1^2--\frac{1}{2}\rho_mC_2^2+C_0C_3+C_1C_2-\frac{1}{4}{\rho_m}^2C_2^2-\frac{1}{2}{\rho_m}^2C_0C_4-\frac{1}{2}{\rho_m}^2C_1C_3+\rho_mC_0C_3+\\+C_1C_2\rho_m-\rho_mC_0C_4-\rho_mC_1C_3\end{array}\right)x^5+$$
$$+\left(\begin{array}{l}\frac{1}{2}C_2^2+\frac{1}{2}\rho_mC_2^2-\frac{1}{2}C_0C_3-\frac{1}{2}C_1C_2+C_0C_4+C_1C_3-\frac{1}{2}{\rho_m}^2C_0C_5-\frac{1}{2}{\rho_m}^2C_1C_4-\frac{1}{2}{\rho_m}^2C_2C_3+\\+\rho_mC_0C_4+\rho_mC_1C_3-\rho_mC_0C_5-\rho_mC_1C_4-\rho_mC_2C_3\end{array}\right)x^6$$

(3.27)

$$\xi^2\left\{\frac{1}{2}\ln(1+\rho_m)\right\}=\left(\frac{1}{2}C_0^2\ln(1+\rho_m)\right)x+\left(C_0C_1\ln(1+\rho_m)-\frac{1}{2}\frac{C_0^2}{(1+\rho_m)}\right)x^2+$$
$$+\left(C_0C_2\ln(1+\rho_m)+\frac{1}{2}C_1^2\ln(1+\rho_m)-\frac{1}{2}\frac{C_0^2}{(1+\rho_m)^2}-\frac{C_0C_1}{(1+\rho_m)}\right)x^3+$$
$$+\left(C_0C_3\ln(1+\rho_m)+C_1C_2\ln(1+\rho_m)-\frac{1}{2}\frac{C_1^2}{(1+\rho_m)}-\frac{1}{2}\frac{C_0^2}{(1+\rho_m)^3}-\frac{C_0C_1}{(1+\rho_m)^2}-\frac{C_0C_2}{(1+\rho_m)}\right)x^4+$$
$$+\left(\begin{array}{l}\frac{1}{2}C_2^2\ln(1+\rho_m)+C_0C_4\ln(1+\rho_m)+C_1C_3\ln(1+\rho_m)-\frac{C_0C_3}{(1+\rho_m)}-\frac{C_1C_2}{(1+\rho_m)}+\\+\frac{1}{2}\frac{C_0^2}{(1+\rho_m)^4}\frac{1}{2}\frac{C_1^2}{(1+\rho_m)^2}-\frac{C_0C_2}{(1+\rho_m)^2}-\frac{C_0C_1}{(1+\rho_m)^3}\end{array}\right)x^5+$$
$$+\left(\begin{array}{l}C_0C_5\ln(1+\rho_m)+C_1C_4\ln(1+\rho_m)+C_2C_3\ln(1+\rho_m)-\frac{1}{2}\frac{C_2^2}{(1+\rho_m)}-\frac{C_0C_4}{(1+\rho_m)}-\\-\frac{C_1C_3}{(1+\rho_m)}-\frac{1}{2}\frac{C_0^2}{(1+\rho_m)^5}-\frac{1}{2}\frac{C_1^2}{(1+\rho_m)^3}-\frac{C_0C_3}{(1+\rho_m)^2}-\frac{C_1C_2}{(1+\rho_m)^2}-\frac{C_0C_2}{(1+\rho_m)^3}-\frac{C_0C_1}{(1+\rho_m)^4}\end{array}\right)x^6$$

(3.28)

Substituting expressions (3.24), (3.25), (3.27) and (3.28) in (3.26), we obtain the following:

$$g(x)=-\frac{3}{16}\rho_m-\frac{5}{32}\rho_m^2-\frac{1}{16}\rho_m^3-\frac{1}{64}\rho_m^4+\ln(1+\rho_m)\left(\frac{19}{16}+\frac{1}{4}\rho_m+\frac{1}{8}\rho_m^2\right)+$$

$$+\left(\begin{array}{l}\frac{3}{16}+\frac{5}{16}\rho_m+\frac{3}{16}\rho_m^2+\frac{1}{16}\rho_m^3+\frac{C_0^2}{2}\rho_m\left(1+\rho_m\right)-\\-\frac{19}{16\left(1+\rho_m\right)}-\frac{\rho_m^2}{8\left(1+\rho_m\right)}-\frac{2\rho_m}{8\left(1+\rho_m\right)}-\frac{1}{4}\left(1+\rho_m\right)\times\ln\left(1+\rho_m\right)\end{array}\right)x$$

$$+\left[\begin{array}{l}\frac{3}{32}-\frac{C_0^2}{2}-\frac{\rho_m C_0^2}{2}-\frac{C_0^4}{24}-\frac{1}{8}\rho_m-\frac{19}{16\left(1+\rho_m\right)^2}-\frac{1}{8}\ln\left(1+\rho_m\right)-\\-\frac{3\rho_m^2}{32}-\frac{\rho_m}{4\left(1+\rho_m\right)^2}\left(1+\frac{\rho_m}{2}\right)+\rho_m C_0 C_1\left(\frac{\rho_m}{2}+1\right)\end{array}\right]x^2+$$

$$+\left[\begin{array}{l}\frac{1}{16}+\frac{C_0^2}{4}+\frac{1}{4\left(1+\rho_m\right)}\left(1+\frac{1}{2}\right)-\frac{19}{16\left(1+\rho_m\right)^3}+\frac{\rho_m C_1^2}{2}+\frac{\rho_m^2 C_1^2}{4}-\\-\frac{\rho_m}{4\left(1+\rho_m\right)^3}\left(1+\frac{\rho_m}{2}\right)-C_0C_1-\frac{C_0^3C_1}{6}+\frac{\rho_m^2C_0C_2}{2}-\rho_m C_0C_1+\rho_m C_0C_2\end{array}\right]x^3$$

$$+\left[\begin{array}{l}-\frac{1}{64}-\frac{C_1^2}{2}-\rho_m C_0C_2+\rho_m C_0C_3+\rho_m C_1C_2+\frac{1}{2\left(1+\rho_m\right)^2}-\\-\frac{3\rho_m}{8\left(1+\rho_m\right)^4}-\frac{19}{16\left(1+\rho_m\right)^4}-\frac{\rho_m C_1^2}{2}+\\-\frac{C_0^2C_1^2}{4}+\frac{C_0C_1}{2}-C_0C_2-\frac{C_0^3C_2}{6}+\frac{\rho_m^2C_0C_3}{2}+\frac{\rho_m^2C_1C_2}{2}\end{array}\right]x^4+$$

$$\left[\begin{array}{l}\frac{C_1^2}{4}+\frac{1}{8\left(1+\rho_m\right)^3}-\frac{19}{16\left(1+\rho_m\right)^5}-\frac{\rho_m}{4\left(1+\rho_m\right)^5}-\frac{\rho_m^2}{8\left(1+\rho_m\right)^5}+\frac{\rho_m C_2^2}{2}-\\-\frac{1}{2}C_0C_2-C_0C_3-C_1C_2+\frac{\rho_m^2C_2^2}{4}-\frac{C_0C_1^3}{6}-\frac{C_0^3C_3}{6}-\\-\frac{C_0^2C_1C_2}{2}+\frac{\rho_m^2C_0C_4}{2}+\frac{\rho_m^2C_1C_3}{2}-\rho_m C_0C_3-\rho_m C_1C_2+\rho_m C_0C_4+\rho_m C_1C_3\end{array}\right]x^5+$$

$$+\left[\begin{array}{l}-\frac{1}{8\left(1+\rho_m\right)^4}+\frac{1}{4\left(1+\rho_m\right)^5}-\frac{C_2^2}{2}-\frac{C_1^4}{24}-\frac{19}{16\left(1+\rho_m\right)^6}+\frac{\rho_m}{4\left(1+\rho_m\right)^5}-\frac{\rho_m C_2^2}{2}-\\-\frac{\rho_m}{4\left(1+\rho_m\right)^6}-\frac{C_0^2C_2^2}{4}+\frac{C_0C_3}{2}+\frac{C_1C_2}{2}-C_0C_4-C_1C_3-\frac{\rho_m^2}{8\left(1+\rho_m\right)^6}-\frac{C_0^3C_4}{6}-\\-\frac{C_0C_1^2C_2}{2}-\frac{C_0^2C_1C_3}{2}+\frac{\rho_m^2C_0C_5}{2}+\frac{\rho_m^2C_1C_4}{2}+\frac{\rho_m^2C_2C_3}{2}-\rho_m C_0C_4-\rho_m C_1C_3+\\+\rho_m C_0C_5+\rho_m C_1C_4+\rho_m C_2C_3\end{array}\right]x^6$$

(3.29)

$$g\left(x\right)=e_0+e_1x+e_2x^2+e_3x^3+e_4x^4+e_5x^5+e_6x^6+\ldots$$

(3.30)

then

$$g(0)-g(x)=-e_1x-e_2x^2-e_3x^3-e_4x^4-e_5x^5-e_6x^6-\ldots \quad (3.31)$$

Let us return to equation (3.13) and determine the subintegral expression also in the form of a power series on *x*. According to formula (3.7)

$$\frac{\partial g}{\partial \xi}=\xi\left(\frac{1}{2}\left(\rho+\frac{\rho^2}{2}\right)-\ln(1+\rho)\right)-\frac{\xi^3}{6} \quad (3.32)$$

According to (3.17) and (3.18)

$$\xi\xi'=\frac{1}{2}\left(\sum_{n=0}^{\infty}C_nx^n\right)^2+x\left(\sum_{n=0}^{\infty}C_nx^n\right)\left(\sum_{n=1}^{\infty}nC_nx^{n-1}\right), \quad (3.33)$$

or

$$\begin{aligned}\xi\xi'=&C_0^2/2+2C_0C_1x+3\left(C_0C_2+C_1^2/2\right)x^2+4\left(C_0C_3+C_1C_2\right)x^3+\\&+5\left(C_0C_4+C_1C_3+C_2^2/2\right)x^4+6\left(C_0C_5+C_1C_4+C_2C_3\right)x^5+\\&+7\left(C_0C_6+C_1C_5+C_2C_4+C_3^2/2\right)x^6+\ldots\end{aligned} \quad (3.34)$$

According to (3.17), (3.24), (3.25) and (3.34) we have:

$$\begin{aligned}\frac{\partial g}{\partial \xi}\xi'=&\frac{\rho_mC_0^2}{4}\left(1+\frac{\rho_m}{2}\right)-\frac{C_0^2}{16}\ln(1+\rho_m)+\\&+\left(-\frac{C_0^2}{4}-\frac{C_0^4}{12}+\rho_mC_0\left(C_1-\frac{C_0}{4}\right)+\frac{C_0^2}{16(1+\rho_m)}+\frac{\rho^2{}_mC_0C_1}{2}\right)x+\\&+\left(\frac{C_0^2}{8}-\frac{C_0^3C_1}{2}-C_0C_1(1_1+\rho_m)+\frac{3\rho_m}{2}\left(\frac{C_1^2}{2}+C_0C_2\right)\left(1+\frac{\rho_m}{2}\right)++\frac{C_0C_1}{4(1+\rho_m)}+\right.\\&\left.+\frac{C_0^2}{16(1+\rho_m)^2}-\frac{\ln(1+\rho_m)}{4}\left(\frac{3C_1^2}{8}+\frac{3C_0C_2}{2}+C_0C_1\right)\right)x^2+\end{aligned}$$

$$+\left(\begin{array}{l}\dfrac{C_0C_1}{2}-\dfrac{3C_0C_2}{2}-\dfrac{3C_1^2}{4}-C_0^2C_1^2-\dfrac{2C_0^3C_2}{3}+3\left(\dfrac{C_1^2}{2}+C_0C_2\right)\left(\dfrac{1}{8(1+\rho_m)}-\dfrac{\rho_m}{2}\right)+\\ +\dfrac{C_0C_1}{4(1+\rho_m)^2}+\dfrac{C_0^2}{16(1+\rho_m)^3}-\dfrac{\ln(1+\rho_m)}{2}\left(C_0C_3+C_1C_2\right)+\\ +2\rho_m\left(C_0C_3+C_1C_2\right)\left(\dfrac{\rho_m}{2}+1\right)\end{array}\right)x^3+$$

$$+\left(\begin{array}{l}-2C_1C_2-2C_0C_3-C_0^3C_4-\dfrac{3C_0C_2}{4}-\dfrac{5C_0^2C_1C_2}{2}+\dfrac{3C_1^2}{8}-\dfrac{5}{6}\left(C_1^3C_0+C_0^3C_3\right)-2\rho_m\left(C_0C_3+C_1C_2\right)\\ +\dfrac{5\rho_m}{2}\left(C_0C_4+C_1C_3+\dfrac{C_2^2}{2}\right)+\dfrac{5\rho_m^2}{4}\left(\dfrac{C_2^2}{2}+C_0C_4+C_1C_3\right)+\dfrac{1}{2(1+\rho_m)}\left(C_0C_3+C_1C_2\right)\\ +\dfrac{3}{8(1+\rho_m)^2}\left(\dfrac{C_1^2}{2}+C_0C_2\right)+\dfrac{C_0C_1}{4(1+\rho_m)^3}+\dfrac{C_0^2}{16(1+\rho_m)^4}-\dfrac{5\ln(1+\rho_m)}{8}\left(C_0C_4+C_1C_3+\dfrac{C_2^2}{2}\right)\end{array}\right)x^4+$$

$$+\left(\begin{array}{l}C_0C_3+C_1C_2-3\left(C_0C_1^2C_2+C_0^2C_1C_3\right)-\dfrac{1}{2}\left(5C_1C_3+5C_0C_4-3C_0^2C_2^2\right)-\dfrac{5}{4}\left(C_2^2+C_1^4\right)-\\ +5\left(\dfrac{1}{8(1+\rho_m)}-\dfrac{\rho_m}{2}\right)\left(C_0C_4+C_1C_3+\dfrac{C_2^2}{2}\right)++\dfrac{1}{2(1+\rho_m)^2}\left(C_0C_3+C_1C_2\right)\\ +\dfrac{3}{8(1+\rho_m)^3}\left(\dfrac{C_1^2}{2}+C_0C_2\right)+\dfrac{C_0C_1}{4(1+\rho_m)^4}+\dfrac{C_0^2}{16(1+\rho_m)^5}\\ +3\left(\rho_m+\dfrac{\rho_m^2}{2}-\dfrac{1}{4}\ln(1+\rho_m)\right)\left(C_0C_5+C_1C_4+C_2C_3\right)\end{array}\right)x^5+$$

$$+\left(\begin{array}{l}-3\left(C_2C_3+C_1C_4+C_0C_5\right)+\dfrac{5}{4}\left(\dfrac{C_2^2}{2}-C_0C_4+C_1C_3\right)-\dfrac{7}{6}\left(C_1^3C_2+C_0^3C_5\right)\\ -\dfrac{7}{2}\left(C_0C_1C_2^2+C_0C_1^2C_3+C_0^2C_2C_3+C_0^2C_2C_3\right)-3\rho_m\left(C_0C_5+C_1C_4+C_2C_3\right)+\\ +\dfrac{7\rho_m}{2}\left(C_2C_4+C_0C_6+C_1C_5+\dfrac{C_3^2}{2}\right)+\dfrac{\rho_m^2}{4}\left(5C_0C_4+7\left(C_0C_6+C_1C_5+C_2C_4+\dfrac{C_3^2}{2}\right)\right)+\\ +\dfrac{6}{8(1+\rho_m)}\left(C_0C_5+C_1C_4+C_2C_3\right)+\dfrac{5}{8(1+\rho_m)^2}\left(\dfrac{C_2^2}{2}+C_0C_4+C_1C_3\right)+\dfrac{1}{2(1+\rho_m)^3}\left(C_0C_3+C_1C_2\right)\\ +\dfrac{3}{8(1+\rho_m)^4}\left(C_0C_2+\dfrac{C_1^2}{2}\right)+\dfrac{C_0C_1}{4(1+\rho_m)^5}+\dfrac{C_0^2}{16(1+\rho_m)^6}-\dfrac{7}{8}\ln(1+\rho_m)\left(C_0C_6+C_1C_5+\dfrac{C_3^2}{2}+C_2C_4\right)\end{array}\right)x^6$$

(3.35)

$$\frac{\partial g}{\partial \xi}\,\xi' = b_1 + b_2x + b_3x^2 + b_4x^3 + b_5x^4 + b_6x^5 + b_7x^5$$

(3.36)

Then the required integral can be represented in the following form:

$$\int_0^x \frac{\partial g(x,\xi)}{\partial \xi}\xi' dx = b_1 x + \frac{b_2 x^2}{2} + \frac{b_3 x^3}{3} + \frac{b_4 x^4}{4} + \frac{b_5 x^5}{5} + \frac{b_6 x^6}{6} + \ldots \tag{3.37}$$

For convenience, we denote the expression in curly brackets in (3.37) as $\phi(x)$, then

$$\int_0^x \frac{\partial g(x,\xi)}{\partial \xi}\xi' dx = \phi(x) \tag{3.38}$$

According to (3.30) and (3.37) for the expression in the square bracket on the left side of equation (3.13) we have

$$g(0) - g(x) + \int_0^x \frac{\partial g(x,\xi)}{\partial \xi}\xi' dx = (b_1 - e_1)x + \left(\frac{b_2}{2} - e_2\right)x^2 + \left(\frac{b_3}{3} - e_3\right)x^3 + \\ + \left(\frac{b_4}{4} - e_4\right)x^4 + \left(\frac{b_5}{5} - e_5\right)x^5 + \left(\frac{b_6}{6} - e_6\right)x^6 \tag{3.39}$$

Using expressions (3.20) and (3.31), write the left part of equation (3.13)

$$\left(\frac{d\xi}{dx}\right)^2\left[g_0 - g_x + \int_0^x \frac{\partial g(x,\xi)}{\partial \xi}\xi' dx\right] = \\ = h_0[b_1 - e_1]x + \left[h_0\left(\frac{b_2}{2} - e_2\right) + h_1(b_1 - e_1)\right]x^2 + \\ + \left[h_0\left(\frac{b_3}{3} - e_3\right) + h_1\left(\frac{b_2}{2} - e_2\right) + h_2(b_1 - e_1)\right]x^3 \\ + \left[h_0\left(\frac{b_4}{4} - e_4\right) + h_1\left(\frac{b_3}{3} - e_3\right) + h_2\left(\frac{b_2}{2} - e_2\right) + h_3(b_1 - e_1)\right]x^4 + \\ + \left[h_0\left(\frac{b_5}{5} - e_5\right) + h_1\left(\frac{b_4}{4} - e_4\right) + h_2\left(\frac{b_3}{3} - e_3\right) + h_3\left(\frac{b_2}{2} - e_2\right) + h_4(b_1 - e_1)\right]x^5 + \\ + \left(h_0\left(\frac{b_6}{6} - e_0\right) + h_1\left(\frac{b_5}{5} - e_5\right) + h_2\left(\frac{b_4}{4} - e_4\right) + h_3\left(\frac{b_3}{3} - e_3\right) + h_4\left(\frac{b_2}{2} - e_2\right) + h_5(b_1 - e_1)\right)x^6 \tag{3.40}$$

Find the integral of the right-hand side of equation (3.13)

$$\int_0^{\rho_m} \frac{\partial g(x,\xi)}{\partial \xi} \xi' dx = \left\{ b_1 \rho_m + \frac{b_2 {\rho_m}^2}{2} + \frac{b_3 {\rho_m}^3}{3} + \frac{b_4 {\rho_m}^4}{4} + \frac{b_5 {\rho_m}^5}{5} + \frac{b_6 {\rho_m}^6}{6} + \ldots \right\} \tag{3.41}$$

$$\int_x^{\rho_m} \frac{\partial g(x,\xi)}{\partial \xi} \xi' dx = F(\rho_m) \tag{3.42}$$

Where

$$F(\rho_m) = b_1 \rho_m + \frac{b_2 {\rho_m}^2}{2} + \frac{b_3 {\rho_m}^3}{3} + \frac{b_4 {\rho_m}^4}{4} + \frac{b_5 {\rho_m}^5}{5} + \frac{b_6 {\rho_m}^6}{6} + \ldots$$

Now we can write the right side of equation (3.13) as a power series

$$P^2 \mathrm{ctg}^2 \alpha_0 + f_m - f_x = P^2 \mathrm{ctg}^2 \alpha_0 + F(\rho_m) - \\ - \left\{ b_1 x + \frac{b_2 x^2}{2} + \frac{b_3 x^3}{3} + \frac{b_4 x^4}{4} + \frac{b_5 x^5}{5} + \frac{b_6 x^6}{6} + \ldots \right\} - \phi(x) \tag{3.43}$$

To summarize, the equation of motion of a charged particle in the octupole-cylindrical field (3.13) is represented as a power series. Further, by equating the terms with equal powers x in expressions (3.40) and (3.43), we determine the coefficients of series (3.16), which allows us to further analyze the corpuscular-optical parameters of the considered system.

The next step involves solving for the coefficients C_n of the power series expansion (3.16) that determines the trajectories of charged particles in the octupole-cylindrical field. This is done by equating the terms with equal powers in equations (3.40) and (3.43), resulting in a system of equations that can be solved to obtain the values of the coefficients C_n.

$$h_0 (b_1 - e_1) = -b_1 \tag{3.44a}$$

$$h_0 \left(\frac{b_2}{2} - e_2 \right) + h_1 (b_1 - e_1) = -\frac{b_2}{2} \tag{3.44b}$$

$$h_0\left(\frac{b_3}{3}-e_3\right)+h_1\left(\frac{b_2}{2}-e_2\right)+h_2\left(b_1-e_1\right)=\frac{b_3}{3} \qquad (3.44c)$$

$$h_0\left(\frac{b_4}{4}-e_4\right)+h_1\left(\frac{b_3}{3}-e_3\right)+h_2\left(\frac{b_2}{2}-e_2\right)+h_3\left(b_1-e_1\right)=\frac{b_4}{4} \qquad (3.44d)$$

$$h_0\left(\frac{b_5}{5}-e_5\right)+h_1\left(\frac{b_4}{4}-e_4\right)+h_2\left(\frac{b_3}{3}-e_3\right)+h_3\left(\frac{b_2}{2}-e_2\right)+h_4\left(b_1-e_1\right)=\frac{b_5}{5} \qquad (3.44e)$$

$$h_0\left(\frac{b_6}{6}-e_0\right)+h_1\left(\frac{b_5}{5}-e_5\right)+h_2\left(\frac{b_4}{4}-e_4\right)+h_3\left(\frac{b_3}{3}-e_3\right)+h_4\left(\frac{b_2}{2}-e_2\right)+h_5\left(b_1-e_1\right)=\frac{b_6}{6} \qquad (3.44f)$$

Based on the expressions obtained for the coefficients h_i, e_i and b_i,, respectively, we can calculate the coefficients C_n in the power series expansion of the trajectory of charged particles in the investigated octupole-cylindrical field. The problem of determining the trajectories is thus reduced to the calculation of these coefficients.

$$h_0=\frac{C_0^2}{4} \qquad (3.45a)$$

$$h_1=\frac{3C_0C_1}{2} \qquad (3.45b)$$

$$h_2=\frac{9C_1^2}{4}+\frac{5C_0C_2}{2} \qquad (3.45c)$$

$$h_3=\frac{7C_0C_3}{2}+\frac{15C_1C_2}{2} \qquad (3.45d)$$

$$h_4=\frac{25C_2^2}{4}+\frac{9C_0C_4}{2}+\frac{21C_1C_3}{2} \qquad (3.45e)$$

$$h_5=\frac{11C_0C_5}{2}+\frac{27C_1C_4}{2}+\frac{35C_2C_3}{2} \qquad (3.45f)$$

$$h_6=\frac{49C_3^2}{4}+\frac{13C_0C_6}{2}+\frac{33C_1C_5}{2}+\frac{45C_2C_4}{2} \qquad (3.45g)$$

$$e_0 = -\frac{3}{16}\rho_m - \frac{5}{32}\rho_m^2 - \frac{1}{16}\rho_m^3 - \frac{1}{64}\rho_m^4 + \ln(1+\rho_m)\left(\frac{19}{16} + \frac{1}{4}\rho_m + \frac{1}{8}\rho_m^2\right) \tag{3.46a}$$

$$e_1 = \frac{3}{16} + \frac{5}{16}\rho_m + \frac{3}{16}\rho_m^2 + \frac{1}{16}\rho_m^3 + \frac{C_0^2}{2}\rho_m(1+\rho_m) - \\ - \frac{19}{16(1+\rho_m)} - \frac{\rho_m^2}{8(1+\rho_m)} - \frac{2\rho_m}{8(1+\rho_m)} - \frac{1}{4}(1+\rho_m)\times\ln(1+\rho_m) \tag{3.46b}$$

$$e_2 = \frac{3}{32} - \frac{C_0^2}{2} - \frac{\rho_m C_0^2}{2} - \frac{C_0^4}{24} - \frac{1}{8}\rho_m - \frac{19}{16(1+\rho_m)^2} - \frac{1}{8}\ln(1+\rho_m) - \\ - \frac{3\rho_m^2}{32} - \frac{\rho_m}{4(1+\rho_m)^2}\left(1+\frac{\rho_m}{2}\right) + \rho_m C_0 C_1\left(\frac{\rho_m}{2}+1\right) \tag{3.46c}$$

$$e_3 = \frac{1}{16} + \frac{C_0^2}{4} + \frac{1}{4(1+\rho_m)}\left(1+\frac{1}{2}\right) - \frac{19}{16(1+\rho_m)^3} + \frac{\rho_m C_1^2}{2} + \frac{\rho_m^2 C_1^2}{4} - \\ - \frac{\rho_m}{4(1+\rho_m)^3}\left(1+\frac{\rho_m}{2}\right) - C_0 C_1 - \frac{C_0^3 C_1}{6} + \frac{\rho_m^2 C_0 C_2}{2} - \rho_m C_0 C_1 + \rho_m C_0 C_2 \tag{3.46d}$$

$$e_4 = -\frac{1}{64} - \frac{C_1^2}{2} - \rho_m C_0 C_2 + \rho_m C_0 C_3 + \rho_m C_1 C_2 + \frac{1}{2(1+\rho_m)^2} - \\ - \frac{3\rho_m}{8(1+\rho_m)^4} - \frac{19}{16(1+\rho_m)^4} - \frac{\rho_m C_1^2}{2} - \frac{C_0^2 C_1^2}{4} + \\ + \frac{C_0 C_1}{2} - C_0 C_2 - \frac{C_0^3 C_2}{6} + \frac{\rho_m^2 C_0 C_3}{2} + \frac{\rho_m^2 C_1 C_2}{2} \tag{3.46d}$$

$$e_5 = \frac{C_1^2}{4} + \frac{1}{8(1+\rho_m)^3} - \frac{19}{16(1+\rho_m)^5} - \frac{\rho_m}{4(1+\rho_m)^5} - \frac{\rho_m^2}{8(1+\rho_m)^5} + \\ + \frac{\rho_m C_2^2}{2} - \frac{1}{2}C_0C_2 - C_0C_3 - C_1C_2 + \frac{\rho_m^2 C_2^2}{4} - \frac{C_0C_1^3}{6} - \frac{C_0^3C_3}{6} - \\ - \frac{C_0^2C_1C_2}{2} + \frac{\rho_m^2C_0C_4}{2} + \frac{\rho_m^2C_1C_3}{2} - \rho_m C_0C_3 - \rho_m C_1C_2 + \rho_m C_0C_4 + \rho_m C_1C_3 \quad (3.46e)$$

$$e_6 = -\frac{1}{8(1+\rho_m)^4} + \frac{1}{4(1+\rho_m)^5} - \frac{C_2^2}{2} - \frac{C_1^4}{24} - \frac{19}{16(1+\rho_m)^6} + \frac{\rho_m}{4(1+\rho_m)^5} - \frac{\rho_m C_2^2}{2} - \\ - \frac{\rho_m}{4(1+\rho_m)^6} - \frac{C_0^2C_2^2}{4} + \frac{C_0C_3}{2} + \frac{C_1C_2}{2} - C_0C_4 - C_1C_3 - \frac{\rho_m^2}{8(1+\rho_m)^6} - \frac{C_0^3C_4}{6} - \\ - \frac{C_0C_1^2C_2}{2} - \frac{C_0^2C_1C_3}{2} + \frac{\rho_m^2C_0C_5}{2} + \frac{\rho_m^2C_1C_4}{2} + \frac{\rho_m^2C_2C_3}{2} - \rho_m C_0C_4 - \rho_m C_1C_3 + \\ + \rho_m C_0C_5 + \rho_m C_1C_4 + \rho_m C_2C_3 \quad (3.46f)$$

$$b_1 = \frac{\rho_m C_0^2}{4}\left(1 + \frac{\rho_m}{2}\right) - \frac{C_0^2}{16}\ln(1+\rho_m) \quad (3.47a)$$

$$b_2 = -\frac{C_0^2}{4} - \frac{C_0^4}{12} + \rho_m C_0\left(C_1 - \frac{C_0}{4}\right) + \frac{C_0^2}{16(1+\rho_m)} + \frac{\rho^2{}_m C_0C_1}{2} \quad (3.47b)$$

$$b_3 = \frac{C_0^2}{8} - \frac{C_0^3C_1}{2} - C_0C_1(1_1 + \rho_m) + \frac{3\rho_m}{2}\left(\frac{C_1^2}{2} + C_0C_2\right)\left(1 + \frac{\rho_m}{2}\right) + + \frac{C_0C_1}{4(1+\rho_m)} + \\ + \frac{C_0^2}{16(1+\rho_m)^2} - \frac{\ln(1+\rho_m)}{4}\left(\frac{3C_1^2}{8} + \frac{3C_0C_2}{2} + C_0C_1\right) \quad (3.47c)$$

$$b_4 = \frac{C_0C_1}{2} - \frac{3C_0C_2}{2} - \frac{3C_1^2}{4} - C_0^2C_1^2 - \frac{2C_0^3C_2}{3} + 3\left(\frac{C_1^2}{2} + C_0C_2\right)\times$$
$$\times\left(\frac{1}{8(1+\rho_m)} - \frac{\rho_m}{2}\right) + \frac{C_0C_1}{4(1+\rho_m)^2} + \frac{C_0^2}{16(1+\rho_m)^3} - \quad (3.47d)$$
$$-\frac{\ln(1+\rho_m)}{2}\left(C_0C_3 + C_1C_2\right) + 2\rho_m\left(C_0C_3 + C_1C_2\right)\left(\frac{\rho_m}{2} + 1\right)$$

$$b_5 = -2C_1C_2 - 2C_0C_3 - C_0^3C_4 - \frac{3C_0C_2}{4} - \frac{5C_0^2C_1C_2}{2} +$$
$$+\frac{3C_1^2}{8} - \frac{5}{6}\left(C_1^3C_0 + C_0^3C_3\right) - 2\rho_m\left(C_0C_3 + C_1C_2\right) +$$
$$+\frac{5\rho_m}{2}\left(C_0C_4 + C_1C_3 + \frac{C_2^2}{2}\right) + \frac{5\rho_m^2}{4}\left(\frac{C_2^2}{2} + C_0C_4 + C_1C_3\right) + \quad (3.47e)$$
$$+\frac{1}{2(1+\rho_m)}\left(C_0C_3 + C_1C_2\right) + \frac{3}{8(1+\rho_m)^2}\left(\frac{C_1^2}{2} + C_0C_2\right) +$$
$$+\frac{C_0C_1}{4(1+\rho_m)^3} + \frac{C_0^2}{16(1+\rho_m)^4} - \frac{5\ln(1+\rho_m)}{8}\left(C_0C_4 + C_1C_3 + \frac{C_2^2}{2}\right)$$

$$b_6 = C_0C_3 + C_1C_2 - 3\left(C_0C_1^2C_2 + C_0^2C_1C_3\right) -$$
$$-\frac{1}{2}\left(5C_1C_3 + 5C_0C_4 - 3C_0^2C_2^2\right) - \frac{5}{4}\left(C_2^2 + C_1^4\right) -$$
$$+5\left(\frac{1}{8(1+\rho_m)} - \frac{\rho_m}{2}\right)\left(C_0C_4 + C_1C_3 + \frac{C_2^2}{2}\right) + + \frac{1}{2(1+\rho_m)^2}\times \quad (3.47f)$$
$$\times\left(C_0C_3 + C_1C_2\right) + \frac{3}{8(1+\rho_m)^3}\left(\frac{C_1^2}{2} + C_0C_2\right) + \frac{C_0C_1}{4(1+\rho_m)^4} +$$
$$+\frac{C_0^2}{16(1+\rho_m)^5} + 3\left(\rho_m + \frac{\rho_m^2}{2} - \frac{1}{4}\ln(1+\rho_m)\right)\left(C_0C_5 + C_1C_4 + C_2C_3\right)$$

$$b_7 = -3\left(C_2C_3 + C_1C_4 + C_0C_5\right) + \frac{5}{4}\left(\frac{C_2^2}{2} - C_0C_4 + C_1C_3\right) - \frac{7}{6}\left(C_1^3C_2 + C_0^3C_5\right)$$
$$-\frac{7}{2}\left(C_0C_1C_2^2 + C_0C_1^2C_3 + C_0^2C_2C_3 + C_0^2C_2C_3\right) - 3\rho_m\left(C_0C_5 + C_1C_4 + C_2C_3\right) +$$
$$+\frac{7\rho_m}{2}\left(C_2C_4 + C_0C_6 + C_1C_5 + \frac{C_3^2}{2}\right) + \frac{\rho_m^2}{4}\left(5C_0C_4 + 7\left(C_0C_6 + C_1C_5 + C_2C_4 + \frac{C_3^2}{2}\right)\right) +$$
$$+\frac{6}{8\left(1+\rho_m\right)}\left(C_0C_5 + C_1C_4 + C_2C_3\right) + \frac{5}{8\left(1+\rho_m\right)^2}\left(\frac{C_2^2}{2} + C_0C_4 + C_1C_3\right) +$$
$$+\frac{1}{2\left(1+\rho_m\right)^3}\left(C_0C_3 + C_1C_2\right) + \frac{3}{8\left(1+\rho_m\right)^4}\left(C_0C_2 + \frac{C_1^2}{2}\right) + \frac{C_0C_1}{4\left(1+\rho_m\right)^5} +$$
$$+\frac{C_0^2}{16\left(1+\rho_m\right)^6} - \frac{7}{8}\ln(1+\rho_m)\left(C_0C_6 + C_1C_5 + \frac{C_3^2}{2} + C_2C_4\right) \qquad (3.47g)$$

By solving the system of equations (3.45) - (3.47), the coefficients C_n can be determined. This approximate-analytical method provides a highly accurate description of the trajectories of charged particles in the field [152].

4 NUMERICAL MODELING OF THE ELECTRON-OPTICAL SCHEME OF THE ENERGY ANALYZER

4.1 Numerical modeling of the electron-optical scheme of the energy analyzer based on the octupole-cylindrical field

This paragraph explores the energy analyzer model through numerical calculations, focusing on conducting a trajectory analysis of charged particle motion within this electron-optical system.

The CAE "Focus" software was used to perform a numerical simulation of the corpuscular optics system and analyze the trajectories of charged particles in the energy analyzer based on the octupole-cylindrical field [153].

Fig. 4.1 illustrates the equipotential portrait of the octupole-cylindrical field for the weight contributions of a circular octupole $\omega = 1$ and a cylindrical field $\mu = 2$.

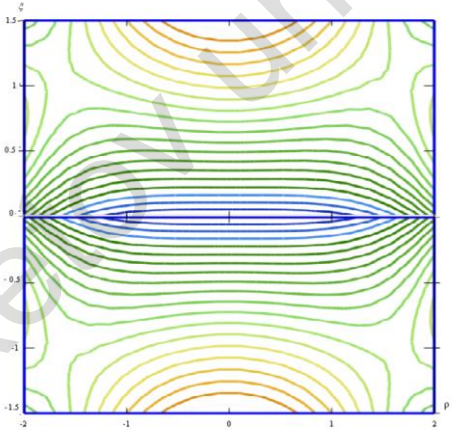

Fig. 4.1. Equipotential field $U(r,z) = \mu \ln r + \omega U_{oct}(r,z)$

Fig. 4.2 illustrates the distribution of the electrostatic field within the energy analyzer which is based on an octupole-cylindrical field configuration. The depicted illustration showcases the upper section of the longitudinal view of the energy analyzer scheme. It demonstrates

the calculation of potential values at grid nodes and the corresponding colorization of the resulting field. Each point is assigned a color based on its potential value, with "warmer" colors indicating higher potentials.

Meanwhile, Fig. 4.3 presents a three-dimensional depiction of the cross-section of the electrostatic octupole-cylindrical field.

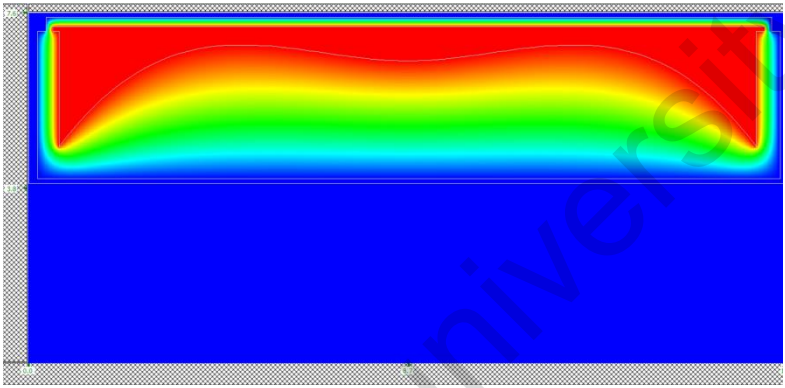

Fig. 4.2. Electrostatic field distribution in the OCF-energy analyzer

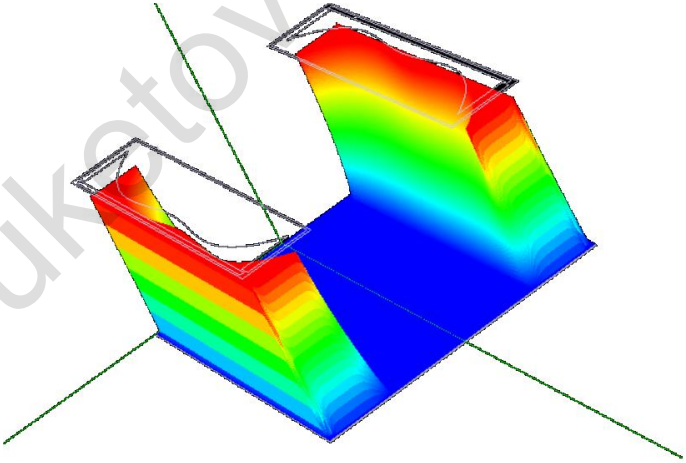

Fig. 4.3. A three-dimensional representation of the field cross-section in the OCF-energy analyzer

Fig. 4.4 shows the electron-optical scheme of the energy analyzer based on the octupole-cylindrical field with ω = 1 and μ = 2. The energy analyzer consists of two coaxial electrodes: the inner electrode *1* has a cylindrical shape with a radius of r_0 and is at zero potential, while the outer electrode *2* has a curvilinear profile and is at a deflecting potential U_0. The electrodes create a field that decelerates and deflects charged particles and behave like an electrostatic mirror. The profile of the outer electrode *2* follows the equipotential surface of the electrostatic octupole-cylindrical field.

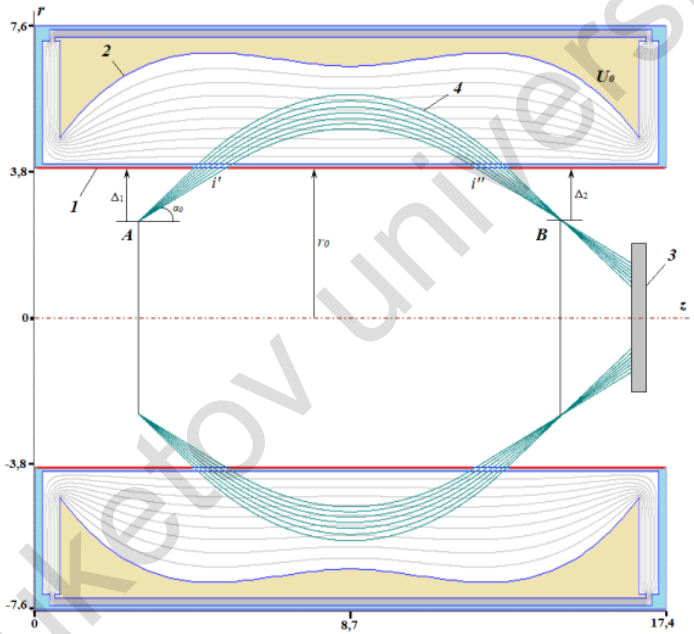

1 - inner grounded cylindrical electrode, 2 - outer deflecting electrode, 3 - a position-sensitive detector, 4 - charged particle beam, A - ring source of charged particles, B - ring image,
i' - entrance ring slit, *i''* - exit ring slit.

Fig. 4.4. The electron-optical scheme of the energy analyzer

The range of initial entering angles of particles into the analyzer is 30-42°. The ratio of the kinetic energy of the charged particle to the potential of the outer electrode is E/U=1.61E[eV]/U[V]=1.61. The position of the source in the coordinate system is x = 2.85; y = 2.5. The potential of the outer cylindrical electrode is 1. The units used for all dimensions are conventional.

The energy analyzer scheme involves the charged particle beam being emitted from the ring source *A*, passing through the entrance slit *i'*, entering the analyzer field, being reflected by the field, returning to the zero potential region through the exit slit *i''*, and then being focused into the ring image *B*. Finally, the particles are detected by a position-sensitive detector *3*. The curvilinear profile of the outer electrode *2* enables the scheme to achieve a sharp 3rd-order angular focusing of charged particles around 36° with a divergence angle of $\Delta\alpha = \pm 6°$.

Fig.4.5 shows the dependence of the particle arrival point (to the point) on the entrance angle α. It follows from Fig. 4.5 that the optimum range of particle entrance angles is the range of angles from 30-42 degrees, which provides the maximum luminosity and the best beam focusing.

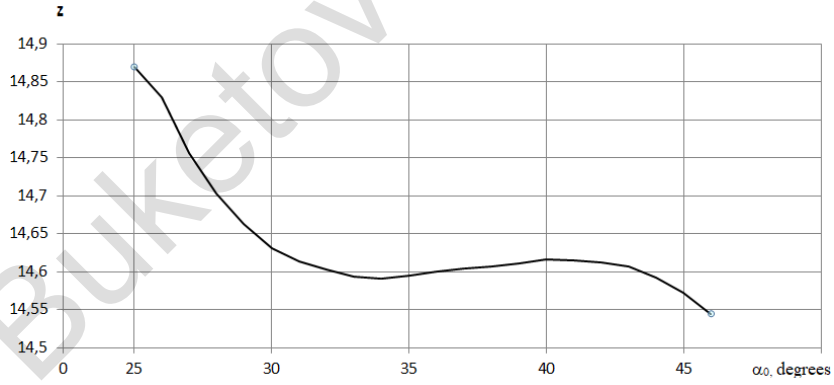

Fig.4.5. Dependence of the particle arrival point on the entrance angle α_0

4.2 Calculation and analysis of electron-optical characteristics of the octupole-cylindrical energy analyzer

Table 4.1 displays the numerical results of the corpuscular-optical parameters for the octupole-cylindrical energy analyzer of the charged particle beam in the "ring-ring" angular focusing regime.

Table 4.1. Corpuscular-optical parameters of the octupole-cylindrical energy analyzer

Parameter	Values
Focusing order	3
Central angle of focusing	36°
Xfoc coordinate of the focus point	14.75°
Yfoc coordinate of the focus point	2.5°
Reflection parameter, *P*	1.0

The order of focusing refers to the specific focusing behavior exhibited by an electron-optical system. It describes the degree or level of focusing achieved by the system, typically denoted by a numerical value. In the context of the discussed energy analyzer, the second-order angular focusing regime is of interest.

By implementing 3-order angular focusing, the energy analyzer can enhance its performance in terms of dispersion, resolution, aberration distortion, and other integral characteristics.

The instrumental function is a significant characteristic of axial electrostatic energy analyzers, as well as many other electron and ion optical devices. The instrumental function of an axial electrostatic energy analyzer is proportional to the dependence of the monoenergetic electron flux passing through the energy analyzer's exit slit on the energy of the electrons. The instrumental function, also known as the transmission curve, instrumental line, instrumental function, or response function, is directly proportional to this dependence. With knowledge of the hardware function, determining the resolving power and transmittance becomes relatively straightforward. In electron optics, the "trajectory" method is commonly employed to obtain the primary characteristics of the analyzed energy analyzer.

To calculate the instrumental function of the octupole-cylindrical energy analyzer, a range of particles is launched from a ring source with initial angles ranging from 30 to 42 degrees and initial energies ranging from 1.60 to 1.62. Fig. 4.6 presents the instrumental function of the octupole-cylindrical analyzer in the third-order "ring-ring" type angular focusing regime.

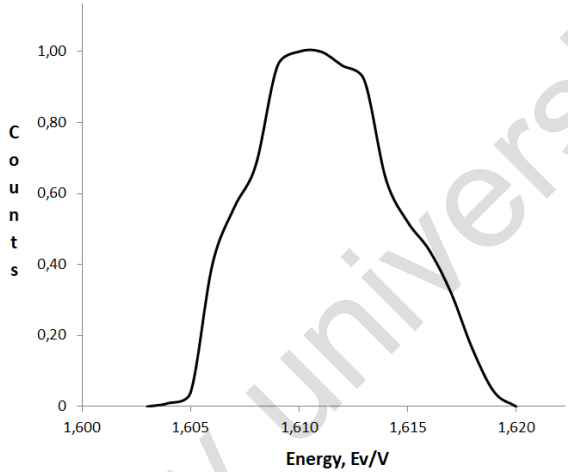

Fig. 4.6. The instrumental function of the octupole-cylindrical energy analyzer at μ =2, ω = 1 (the "ring-ring" type angular focusing regime)

The octupole-cylindrical energy analyzer has a relative energy resolution at half-height of its instrumental function of 0.5% when using an exit diaphragm with a radius of $0.012r_0$, and a luminosity of $\Omega/2\pi$=12.3%. These numerical simulation results are in good agreement with the approximate-analytical method calculations.

The numerical model of the octupole-cylindrical energy analyzer has been obtained. The corpuscular-optical properties of the electron-optical system are calculated. Angular focusing conditions have been determined for particle trajectories with significant angular divergence of the beam in the axial plane. The energy analyzer is characterized by compactness, high focusing quality and energy resolution, and can be used to develop a small-sized highly sensitive electron spectrometer [154, 155].

5 DESIGN OF THE ALL-SKY SPECTROMETER OF HOT COSMIC PLASMA

5.1 Devices for the simultaneous angular and energy analysis of cosmic plasma

The objects of research in the field of space plasma physics are the radiation belts of the Earth, the solar wind, the collisionless shockwave of the Earth's magnetosphere, tail of the magnetosphere, the polar lights, the kilometric radiation of the Earth, etc. These studies, in particular, include the study of such characteristics of the hot plasma distribution as the ionic composition, the shape of the energy spectra and angular distributions, as well as the determination of its structure and the nature of the processes occurring in it.

Energy and mass analyzers of charged particle beams, specifically for ions and electrons with energy ranges spanning from a few electron volts up to tens of kiloelectron volts, are the most commonly utilized instruments for researching hot space plasma. Energy and mass analysis of moving particles is carried out due to their spatial separation in electric and magnetic fields. In terms of mass-dimensional indicators, devices with electrostatic deflection of charged particles are out of competition. An additional parameter that needs to be measured during research in space is the direction of arrival of particles. The direction of their arrival is definitely related to the position of the particle source on the celestial sphere.

Devices for the simultaneous angular and energy analysis of cosmic plasma have passed through several stages in their development. At the initial stages of the engineering development, simple single-channel spectrometers [156], or their combinations, were used to measure the three-dimensional velocity distribution function. The next step in their progress is the development of a spectrographic method for registration of charged particles. In the design of the spectrograph [157], a pair of plates was used that ensured the dispersion of particle flows with respect to energy, which made it possible to simultaneously register electrons and ions of various energies using a line of detectors. The use of quarter-spherical and hemispherical analyzers with a knife-edge field of view, the

acceptance angle (for particle reception) of which reached 140°-160° [158] can be considered the next achievement of space plasma diagnostics methods.

The “main tool” of space research today is rightly considered the axially symmetric top-hat analyzer [159] which is selective in terms of kinetic energy E and the direction of motion of charged particles. The selection of particles by energy is provided by a pair of concentric hemispherical electrodes: a grounded outer hemisphere and an inner hemisphere with a deflecting potential V. Two parallel, closely spaced disks of a sufficiently large radius, located at the top of the outer hemisphere parallel to the base of the hemispheres, the polar angle $\theta = 90^{\circ}$ of motion of the registered particles in a spherical coordinate system is fixed. By gradually changing the potential V of the inner hemisphere, one can scan the entire spectrum of energies E of charged particles. Registration of the particle distribution by azimuth angle φ is ensured by using a plane position-sensitive detector as a collector, since a particle with a certain angle φ is displayed by a single point on the circumference of the entire image. Measurement of the distribution function of charged particles in the entire range of 4π sr is provided for the half period of rotation of the satellite around its axis.

The top-hat analyzer is successfully used to investigate key regions of the electromagnetic plasma not only of the Earth, but also of other planets of the solar system [160].

Top-hat analyzer is still in the focus of interest of many developers of devices for diagnostics of cosmic plasma, proposing ways to improve its parameters [161, 162] and studying the influence of various external factors on the main characteristics of the device [163].

The scope of the top-hat analyzer is constantly expanding. In particular, with its help, the plumes of charged particles generated by an ion engine in the far field have been investigated in [164]. The work [165] presents the results of observation of low-altitude ionospheric sources of high-latitude ion up flow/out flow. The primary challenge addressed by the theoretical model developed was the measurement of ions with extremely low energies (in the range of tenths of an eV) at altitudes ranging from 200 to 350 km.

The disadvantage of the top-hat analyzer is the significant time cycle for registration of the angular dependences in the total solid angle of 4π sr and low accuracy in determining the polar angles due to the principle of mechanical displacement (rotation) underlying the measurements.

Over the past 20 years, plasma analyzers with a large field of view have been continuously developed, including those based on a top-hat analyzer with entrance optics, which allows scanning the polar angles θ in a rather wide range [166].

A good example of plasma analysis systems, built on schemes other than top-hat, is the Fast Imaging Plasma Spectrometer (FIPS) [167], a simplified scheme of which has proven itself well in the flight of the "Messenger" interplanetary station and has shown that it really is not only an alternative to the top-hat, but also allows to carry out unique measurements in various plasma environments. The FIPS energy and mass analyzer with a field of view of almost 2π sr consists of a wide-angle two-chamber electrostatic analyzer that forms an image of the angular distribution of ions on a multi-beam collimator located in front of the time-of-flight (TOF) camera.

In parallel, more efficient 2π or 4π systems were being developed, which will probably soon be mounted on spacecrafts.

O.L. Weisberg proposed and investigated a new method for the simultaneous measurement of the velocity vector of charged particles in a solid angle of 2π sr [168]. The complete view of the celestial hemisphere is based on a scheme (Fig. 3.1) that involves the transmission of a particle flow (1) which is emitted by sources (2) distributed in space through a ring diaphragm (3).

Due to the design characteristics of the device, the range of entrance angles in each meridian section is divided into two subranges from -90° to 0° and from 0° to +90° relative to the axis of symmetry 0z. In this geometry, only a hemisphere section of radius r_0, which is an infinitesimal value with respect to the radius of the virtual celestial sphere, is excluded from consideration. Further, a wide entrance flow of charged particles is converted into a narrow-collimated one, subjected to energy analysis and detected by a position-sensitive detector, with each coordinate on the detector plane being associated with the direction to the source on the celestial hemisphere.

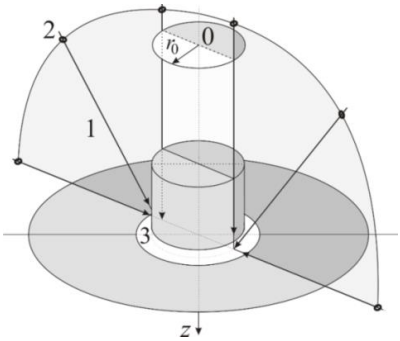

Fig.5.1. Entrance of particles into the particle analysis device: 1 – particle flow, 2 – sources of particles distributed on the virtual celestial sphere, 3 – entrance ring diaphragm.

Figure 5.2 illustrates the electron-optical scheme of a device named 'CAMera' that performs simultaneous energy and angular analysis of charged particle flows within a solid angle of 2π sr [168]. Particle flow (1) enters the main electrostatic elliptical mirror (2) through the ring aperture (3) and is reflected by the mirror into a narrow-collimated beam. The selection of energy or energy scanning is carried out using a secondary plane mirror (4). A point diaphragm (5) cuts particles with the energy of analyzer settings (4) out from the flow, the particles being recorded by the position-sensitive detector (6). Note the fact that each charged particle moving in the analyzer four times intersects the plane of the grid electrodes, and one of these electrodes has a complex geometric shape.

The successful development and testing of plasma analyzers DI-Aries (DI is for Sensor of Ions in Russian and Aries is for Zodiac constellation) [169] and PICAM (Planetary Ion CAMera) [170, 171] have confirmed a new concept based on rotationally symmetric electrostatic mirrors for the creation of ion analyzers with an instant half-spatial overview field. At each step of energy measurement, ion optics provides a two-dimensional image of the angles of ion motion on a microchannel detector with a high time and acceptable angular resolution. Current and future research will mainly focus on increasing the geometric factor of the device and achieving a more simple and accurate mechanical design [172].

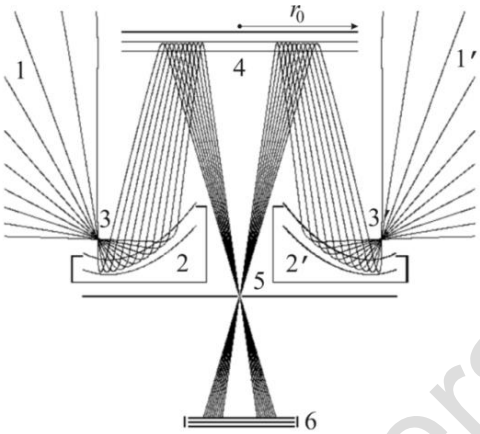

Fig.5.2. Meridian section of the "CAMera" analyzer: 1-1' – particle flow, 2-2' – main elliptical mirror, 3-3' – entrance ring diaphragm, 4 – secondary plane mirror, 5 – exit point diaphragm, 6 – position-sensitive detector.

The disadvantages of "CAMera" type analyzers are a large number of grids and technological difficulties in the manufacture of elliptical grid mirrors. The purpose of this research is to develop a simplified energy analyzer design with a minimum number of grids to provide a 2π-view of the celestial sphere.

5.2 Development of the all-sky spectrometer of hot cosmic plasma

1. The idea of the proposed spectrometer. The idea of the analyzer design proposed in this work was to use distributed fields created by devices of simple design. In this work [173], the software for numerical modeling of electron optics systems CAE "Focus" as a main tool for developing the design of the device and its stages. Part of the studies involved using approximately-analytical methods to synthesize electrostatic fields for analyzing the energy of charged particle beams [174].

2. Modeling methods.

Electron and ion optics modeling software "Focus"

Traditionally, numerical modeling of electron-optical systems (EOS) consists of three distinct sections:

- computing the electrostatic and magnetic fields within the operational volume.

- computing the trajectories of charged particles within the electromagnetic field generated by the system.

- computing the overall characteristics of the EOS, including specific order angular focusing, dispersion, resolution, aberration distortion, and other relevant parameters.

CAE "Focus" comprises multiple software modules, each designed to tackle a specific problem independently.

The Design module is a graphical editor. It is designed for the formation and modification of the EOS design. The cross-section of the electrode system of each EOS can be represented by the union of the following primitives - a segment, a circular arc, a parabola, a hyperbola, a spline, a rectangle and an ellipse. The CAE "FOCUS" software module allows for the simulation of designs with electrodes of finite thickness and arbitrary shape, as each electrode with its specified potential is a closed loop. This feature enables the simulation of designs that closely resemble real devices. Moreover, the module facilitates three-dimensional representation of the simulated schemes.

At present, for the numerical solution of potential theory problems, three following methods are widely used: the finite difference method (FDM), the finite element method (FEM), and the boundary element method (BEM).

The most advanced numerical methods for solving problems of mathematical physics that appeared in the computer era include the BEM [175]. BEM should be considered as a truly numerical implementation of the well-known method of integral equations [176]. BEM (Boundary Element Method) has several advantages such as a simple algorithm presentation and the capability of solving both external and internal problems of potential theory. It can handle arbitrary boundary configurations of the study area, including elements of different scales.

Along with the obvious advantages, the BEM has a disadvantage that is the singular behavior of integrand functions, which leads to an

unacceptably high computational error. The development of an original numerical mathematical method [177] for exclude singularities in the integrand functions allowed to make BEM a powerful tool for calculation electric fields in systems with almost arbitrary boundary configuration and to provide a level of calculation accuracy limited only by round-off errors.

The created mathematical apparatus for determination of the potential distribution function in the EOS by the boundary element method is the basis of the *Field_E* module of the "FOCUS" software.

In order to simulate magnetic fields, the *Field_M* module has been developed and integrated into the CAE "FOCUS". The module realizes the solution of the problem of calculating the distribution function of the magnetic field induction of a set of solenoids by directly applying one of the basic laws of magnetostatics – the Biot-Savart law. The spatial position of each solenoid is defined by the coordinates of its upper base center and two angles that determine the orientation of its axis in space. The problem is solved by representing the resulting field as a superposition of magnetic fields of a set of solenoids, where the field of each of them, in turn, is determined as a superposition of magnetic fields of elementary circular currents (coils) [178].

The *Path_S* of CAE "FOCUS" module is intended for trajectory express analysis of EOS.

The Path_D module provides users with a more robust set of user-defined functions and analytical capabilities for the 3D trajectory analysis of systems with alternating electric and direct magnetic fields. The solution of the equations of charged particles motion is carried out by the Runge-Kutta-Felberg method, which makes it possible to control the calculations accuracy.

Based on the results of the trajectory analysis of EOS, the conditions for angular and time-of-flight focusing are automatically determined. To search for focusing conditions, original numerical methods have been proposed and developed [179, 180].

The developed mathematical methods and algorithms, implemented in the CAE "Focus", were deeply tested according to standard methods. After comparing the calculated data with known

analytical solutions, it was determined that the following characteristics can be achieved in real-time:

- potentials calculation (up to area boundaries) with an accuracy of not worse than 10^{-4} %, and in the case of rectilinear sections of electrodes, accuracy is limited only by round-off errors;

- particle trajectory calculation with an accuracy of not worse than 10^{-3}%;

- parameters calculation for searching for focusing conditions (angular, spatial, time-of-flight) with an accuracy of not worse than 10^{-2}%.

Numerical method for search high-order angular focusing conditions. The quality criterion for most electron and ion optics systems is the order of the angular focusing they provide.

The focusing condition of *N* order is expressed by the equality of partial derivatives to zero with respect to the initial angle α in the meridian section $x0y$

$$y'(\alpha_0)=y''(\alpha_0)= ... =y^{(N)}(\alpha_0)=0, \qquad (5.1)$$

in the Taylor series expansion, the coordinates y the trajectory intersection with the focal plane

$$y(\alpha)=y(\alpha_0)+(\partial y/\partial\alpha)_0 \Delta\alpha+1/2(\partial^2 y/\partial\alpha^2)_0 \Delta\alpha^2+... , \quad (5.2)$$

where $\Delta\alpha=(\alpha-\alpha_0)$, α_0 is the initial angle of the central trajectory.

The original numerical method for search the angular focusing conditions of particle flows is described in sufficient detail in [181].

The following is a brief summary of instructions for using the method.

On a discrete set of initial angles α_i, i=1, 2, ..., L of particle motion in a certain selected range of angles $[\alpha_{min}, \alpha_{max}]$, a continuous function is constructed

$$F(\alpha)=R''(\alpha)\, t'(\alpha)-R'(\alpha)\, t''(\alpha), \qquad (5.3)$$

where $R(\alpha)=y_c(\alpha)+x_c(\alpha)$ t(α) , $t(\alpha)=\mathrm{tg}(\gamma)$; $\gamma(\alpha)$ and $x_c(\alpha)$, $y_c(\alpha)$ are the angle and coordinates at any convenient point of the final straight

section of the trajectory. Derivatives are calculated using the formulas for numerical differentiation [182].

Then the algebraic equation is solved

$$F(\alpha)=0 \qquad (5.4)$$

with respect to $\alpha=\alpha_0$ and the coordinates of the focus point are determined by the formulas:

$$x_0=R'(\alpha_0)/t'(\alpha_0),\ y_0=R(\alpha_0)-x_0\cdot t(\alpha_0). \qquad (5.5)$$

To establish the angular focusing order, the cross-correlation of the function $F(\alpha)$ with the power function $S(\alpha)=(\alpha-\alpha_0)^{m+1}$ is estimated by the formula

$$\rho_0(m)=R_{FS}/(K_F\cdot K_S)^{1/2}, \qquad (5.6)$$

with a sequential change in the value of $m=0, 1, ..., M$ (M is the upper search boundary). Here $R_{FS}=\frac{1}{L}\sum_{i=1}^{L}(F_i-\overline{F})(S_i-\overline{S})$,

$K_F=\frac{1}{L}\sum_{i=1}^{L}(F_i-\overline{F})^2$, $K_S=\frac{1}{L}\sum_{i=1}^{L}(S_i-\overline{S})^2$, $\overline{F}=\frac{1}{L}\sum_{i=1}^{L}F_i$, $\overline{S}=\frac{1}{L}\sum_{i=1}^{L}S_i$.

Next, the value of m $(0\le m\le M)$ is determined for which $\rho_0(m)=\max\{\rho_0(0), \rho_0(1), ..., \rho_0(M)\}$. The proximity of $\rho_0(m)$ to 1 will indicate the mutual correlation of $F(\alpha)$ and $S(\alpha)=(\alpha-\alpha_0)^{N+1}$, i.e. focusing of the $N=m+2$ order. The upper search limit M is selected for practical reasons no more than 20 ÷ 25.

Multipole approach for electrostatic field synthesis.

Two-dimensional electrostatic multipoles with a rectilinear symmetry axis are well known and widely used as focusing, deflecting, and correcting elements in electron and ion optics. It is important to develop a multipole approach to solving the external Dirichlet problem in a cylindrical coordinate system [183]. It has been shown [184] that if on a cylindrical surface the potential and its first derivative with respect to the radial component are given by power series in the axial component, then the external field is the sum of

circular multipoles. Based on this, new multipole-cylindrical fields have been calculated, which are of interest for practical application in corpuscular optics.

The construction of axially symmetric electrostatic multipole-cylindrical fields is based on a superposition of a cylindrical field and circular multipoles of various orders. This method was first described in [185]. Then the proposed approach was applied to study a family of multipole-cylindrical fields formed when the zero equipotential surface of a cylindrical field coincided with the zero equipotential surfaces of some circular multipoles. The considered axially symmetric fields have a simple structure and are promising for use in the mirror regime of reflection of a charged particle beam.

The class of multipole-cylindrical fields does not allow separation of variables in the equations of charged particles motion, that is, it is impossible to obtain an analytical solution. The calculation of the trajectories by the numerical method, in comparison with the analytical one, significantly complicates the search for the condition of angular focusing of a charged particle beam. The method of analytical description of trajectories by an optimally selected superposition of power series describing the trajectory in the plane in integro-differential form and the condition for stitching the trajectory branches at its vertex is applied for quadrupole-cylindrical, hexapole-cylindrical, decapole-cylindrical and octupole-cylindrical fields. Operating with finite sums of the additives that make up the power series, as shown in these works, makes it possible to describe the corpuscular-optical properties of systems with sufficient accuracy.

The potential of a hexapole-cylindrical field is described in the r, z coordinate system by the following expression:

$$U(r,z) = \mu \ln r + g U_h(r,z), \tag{5.7}$$

where

$$U_h(r,z) = \frac{1}{2}\left\{\ln r\left[z^2 - \frac{1}{2}r^2 - \frac{1}{2}\right] + \frac{1}{2}r^2 - \frac{1}{2}\right\} \tag{5.8}$$

is a circular hexapole, μ is the coefficient specifying the weight contribution of the cylindrical field ln*r*, γ is the weight component of the circular hexapole.

The outer electrode, to which the deflection potential U_o is applied, has a curved profile, the shape of which is determined by the equation:

$$z = \pm\sqrt{\frac{4\frac{U(r,z)}{V} + \ln r\left(r^2 + 1 - m\right) - r^2 + 1}{2 \times \ln r}}\ , \qquad (5.9)$$

where $U(r,z)$ is the distribution of the hexapole-cylindrical field.

Fig.5.3 shows the energy analyzer scheme with a hexapole-cylindrical field for a cylindrical field component μ=2 and a circular hexapole γ=1 [186]. The analyzer consists of two coaxial cylindrical electrodes, with the inner electrode remaining cylindrical and the outer electrode having a curvilinear profile relative to the surface of the inner cylindrical electrode. The hexapole-cylindrical field is formed between these two electrodes, with the outer electrode serving as the equipotential surface of the field.

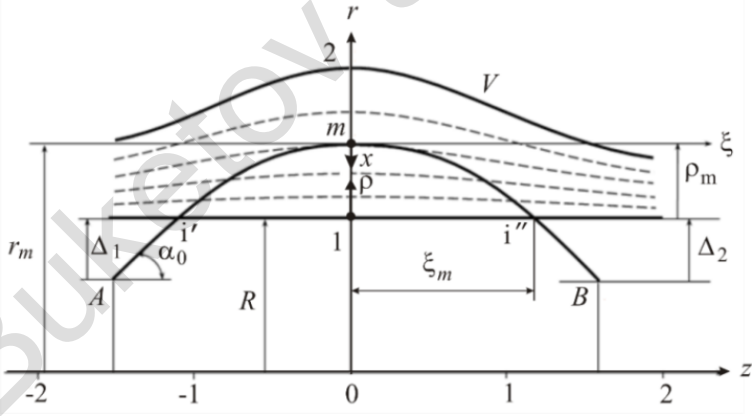

Fig. 5.3. Energy analyzer scheme based on a hexapole-cylindrical field:
A – source, *i'* – entrance ring slit, *i''* – exit ring slit,
B – receiver

Approximate-analytical approach to calculating the parameters of an analyzer with a hexapole-cylindrical field is as follows.

The distribution of a hexapole-cylindrical field Eq. (5.7) in coordinates x,ξ (see Fig.5.3) has the following form:

$$U(x,\xi) = V \cdot g(x,\xi) , \tag{5.10}$$

where

$$g(x,\xi) = \frac{1}{4} \cdot \left\{ \ln(H-x) \left[2\xi^2 - (H-x)^2 + 7 \right] + (H-x)^2 - 1 \right\} ,$$

$$H = 1 + \rho_m . \tag{5.11}$$

The trajectory of a particle in an electrostatic hexapole-cylindrical mirror has a vertex located within the field area and is not generally described by an elementary function. This trajectory is known as a "return" trajectory and consists of two symmetric branches with respect to the vertex. The integro-differential equation of motion of a charged particle along the “return” trajectory in the hexapole-cylindrical field has the following form:

$$(\xi')^2 \left[g_0 - g_x - \int_0^x \ln(H-x)\, \xi\xi'\, dx \right] = P^2 \cot^2\alpha_0 - f_m + \int_0^x \ln(H-x)\, \xi\, \xi'\, dx , \tag{5.12}$$

where

$$g_0 = g(x_m, \xi_m) = \ln H \left[-\frac{H^2}{4} + \frac{7}{4} \right] + \frac{H^2}{4} - \frac{1}{4} , \; g_x = g\left[x,\, \xi(x) \right] . \tag{5.13}$$

and $P = \sqrt{\frac{E_0}{qV}} \sin^2 \alpha_0$ is the reflection parameter linking the geometric and energy parameters of the mirror, E_0 and q are initial energy and charge of a particle respectively, V is potential of the deflection electrode.

To solve the integro-differential Eq.(5.12), the expansion method of the solution of equation ξ in a fractional power series is used:

$$\xi = \xi(x) = \sqrt{x} \left(C_0 + C_1 x + C_2 x^2 + C_3 x^3 + C_4 x^4 + C_5 x^5 + \ldots \right) \tag{5.14}$$

Having obtained the expansion of the derivative ξ' in a series from Eq. (5.14), and also using the expansion

$$\ln(H-x) = \ln H - \frac{x}{H} - \left(\frac{x}{H}\right)^2 - \left(\frac{x}{H}\right)^3 - \left(\frac{x}{H}\right)^4 - \left(\frac{x}{H}\right)^5 - \ldots \qquad (5.15)$$

it is possible to solve the integro-differential Eq.(5.12) with respect to the unknown coefficients C_0, C_1, …, i.e. determine the trajectory of the particle $\xi = \xi(x)$ (see Eq. (5.14)).

Below are the results of calculating the main parameters of the trajectory based on the analysis of the obtained solution.

The projection of the trajectory onto the ρ axis from the entry point to the turning point has the expression:

$$\rho_m = 0.5P^2 + 0.125P^4 + \left(0.013525 - 0.0625\cot^2\alpha_o\right)P^6 + \ldots \qquad (5.16)$$

The projection of the trajectory onto the symmetry axis of the mirror in the same section of motion is determined by the formula

$$\xi_m = \xi(x)\big|_{x=\rho_m} = \sqrt{\rho_m}\, C_o S\,, \qquad (5.17)$$

where

$$C_o = \cot\alpha_o \sqrt{2.0P^2 + P^4 + 0.625P^6 + \left(0.52778 - 0.125\cot^2\alpha_o\right)P^8 + \ldots}\,, \qquad (5.18)$$

$$S = 1 - 0.04167P^2 - \left(0.03073 + 0.02083\cot^2\alpha_o\right)P^4 - \left(0.02755 + 0.0092\cot^2\alpha_o\right)P^6 + \ldots \qquad (5.19)$$

The sum expresses the total projection of the trajectory onto the z-axis from source A to its image B, relative to the symmetry of the "return" trajectory with respect to the r-axis, and is given in terms of fractions of the radius R of the inner cylinder:

$$l = \frac{L}{R} = \Delta \cot\alpha_0 + 2\xi_m , \quad \Delta = \Delta_1 + \Delta_2 . \tag{5.20}$$

To analyze the characteristics of an electrostatic hexapole-cylindrical energy analyzer, the spatial focusing coefficients of the 1st, 2nd and 3rd orders have been calculated: $\frac{dl}{d\alpha}$, $\frac{d^2l}{d\alpha^2}$, $\frac{d^3l}{d\alpha^3}$. The conditions for the second-order angular focusing the with respect to the small deviation of the non-equilibrium trajectory from the axial orbit have been found: $\frac{dl}{d\alpha} = \frac{d^2l}{d\alpha^2} = 0$. The specific energy dispersion is calculated as a measure of the resolving capability for narrow ring slits *A* and *B*. It is determined as the ratio of the linear energy dispersion to the width s_0 of the image line.

$$\delta = \frac{D}{s_0} = \frac{D}{A_{\text{III}} \cdot (\Delta\alpha)^3} , \tag{5.21}$$

where $D = \frac{\partial l}{\partial E} E_0$ is the value of the relative linear energy dispersion, $A_{\text{III}} = \frac{1}{3!} \frac{d^3l}{d\alpha^3}$ is cubic angular aberration.

Table 5.1 displays a small example illustrating the main electron-optical characteristics of the analyzer. These characteristics are calculated based on the reflection parameter *P* and fulfill the requirements for second-order angular focusing: α_o is entrance angle of the trajectory; ρ_m is the coordinate of the trajectory vertex point in the mirror field; $\Delta = \Delta_1 + \Delta_2$ is the value of the total removal of the source and its image from the inner cylindrical electrode , ξ_m is a half projection of the trajectory onto the symmetry axis in the mirror field; *l* is a focal length; *D* is the value of relative linear energy dispersion; A_{III} is the cubic angular aberration, Δl is the value of the aberrational image expansion; δ is the value of the specific energy dispersion.

Table 5.1. The main electron-optical characteristics of the hexapole-cylindrical analyzer

P	α_o	ρ_m	Δ	ξ_m	l	D	A_{III}	$/\Delta l/$	δ
0.10	30.165°	0.005	0.010	0.0173	0.0518	0.0346	-0.158	0.0009	27.95
0.50	33.922°	0.130	0.264	0.400	1.193	0.849	-2.809	0.0160	53.12
0.95	44.977°	0.465	0.787	1.131	3.050	2.417	-0.394	0.0061	385.26

Modeling an entrance optics of the spectrometer. Based on the results of numerical calculations, the design of an entrance lens system has been proposed that converts the flow of charged particles emitted from different points of the celestial hemisphere into a narrow hollow conical beam (Fig. 5.4). The electrodes of the lens system are formed by the simplest and therefore technologically advanced primitives – discs, cylinders and cones.

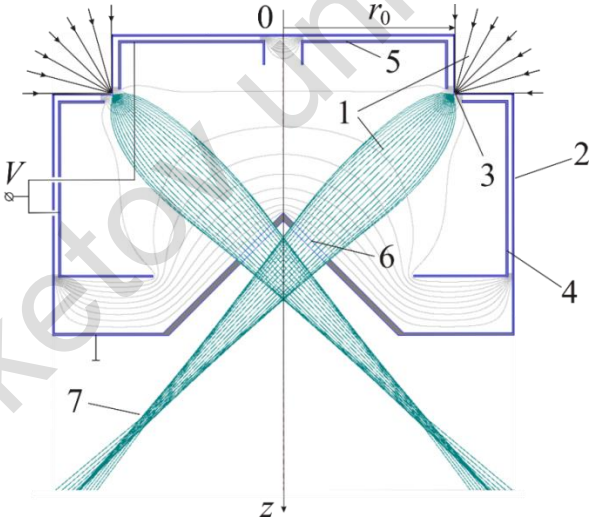

1 – a particle flow, 2 – a device body (an outer electrode), 3 – an entrance ring diaphragm, 4, 5 – inner U-shaped electrodes, 6 – an exit window, 7 – a focal point.

Fig. 5.4. The meridional section of the entrance lens system of a simple design with a full view of the celestial hemisphere

Charged particles (1) (Fig. 5.4) with energy E_0 (E_0/V=1), emitted by sources distributed in some way over the surface of the hemisphere of the sky with a large radius, moving along radial trajectories in the direction of the device body (2), penetrate through the entrance ring diaphragm (3) (see. Fig. 5) into the field of a single conical electrostatic lens, formed by a zero potential on the outer electrode (2) and potentials V on the inner electrodes (4) and (5) of the "U"-shaped section, applied from an external power source. Flow (1), having experienced the focusing effect of this field, enters into the external space through a window (6) covered with a fine-structured metal mesh in the conical surface of the outer electrode (2), forming a hollow narrow-collimated truncated cone with a smaller base located in the focal region (7).

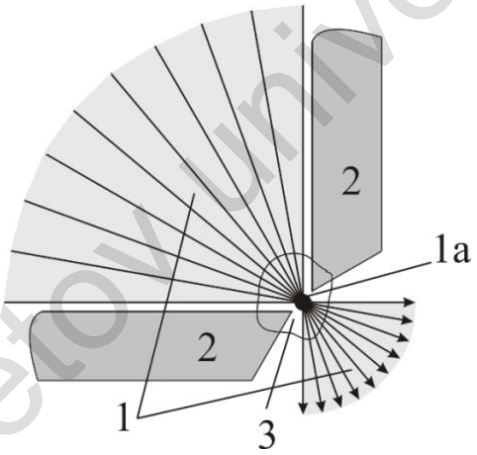

1 – a charged particle beam, 1a – a virtual source, 2 – the device body, 3 – a ring diaphragm.
Fig. 5.5. Scheme of particle flow passing through the entrance ring diaphragm (transaxial section)

A detailed numerical analysis of the lens system scheme (Fig. 4) shows that a single conical lens is represented by two areas which play the role of successive collecting lenses that is a short focus and a long focus ones.

Fig. 5.6 shows the effect of a parallel beam focusing with an initial relative electron energy E/V=1 by the first collecting lens. The initial angle of entry of a parallel charged particle beam into the lens field is -45° with respect to the 0z symmetry axis. The focal length, which is calculated from the center of the entrance diaphragm (3) equal to f_1=0.15 r_0. In the modeling, the outer electrode was considered transparent to the particle beam.

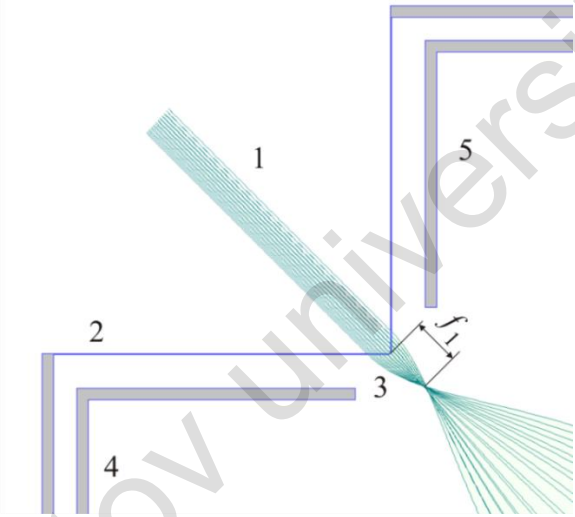

1 – a particle beam, 2 – the device body (an outer electrode), 3 – the entrance ring diaphragm, 4, 5 – inner U-shaped electrodes.
Fig. 5.6. Entrance collecting lens

In the case of emission of a divergent flow by a thin ring source 1a (Fig. 5) located in the area of the entrance diaphragm 3, after transit through the first lens, charged particles enter the area of the second lens in an almost parallel flow perpendicular to the equipotential of 0.7V and, therefore, are collected at focus 7 of this lens (see Fig. 4).

The exact estimate of the distance “source 3 – image 7” (Fig. 4) obtained in accordance with numerical calculations is about 3.3 r_0; this provides the second-order angular focusing near the central angle of 45°.

Modeling of the second stage of the spectrometer. The second stage of the analyzer must have sufficient particle energy dispersion to ensure the required level of energy resolution and it must focus the diverging entrance particle flow onto an ring slit in front of the position-sensitive detector organizing the angular measurement scheme. The central angle of departure from the first stage of the device is approximately 45°; therefore, the second stage must have a high angular focusing order (higher than the first one) relative to the trajectory of a particle with such an initial angle. A wide range of the second-order focusing angles within 30°-50° and a number of other unique electron-optical characteristics are provided by designs of devices with hexapole-cylindrical fields $U(r,z) = \mu \ln r + \gamma U_h(r,z)$ (see Section 2.3). From the analysis of the calculated data of work [186], it follows that the angle of the required value of 45° can be obtained in the scheme with μ=2 and γ=1. Examples of theoretically calculated parameters of the analyzer of this scheme are presented in Table 5.1.

The case of P=0.95 satisfies the conditions of the problem solved in the article. In addition, this scheme is distinguished by a high level of specific energy dispersion δ=385.26, which is approximately 6 times higher than the specific dispersion of a cylindrical mirror analyzer, having δ=65.5 for a better "axis-axis" focusing scheme. Another advantage of the scheme is the small value of the third-order angular aberration A_{III}, which guarantees a narrow focus of highly divergent particle flows.

Presented in Table 5.1 characteristics were calculated for electrodes of infinite length along the *z*-axis. In a real device, the length of the electrodes must be limited. With limited length, the influence of edge effects can be neglected if the places of the electrode shape distortion are located at a considerable distance from the particle transit area. Fig.7 shows the electron-optical scheme of the hexapole-cylindrical analyzer of real dimensions, as well as the central trajectory of a particle with the initial conditions corresponding to the regime of P=0.95 in Table 5.1: the initial angle α_0=44.9774° and the relative initial energy $\frac{E_0}{V} = \left(\frac{P}{\sin\alpha_0}\right)^2 = \left(\frac{0.95}{\sin 44.9774°}\right)^2 \approx 1.806$. Table 5.2 compares the main characteristics of the calculated trajectories

(Table 5.1) numerically and analytically. The comparison results show a high degree of coincidence of the parameters of the idealized and real schemes. From the above, the conclusion is drawn that the hexapole-cylindrical analyzer can be considered as the second stage of the designed device.

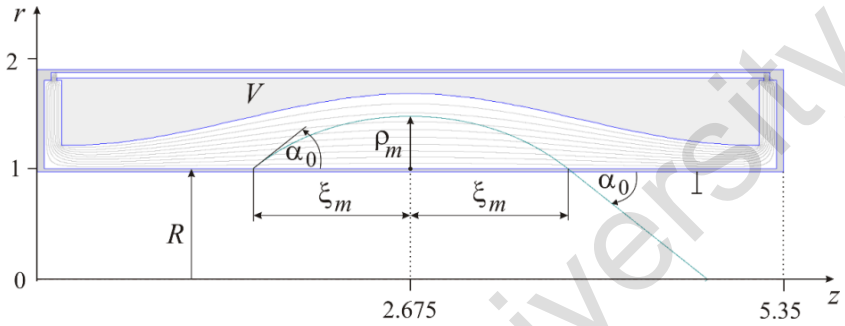

Fig. 5.7. The electron-optical scheme of the second stage of the analyzer: $R = 1$.

Table 5.2. Comparison of the main characteristics of the trajectories calculated numerically and analytically

Parameter	P	α_o	ρ_m	ξ_m	D
Idealized scheme	0.950	44. 977°	0.465	1.131	2.417
Real scheme	0.946	44.980°	0.475	1.131	2.027

Indeed, the trajectory analysis of the second hexapole-cylindrical stage (Fig. 5.8), when the particles that left the first stage are launched to its entrance (Fig. 5.4), reveals rather sharp angular focusing (of the second-order) near 45° of the initial particle beam. Note, that it had the polar angles spread within the range from 0° to 90° at the first stage entrance. In the modeling, the first and second stages are matched along the central trajectory of a particle incoming the second one at a distance of ξ_m from the top of the outer electrode.

Modeling of the spectrometer of energy and angular dependences. The electron-optical scheme and the results of the trajectory analysis of the entire device as a sequence of two stages are

shown in Fig. 5.9. The scheme of the device provides the second-order angular focusing near the trajectory α_0=44.9° in the meridional section with coordinates z = 19.9, r = 1.45. The design of the device includes a narrow entrance ring slit (1), the first stage exit window (2), entrance (3) and exit (4) windows of the second stage, entrance (5) and exit (6) ring-shaped limiting diaphragms. Windows (2), (3) and (4) are tightened with a fine-structured metal mesh, preventing potential sag and providing charged particle transit. Ring-shaped diaphragms (5) and (6) are located in the smallest section of the particle flow. The potential of the first stage focusing electrodes is $V_1=V=E_0$[eV], the potential of the second stage outer electrode is $V_2=0.556V=0.556E_0$[eV], where V is the voltage of the external power source, E_0[eV] is the particle energy in eV.

Fig. 5.10 shows the instrumental function of the energy analyzer, which is the dependence of the relative number of particles N/N_0, registered by the collector, on the relative energy E_0/V. The basic energy resolution of the device is $R_0 = \Delta E_0/E_0 = 4.9$ %, the resolution at half-height of the instrumental function is $R_{1/2} = \Delta E_{1/2}/E_0 = 1.1$ %, the luminosity is $\Omega \approx 100\%$ of 2π. Here, ΔE_0, $\Delta E_{1/2}$ are the energy transmission bandwidth based at the bottom and half-height of the instrumental function.

Each polar angle of the celestial sphere corresponds to a circle of a certain radius on the surface of the plane coordinate-sensitive detector (7) (Fig. 5.9). Furthermore, each point of this circle determines the azimuthal direction to the particle source within the range from 0 to 2π. Thus, the angular resolution of the device is determined by the spatial resolution of the used position-sensitive detector.

The two-stage, fairly simple design of the all-sky spectrometer of hot cosmic plasma, is proposed in the work. The first stage of the device is the axially symmetric lens system of an original design, which transforms a wide 2π sr entrance particle beam into a narrow one in the form of a hollow cone. The second stage of the device functions as a hexapole-cylindrical energy analyzer for the beam. The electron-optical scheme of the device is developed using both numerical and approximate-analytical methods, specifically setting it up to operate in the second-order angular focusing regime.

A plane position-sensitive detector can be used as a particle collector, providing an additional function for recording angular dependences.

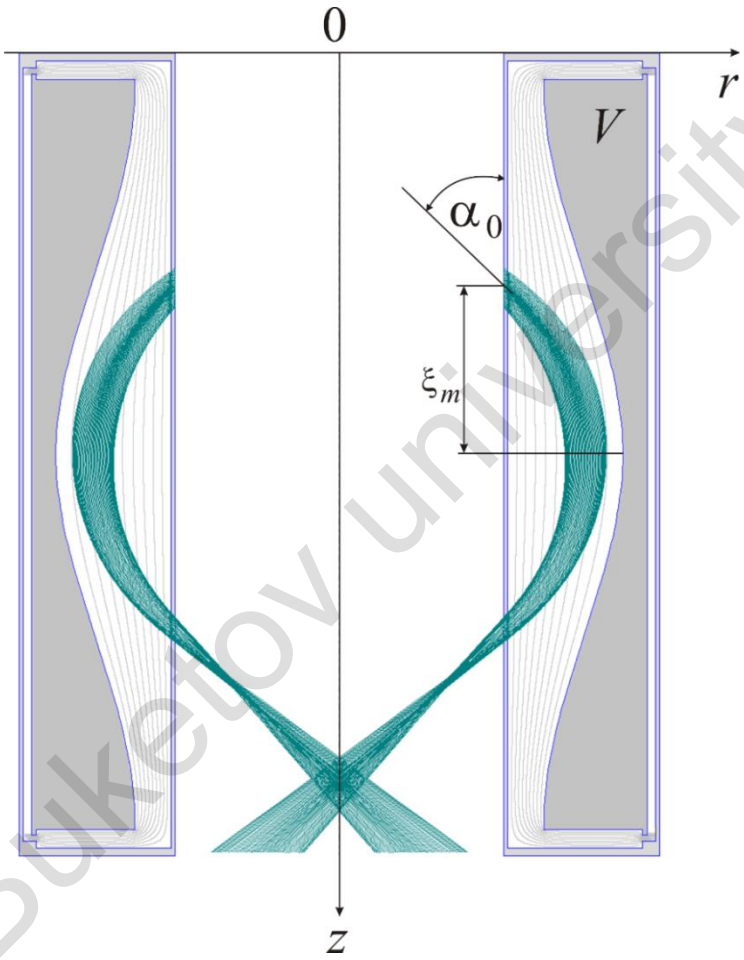

Fig. 5.8. Trajectories of particles in the second stage of the analyzer after passing through the first stage.

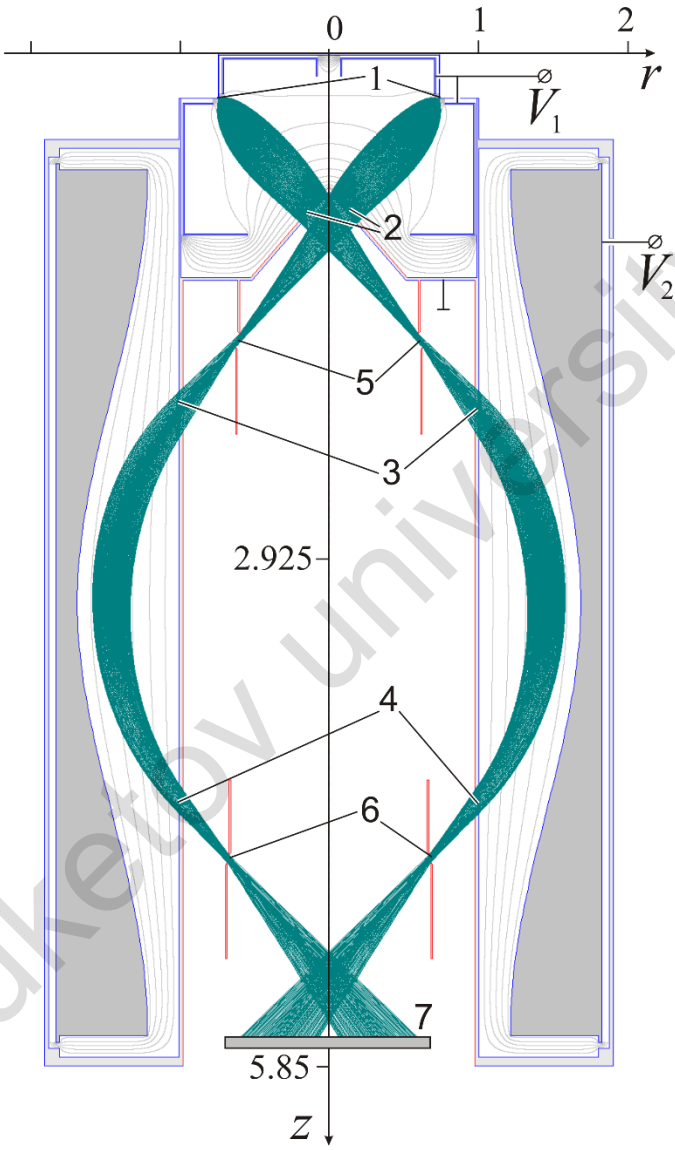

Fig. 5.9. The electron-optical scheme of the all-sky spectrometer of hot cosmic plasma: E_0/V_1=1, E_0/V_2≈1.8.

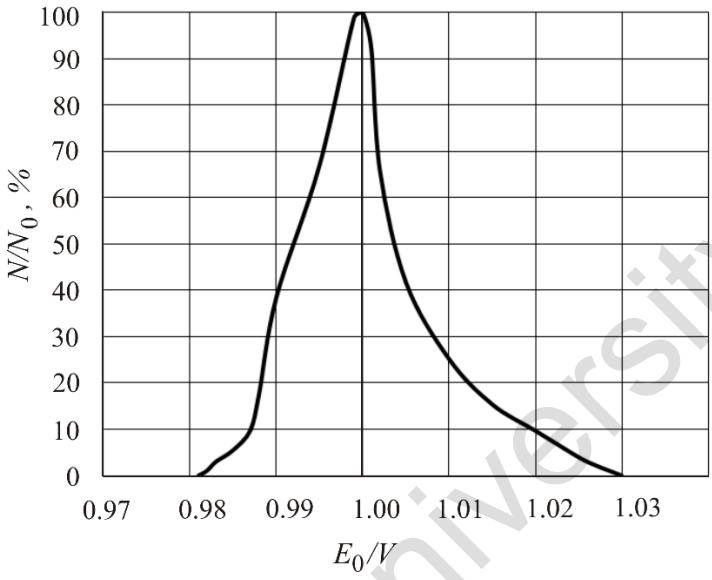

Fig. 5.10. The instrumental function of the spectrometer.

Conclusion

The monograph presents the results of calculations and modeling of electron-optical schemes of electrostatic mirror energy analyzers of charged particles.

Energy analyzers play a crucial role in various fields of scientific research and technological applications. Energy analyzers are sophisticated instruments designed to measure and analyze the energy distribution of charged particle beams. Their versatile nature and precise capabilities make them indispensable tools in numerous scientific and technological endeavors.

Energy analyzers find extensive use in materials science and nanotechnology research. They enable the characterization of energy states, electronic structure, and surface properties of materials. In particle physics experiments, energy analyzers play a crucial role in identifying and characterizing particles, measuring their energies, and studying fundamental particle interactions. Energy analyzers are employed in space missions and astronomy to study the properties of charged particles in the space environment. The versatility and reliability of energy analyzers make them essential tools for scientists and engineers in a wide range of disciplines.

Based on the theoretical schemes, electrostatic energy analyzers with high electron-optical characteristics for space research were developed. The choice of the type of corpuscular flux energy analyzer and its electron-optical scheme in the creation of portable equipment for the study of space plasma was justified. A high-resolution octupole-cylindrical light analyzer was developed. A two-stage, fairly simple construction of an all-sky spectrometer of hot cosmic plasma was proposed.

Various methods of calculation and design of corpuscular-optical systems were used in solving the set problems. The approximate analytical method for calculating the trajectories of charged particles in electrostatic fields was used. For numerical modeling of energy analyzers, the most modern software packages were used, in particular, the numerical program "Focus" of Ryazan State Radio Engineering University for modeling axially symmetric corpuscular-

optical systems, as well as the software tool MathCAD Professional for solving mathematical problems of varying degrees of complexity.

All the results concerning the design of specific scheme of electrostatic energy analyzers are of great importance for physical electronics, scientific instrumentation, and etc. The practical value of the work lies in the development of specific corpuscular-optical schemes intended for for the analysis of corpuscular flows.

References

1 Uglov V.V., Cherenda N.N., Anishchik V.M. Metody analiza elementnogo sostava poverkhnostnykh sloyev [Methods for analysis of the elemental composition of surface layers.]. - Minsk.: BGU, 2007. – 158 p. [in Russian]

2 Vudraf D., Delchar T. Sovremennyye metody issledovaniya poverkhnosti [Modern methods of surface research]. – Moscow: Mir, 1989. – 568 p. [in Russian]

3 Zigban K., Nordling T., Fal'man A., Nordberg R. Elektronnaya spektroskopiya [Electron spectroscopy]. – Moscow: Mir, 1971. – 493 p. [in Russian]

4 Silad'i M. Elektronnaya i ionnaya optika [Electron and ion optics]. – Moscow: Mir, 1990. – 639 p. [in Russian]

5 Glazer V. Osnovy elektronnoy optiki [Fundamentals of electron optics]. – Moscow: Gos.izd.tekhn.-teor. literatury, 1957. – 763 p. [in Russian]

6 Kozlov I.G. Metody energeticheskogo analiza elektronnykh potokov [Methods of energy analysis of electron flows]. - Moscow: Atomizdat, 1971. - 189 p. [in Russian]

7 Kul'ment'yev A.I., Kul'ment'yeva O.P. Metody analiza poverkhnosti tverdykh tel [Methods for analyzing the surface of solids]. - Sumy: SumGU, 2008. - 158 p. [in Russian]

8 Afanas'yev V.P. Elektronnaya i ionnaya spektroskopiya tverdykh tel [Electron and ion spectroscopy of solids] // Sorosovskiy Obrazovatel'nyy Zhurnal. – 1999. – V. 5, № 2. – pp.110–116. [in Russian]

9 Afanas'yev V.P., Yavor S.Ya. Elektrostaticheskiye energoanalizatory dlya puchkov zaryazhennykh chastits [Electrostatic energy analyzers for beams of charged particles]. - Moscow: Nauka, 1978. - 224 p. [in Russian]

10 Hamada Y., Fujisawa A., Iguchi H., Nishizawa A., Kawasumi Y. A tandem parallel plate analyzer // Rev. Sci. Instrum. – 1997. – Vol. 68, № 5. - pp.2020-2022.

11 Boumsellek S., Tuan V.N., Esaulov V.A. Electrostatic analyzer and optics for low – energy electron spectroscopy // Rev. Sci. Instrum. – 1990. – Vol. 61, № 7. - pp.1854-1857.

12 Yuan D., Kuo T., Cojocaru G., Jayamanna K., Mcdonald M., Schmor P., Yin Y. Design of a parallel-plate energy spread analyzer // Rev. Sci. Instrum. – 1998. – Vol.69, № 2. - pp. 1194-1196.
13 Calabrese D., Yenen O., Wiese L.M, Jaecks D. H. Two-stage parallel-plate energy analyzer for simultaneous detection of positive, negative, and neutral particles // Rev. Sci. Instrum. – 1994. - Vol. 65, № l. - pp.116-122.
14 Fishkova T.YA. Sistema monokhromatizatsii elektronnogo puchka [System of electron beam monochromatization] // Prikladnaya fizika. - 2011. - № 2. - pp. 33-36. [in Russian]
15 Ovsyannikova L.P., Fishkova T.Ya., Shpak Ye.V. Tsilindricheskoye zerkalo s zakrytymi tortsami dlya analiza po energii vtorichnykh puchkov zaryazhennykh chastits so skanirovaniyem poverkhnosti obraztsa [Cylindrical mirror with closed ends for energy analysis of secondary beams of charged particles with scanning of the sample surface] // Pis'ma v ZhTF – Technical Letters. – 1995. - V.21, № 21. - pp. 19-22. [in Russian]
16 Trubitsyn A.A. Novyy elektrostaticheskiy analizator s uglovym i energeticheskim razresheniyem [New electrostatic analyzer with angular and energy resolution] // Pis'ma v ZhTF – Technical Letters. - 1995. - V.21, № 13. - pp. 19-22. [in Russian]
17 Zashkvara V.V., Ashimbaeva B.U. Cylindrical mirror analyzer with adjustable angular focusing // J. Electron Spectrosc. Relat. Phenom. – 1998. - Vol. 94, is.1-2. – P.89-96.
18 Yi-sha Ku, Ching-shen Su. Design and performance of a cylindrical reflection mirror analyzer for low energy ion scattering studies // Rev.Sci.Instrum. -1991. - Vol.62, № 6. - P.1471-1474.
19 Read F.H., Cubric D., Kumashiro S., Walker A. The parallel cylindrical mirror analyzer: axis-to-axis configuration // Nuclear Instruments and Methods in Physics Research. – 2004. - № A 519. – P.338–344.
20 Zou Y., Cui Y., Yun V., Valfells A. and other. Compact high-resolution retarding field energy analyzer for space-charge-dominated electron beams // Phys.rev.special topics - accelerators and beams. – 2002. – Vol. 5, № 072801. - P.1-7.

21 Tokesi K., Kover L., Varga D. A modified distorted field electrostatic analyzer // Nuclear Instruments and Methods in Physics Research. - 1994. - № A 348. - P.173-176.
22 Ovsyannikova L. P., Fishkova T. YA. Elektrostaticheskiy energofil'tr s dvoynoy fokusirovkoy [Electrostatic energy filter with double focusing] // Prikladnaya fizika. – 2008. - №5. - pp. 86-88. [in Russian]
23 Bundaleski N., Rakocevic Z., Terzic I. Optical properties of the 127^0 cylindrical energy analyzer used in LEIS experiments // Nuclear Instruments and Methods in Physics Research. - 2002. - № B 198. - pp.208-219.
24 Iwamoto K., Matsumoto A. Ion energy loss spectroscopic apparatus using cylindrical electrostatic energy analyzer equipped with the Matsuda plate // Rev. Sci. Instrum. - 1997. - Vol. 68, № 8. - pp.3042-3045.
25 Fujisawa A., Iguchi H., Sasao M., Hamada Y. Second-order focusing property of 210^0 cylindrical energy analyzer // Rev. Sci. Instrum. –1995. – Vol. 66, № 3. - pp.2524- 2527.
26 Williams J.F., Chen X., Wilkie P. Miniature electrostatic electron energy analyzers and S-shaped deflector // Rev.Sci.Instrum. – 2008. – Vol 79, № 023104. - P.1-4.
27 Ishii K., Ohkawara H., Maeda Y., Katanuma I., Yatsu K., Miyoshi S. The energy component analyzer and spectrum analysis of end-loss ions in a tandem mirror // Rev. Sci. Instrum. – 1991. – Vol. 62, № 4. - P.899-905.
28 Read F.H. The parallel cylindrical mirror electron energy analyzer // Rev. Sci. Instrum. – 2002. – Vol. 73, № 3. - pp.1129-1139.
29 Rubio-Zuazo J., Escher M., Merkel M., Castro G.R. High Voltage-Cylinder Sector Analyzer 300/15: A cylindrical sector analyzer for electron kinetic energies up to 15 keV // Rev. Sci. Instrum. – 2010. – Vol. 81, № 043304. - pp.1-8.
30 Varga D., Tokesi K., Rajta I. Design of an electrostatic electron spectrometer for simultaneous energy and angular distribution measurements // J. Electron Spectrosc. Relat. Phenom. – 1995. – Vol. 76. - pp. 433- 436.

31 Teodorescu C. M., Gravel D., Ruhl E. and other. Retractable miniature double pass cylindrical mirror analyzers// Rev. Sci. Instrum. - 1998. - Vol. 69, № 11. - pp.3805-3808.
32 Petrov V.N., Kamochkin A.S. Energy analyzer for spin polarized Auger electron spectroscopy // Rev. Sci. Instrum. - 2004. - Vol. 75, № 5. - pp.1274-1279.
33 Kobayashi E., Seo J., Nambu A., Mase K. Development of a miniature double-pass cylindrical mirror electron energy analyzer (DPCMA), and its application to Auger photoelectron coincidence spectroscopy (APECS) // Surface Science. – 2007. – Vol. 601. – P. 3589–3592.
34 Koscielniak P., Kaszczyszyn S., Szuber J. A new type of electron energy analyzer based on three coaxial cylindrical electrodes for Auger electron spectroscopy // Vacuum. – 2001. – Vol. 63. - pp.361-66.
35 Dogan M., Sise O., Ulu M.. Design of electron energy analyzers for electron impact studies // Radiation Physics and Chemistry. – 2007. – Vol. 76. – P. 445–449.
36 Davydov S.N., Danilov M.M., Korablev V.V. Sfericheskoye zerkalo kak instrument dlya elektronnoy spektroskopii sovpadeniy [Spherical mirror as a tool for electronic coincidence spectroscopy] // Zhurnal tekhnicheskoy fiziki. – 1999. - V.69, № 1. - pp.109-113. [in Russian]
37 Berntsen M.H., Palmgren P., Leandersson M. and other. A spin- and angle-resolving photoelectron spectrometer// Rev. Sci. Instrum. – 2010. – Vol. 81, №035104. - pp.1-5.
38 Belov V.D., Yavor M.I. High-resolution energy analyzer for photoelectron diffraction studies // Nuclear Instruments and Methods in Physics Research. – 2007. -№ A 575. – P. 262–265.
39 Baraldi A., Dhanak V.R. Design study of a double pass hemispherical electron energy analyser with multichannel detection // J. Electron Spectrosc. Relat. Phenom. - 1994. - Vol. 67. – P. 211-220.
40 Zashkvara V.V., Il'in A.M., Kryuchkov V.F. Dva sluchaya fokusirovki osesimmetrichnogo puchka zaryazhennykh chastits v giperbolicheskom pole [Two cases of focusing of an axisymmetric beam of charged particles in a hyperbolic field] // Zhurnal tekhnicheskoy fiziki. – 1976. - V.46. - pp.1572-1573. [in Russian]

41 Mamontov Ye.V., Ivlev D.A. Giperboloidnyy mass-spektrometr na usechennoy lovushke [Hyperboloid mass spectrometer on a truncated trap] // Pis'ma v ZhTF. – 1999. - V.25., №. 10. - pp. 51-56.[in Russian]
42 Jacka M., Kirk M., El Gomati M. M., Prutton M. A fast, parallel acquisition, electron energy analyzer: The hyperbolic field analyzer // Rev. Sci. Instrum. – 1999. - Vol. 70, № 5. - pp.2282-2287.
43 Jacka M., Kale A., Traitler N. Hyperbolic field electron energy analyzer with second order focusing // Rev. Sci. Instrum. – 2003. – Vol.74, № 10. - pp.4298-4300.
44 Iwasaki K., Mitsuke K. Development of a conical energy analyzer for angle-resolved photoelectron spectroscopy // Surface Review and Letters. – 2002. – Vol. 9, № 1. – P. 583-586.
45 Khursheed A. Design of a parallel magnetic box energy analyzer attachment for electron microscopes // J. Electron Spectrosc. Relat. Phenom. -2011. – Vol. 184. – P.57-61.
46 Miron C., Simon M., Leclercq N., Morin P. New high luminosity «double toroidal» electron spectrometer // Rev. Sci. Instrum. – 1997. – Vol. 68, № 10. - pp. 3728-3737.
47 Nishimura T., Ikeda A., Kido Y. A new toroidal electrostatic analyzer and application to surface analysis // Rev. Sci. Instrum. – 1998. – Vol. 69, № 4, - pp.1671-1675.
48 Belov V.D., Yavor M.I. New type of high-resolution high-transmission energy analyzers based on toroidal mirrors // J. Electron Spectrosc. Relat. Phenom. – 1999. - Vol. 104. – P. 47-54.
49 Tadich A., Riley J., Huwald E. and other. Full Hemisphere Fermi Surface Mapping Using A Novel Toroidal Electron Spectrometer // The 10th International Conference on Synchrotron Radiation Instrumentation. – Melbourne, 2009. - 943p.
50 Trubitsyn A.A. Modelirovaniye ionno-opticheskikh sistem dlya mass-spektrmetrov s kvadrupol'nym fil'trom mass [Simulation of ion-optical systems for mass spectrometers with a quadrupole mass filter]// Zhurnal tekhnicheskoy fiziki (Kratkiye soobshcheniya). -2003. - V.73, №.6. - pp. 136-137. [in Russian]
51 Le Guen K., Ceolin D., Guillemin R. and other. Development of a four-element conical electron lens dedicated to high resolution

Auger electron–ion(s) coincidence experiments // Rev. Sci. Instrum. – 2002. - Vol. 73, № 11. - pp.3885-3894.
52 Belov V.D. Immersionnyye linzy v aksial'no-simmetrichnykh elektrostaticheskikh sistemakh sfericheskogo sektornogo deflektora s prostranstvennoy fokusirovkoy vtorogo poryadka [Immersion lenses in axially symmetric electrostatic systems of a spherical sector deflector with second-order spatial focusing] // Nauchnoye priborostroyeniye. – 2006. - V.16, № 4. - pp. 31-40. [in Russian]
53 Fishkova T.Ya. Kombinirovannaya elektrostaticheskaya linza [Combined electrostatic lens] // Pis'ma v ZhTF. – 2009. - V.35, №9. - pp. 31-36. [in Russian]
54 Zashkvara V.V., Ashimbaeva B.U. Time-of-flight focusing in a system consisting of electrostatic mirrors with two-dimensional fields// Nuclear Instruments and Methods in Physics Research. – 1995. – № A 364, is.3. – P.401-408.
55 Hansch P., Norby J.R., Evans S.H., Van Woerkom L.D. An ellipsoidal mirror time-of-flight photoelectron energy analyzer // Rev. Sci. Instrum. - 1995. – Vol.66, № 12. - pp.5512-5515.
56 Semkin N.D., Piyakov I.V., Voronov K.Ye., Pomel'nikov R.A. Perspektivy razvitiya vremyaproletnykh mass-spektrometrov dlya analiza gazovykh i pylevykh chastits [Prospects for the development of time-of-flight mass spectrometers for the analysis of gas and dust particles] // Prikladnaya fizika. – 2002. - № 2. - pp. 124-141. [in Russian]
57 Verenchikov A.N., Yavor M.I., Khasin YU.I., Gavrik M.A. Mnogootrazhatel'nyy planarnyy vremyaproletnyy mass-analizator I. Analizator dlya parallel'nogo tandemnogo spektrometra [Multireflective planar time-of-flight mass analyzer I. Analyzer for a parallel tandem spectrometer] // Zhurnal tekhnicheskoy fiziki. – 2005. - V.75, № 1. - pp.74-83. [in Russian]
58 Hilbert A., Barwick B., Fabrikant M., Uiterwaal C.J.G.J., Batelaan H.. A high repetition rate time-of-flight electron energy analyzer // Applied physics letters. - 2007. – Vol. 91, № 173506. - pp.1-3.
59 Zashkvara V.V., Masyagin V.E., Ashimbaeva B.U., Kovalik A. and other. Verification of focusing properties of the multicascade

electrostatic analyzer // J. Electron Spectrosc. Relat. Phenom. – 1995. - Vol. 71. – P.87 – 92.
60 Ovsyannikova L.P., Fishkova T.YA. Magnitostaticheskiy mass-analizator tipa ploskogo zerkala s fokusirovkoy vtorogo poryadka [Magnetostatic mass analyzer of the flat mirror type with second-order focusing] // Pis'ma ZhTF. – 2002. - V.28, № 4. - pp.65-70. [in Russian]
61 Trubitsyn A.A. Cylindrical mirror analyzer with high energy resolution // J. Electron Spectrosc. Relat. Phenom. – 1995. – Vol.73. – P. 305-310.
62 Ovsyannikova L.P., Fishkova T.YA. Elektrostaticheskiy spektrograf v vide usechennogo tsilindra [Electrostatic spectrograph in the form of a truncated cylinder] // Zhurnal tekhnicheskoy fiziki. – 2001. - V.71 (11) - pp.133-135. [in Russian]
63 Belov V.D., Yavor M.I. High-resolution energy analyzer with a large angular acceptance for photoelectron spectromicroscopy applications// Rev. Sci. Instrum. – 2000. - Vol. 71, № 4. - P.1651-1655.
64 Downie P., Reynolds D.J., Powis I. Parallel, multichannel energy and angle resolving electrostatic electron analyzer // Rev. Sci. Instrum. - 1995. – Vol. 66, № 7. - pp.3807-3818.
65 Kienle M., Plies E. An off-axis multi-channel analyzer for secondary electrons // Nuclear Instruments and Methods in Physics Research. – 2004. - № A519. – P. 325–330.
66 David D.E., Popovic D.B., Antic D., Michl J. A multichannel electron energy loss spectrometer for low-temperature condensed films //J. of Chem.Phys. - 2004. – Vol. 121, № 21, - pp.10542 -10550.
67 Ovsyannikova L.P., Fishkova T.YA. Mnogokanal'nyy energofil'tr v vide tsilindra s zakrytymi tortsami i osevym nitevidnym elektrodom [Multichannel energy filter in the form of a cylinder with closed ends and an axial filamentous electrode] // Pis'ma ZhTF. – 2004. - V.30 (20). - pp.25-29. [in Russian]
68 Cizmar P., Müllerová I., Jacka M., Pratt A. New multichannel electron energy analyzer with cylindrically symmetrical electrostatic field // Rev. Sci. Instrum. - 2007. - Vol. 78, № 053714. - pp.1-5.
69 Tepermeister I., Sawin H.H. Modeling and construction of a novel electron energy analyzer for rapid X-ray photoelectron

spectroscopy spectra acquisition // Rev. Sci. Instrum. – 1992. –Vol. 83, № 8. - pp.3828- 3834.
70 Hu D.Q., Leung K.T. Simion study of the fringing field effects in deflector-type electrostatic electron energy analyzers: A new flexible Jost-based correction scheme // Rev. Sci. Instrum. – 1995. – Vol. 66, № 4. - pp.2865-2870.
71 Kelly M.A. A new electron energy analyzer for electron spectroscopy // J. Electron Spectrosc. Relat. Phenom. - 1999. - Vol. 98–99. – P.55–66.
72 Shiraki S., Ishii H., Nihei Y. Development of a high-performance angle-resolving electron energy analyzer // J. Electron Spectrosc. Relat. Phenom. – 2001. -Vol. 114-116. – P. 1043–1048.
73 Nandi T., Ahmad N., Singh H.K., Pillay R.G. Inclined straight electrostatic analyzer // Rev. Sci. Instrum. – 2004. – Vol. 75, № 11. - pp.5041-5043.
74 Vorob'yev G.S., Drozdenko A.A., Nagornyy D.A. Ustanovka dlya izmereniya staticheskikh kharakteristik vysokointensivnykh elektronnykh puchkov [Installation for measuring the static characteristics of high-intensity electron beams] // Pribory i tekhnika eksperimenta. – 2009. - № 1. - pp. 115-118. [in Russian]
75 Mar'in B.V., Polandov A.G. Segmentoidnyye elektrostaticheskiye analizatory dlya registratsii nizkoenergichnykh zaryazhennykh chastits [Segmentoid electrostatic analyzers for detecting low-energy charged particles] // Pribory i tekhnika eksperimenta. – 2002. – № 3. - pp. 73-77. [in Russian]
76 Golikov YU.K. Opredeleniye elektrostaticheskikh poley po zadannym kharakteristikam dvizheniya zaryazhennykh i dipol'nykh chastits [Determination of electrostatic fields according to the given characteristics of the movement of charged and dipole particles]: abstract of the thesis. … Dr. phys.-math. Sciences: 01.04.04. - Leningrad, 1985. - 20 p. [in Russian]
77 Golikov YU.K., Utkin K.G., Cheparukhin V.V. Raschet elementov elektrostaticheskikh elektronno-opticheskikh system [Calculation of elements of electrostatic electron-optical systems]. - Leningrad: LPI, 1984. - 78 p. [in Russian]

78 Zashkvara V.V., Tyndyk N.N. Electrostatic axially symmetric multipole in deflector-type analyzers // Nuclear Instruments & Methods in Physics Research. – 1992. – № A 313. – P. 315-327.
79 Zashkvara V.V., Tyndyk N.N. Axially symmetric multipole in magnetic analyzers // Nuclear Instruments & Methods in Physics Research. – 1992. – № A 321. – P. 439-446.
80 Zashkvara V.V., Tyndyk N.N. Two-sector electrostatic deflector based on superposition of cylindrical field and axially symmetric multipoles // Nuclear Instruments & Methods in Physics Research. – 1993. – № A 328. – P. 416-434.
81 Zashkvara V.V., Tyndyk N.N. Osesimmetrichnyye elektrostaticheskiye mul'tipoli, ikh prilozheniye [Axially-symmetric electrostatic multipoles, their application] // Zhurnal tekhnicheskoy fiziki. – 1991. – V.61, №4. – pp.148-157. [in Russian]
82 Zashkvara V.V., Tyndyk N.N. Mul'tipol'nyye resheniya volnovogo uravneniya [Multipole solutions of the wave equation] // Zhurnal tekhnicheskoy fiziki. – 1998. - V.68, № 6. - pp.9-14. [in Russian]
83 Zashkvara V.V. On circular multipole calculations // Nuclear Instruments & Methods in Physics Research. – 1995. – № A 354. – P. 171-174.
84 Zashkvara V.V., Tyndyk N.N. Nelaplasovy krugovyye mul'tipoli [Non-Laplace circular multipoles] // Zhurnal tekhnicheskoy fiziki. - 1995. - V.65, Issue. 7. - pp.154-1666. [in Russian]
85 Zashkvara V.V., Tyndyk N.N. Potential fields based on circular multipole series // Nuclear Instruments & Methods in Physics Research. – 1996. – № A 370. – P. 452-460.
86 Zashkvara V.V., Tyndyk N.N. The method for the calculation of multipole-cylindrical fields // Nuclear Instruments & Methods in Physics Research. – 1999. – № A 370. – P. 223-231.
87 Spivak-Lavrov I.F. Resheniye zadachi Dirikhle dlya uravneniya Laplasa v sluchaye mnogosvyaznoy oblasti s tochechnoy simmetriyey [Solution of the Dirichlet problem for the Laplace equation in the case of a multiply connected domain with point symmetry] // Zhurnal tekhnicheskoy fiziki. – 1999. - V.69 (3). - pp. 1 - 9. [in Russian]

88 Zashkvara V.V., Ashimbaeva B.U.,.Chokin K.Sh. Calculation of trajectories in a multipole cylindrical field // J. Electron Spectrosc. Relat. Phenom. - 2002. – Vol.122. - pp.195-202.
89 Zashkvara V.V., Ashimbayeva B.U., Chokin K.SH., Masyagin V.Ye. Raschet trayektoriy zaryazhennykh chastits v elektrostaticheskom neodnorodnom pole [Calculation of the trajectories of charged particles in an electrostatic inhomogeneous field]// Izvestiya NAN RK, Ser.fiz.-mat. - 2000. - №2.- pp.72-78. [in Russian]
90 Golikov Yu.K., Grigor'yev D.V., Shorina T.A. Elektricheskiye polya s kol'tsevymi osobennostyami v korpuskulyarnoy optike [Electric fields with ring singularities in corpuscular optics] // Pis'ma v ZhTF. – 1999. - V. 25 (9). - pp. 23-27. [in Russian]
91 Golikov Yu.K., Utkin K.G., Grigor'yev D.V. Obratnyye zadachi teorii elektrostaticheskikh energoanalizatorov. I [Inverse problems of the theory of electrostatic energy analyzers. I] // Zhurnal tekhnicheskoy fiziki. – 1999. - V.69 (9). - pp. 128-131. [in Russian]
92 Gabdullin P.G., Golikov Yu.K., Krasnova N.K., Davydov S.N. Primeneniye formuly Donkina v teorii energoanalizatorov. I [Application of the Donkin formula in the theory of energy analyzers. I] // Zhurnal tekhnicheskoy fiziki. – 2000. - V.70 (2). - pp. 91-94. [in Russian]
93 Gabdullin P.G., Golikov Yu.K., Krasnova N.K., Davydov S.N. Primeneniye formuly Donkina v teorii energoanalizatorov. II [Application of the Donkin formula in the theory of energy analyzers. II] // Zhurnal tekhnicheskoy fiziki. – 2000. - V.70 (3). - pp. 44-47. [in Russian]
94 Golikov Yu.K., Krasnova N.K. Elektricheskiye polya, odnorodnyye po Eyleru, dlya elektronnoy spektrografii [Euler-homogeneous electric fields for electron spectrography] // Zhurnal tekhnicheskoy fiziki. – 2011. - V. 81 (2). - pp.9-15. [in Russian]
95 Golikov Yu. K., Krasnova N. K., Solov'yev K. V., Grigor'yev D. V. O nekotorykh analiticheskikh svyazyakh osesimmetrichnykh i dvukhmernykh laplasovykh poley [On some analytical relationships between axisymmetric and two-dimensional Laplacian fields] // Prikladnaya fizika. – 2004. - №1. - pp.48-49. [in Russian]

96 Golikov Yu.K., Krasnova N.K., Solov'yev K.V. Trekhmernyye laplasovy potentsialy s kompleksnym predstavleniyem [Three-dimensional Laplacian potentials with complex representation] // Zhurnal tekhnicheskoy fiziki. – 2006. -V. 76 (1). - pp. 24-27. [in Russian]
97 Golikov Yu. K., Solov'yev K.V. Novyye analiticheskiye predstavleniya mul'tipol'nykh elektromagnitnykh struktur [New analytical representations of multipole electromagnetic structures] // Prikladnaya fizika. – 2006. – №6. - pp.5-7. [in Russian]
98 Zashkvara V.V., Ashimbaeva B.U., Chokin K. Sh., Rysavy M. Effect of the fringe field of one-dimensional aperture gratings on the transmission and focusing of the cylindrical mirror analyzer // J. Electron Spectrosc. Relat. Phenom. – 1992. - Vol.58. – P. 271 – 283.
99 Ovsyannikova L.P., Fishkova T.Ya. Dvukhperiodnyy tsilindricheskiy energoanalizator s tortsevymi elektrodami [Two-period cylindrical energy analyzer with end electrodes] // Zhurnal tekhnicheskoy fiziki. - 1997. - V.67, No. 8. - pp. 89-91. [in Russian]
100 Yavor S.Ya. Fokusirovka puchkov zaryazhennykh chastits s raspredeleniyem energii po secheniyu v dispergiruyushchikh sistemakh [Focusing of beams of charged particles with energy distribution over the cross section in dispersive systems] // Zhurnal tekhnicheskoy fiziki. - 1997. - V.67, No. 12. - pp.50-53. [in Russian]
101 Yavor S.Ya. Fokusirovka puchkov zaryazhennykh chastits s energouglovoy korrelyatsiyey v ploskom kondensatore [Focusing of beams of charged particles with energy-angle correlation in a flat capacitor] // Zhurnal tekhnicheskoy fiziki. - 1998. - V.68, No. 10. - pp.138-139. [in Russian]
102 Golikov Yu. K., Krasnova N. K., Solov'yev K. V., Grigor'yev D. V., Lyubchich A.D. Soglasuyushchiye i korrektiruyushchiye elektricheskiye zerkala v elektronnoy optike [Matching and correcting electric mirrors in electron optics] // Prikladnaya fizika. - 2002. - № 3. - pp. 55-67. [in Russian]
103 Golikov Yu.K., Kholin N.A., Shorina T.A. Teoriya i praktika kvazikonicheskikh energoanalizatorov [Theory and practice of quasi-conical energy analyzers] // Nauchnoye priborostroyeniye. – 2009. - V.19, №2. - pp. 13-24. [in Russian]

104 Tsuno K. Electron optical analysis of a high-resolution electron energy loss spectrometer with a retarding Wien filter // Rev. sci. instrum. – 1992. – Vol. 63, № 9. - pp.4112-4121.
105 Mattel R., McBreen P. H. Optimization of the geometric disposition of the deflecting electrodes in HREELS spectrometers // Rev. sci. instrum. - 1992. – Vol.63, № 5. - P.3007-3012.
106 Glikman L.G., Goloskokov Yu.V., Karetskaya S.P. K teorii fokusirovki puchkov zaryazhennykh chastits v dvumernom elektrostaticheskom pole so sredney ploskost'yu I [On the theory of focusing beams of charged particles in a two-dimensional electrostatic field with a mean plane I] // Zhurnal tekhnicheskoy fiziki. – 1996. - V.66, №5. - pp. 118-127. [in Russian]
107 Demin S.K., Safronov S.I., Tarasov R.P. Chislennyy analiz i sintez elektronno-opticheskikh sistem slozhnoy struktury I [Numerical analysis and synthesis of electron-optical systems of complex structure I] // Zhurnal tekhnicheskoy fiziki. - 1998. - V.68, №2. - pp.97-103. [in Russian]
108 Yavor M.I. Raschet fokusirovki i aberratsiy puchkov zaryazhennykh chastits v polyarno-toroidal'nykh analizatorakh [Calculation of focusing and aberrations of charged particle beams in polar-toroidal analyzers] // Zhurnal tekhnicheskoy fiziki. – 1998. - V. 68, № 4. - pp.107-111. [in Russian]
109 Duglas D.Dzh., Glebova T.A., Konenkov N.V., Sudakov M.YU. Prostranstvennyye garmoniki polya kvadrupol'nogo fil'tra mass s kruglymi elektrodami [Spatial harmonics of the field of a quadrupole mass filter with round electrodes]// Zhurnal tekhnicheskoy fiziki. - 1999. - V.69, No.10. - pp. 96-101. [in Russian]
110 Ovsyannikova L.P., Fishkova T.YA. Nagruzochnyye kharakteristiki elektrostaticheskoy koaksial'noy linzy [Load characteristics of an electrostatic coaxial lens] // Zhurnal tekhnicheskoy fiziki. – 1999. - V.69, No.6. - pp. 123-126. [in Russian]
111 Ovsyannikova L.P., Fishkova T.Ya. Mass-analizator zerkal'nogo tipa s tsilindricheskoy formoy polyusov [Mirror-type mass analyzer with cylindrical poles] // Zhurnal tekhnicheskoy fiziki (kratkiye soobshcheniya). – 2002. - V.72, No.10. - pp.119-123. [in Russian]
112 Ovsyannikova L.P., Fishkova T.Ya. Energoanalizator s tsilindricheskoy formoy elektrodov [Energy analyzer with a

cylindrical shape of electrodes] // Pis'ma ZhTF. - 2004. - V.30, No.7. - pp.36-41. [in Russian]
113 Sagara T., Boesten L., Nishida S., Okada K. Resolution improvements for hemispherical energy analyzers// Rev. sci. instrum. – 2000. - Vol.71, № 11. - pp.4201-4207.
114 Kugeler O., Marburger S., Hergenhahn U. Calculation and measurement of the time-of-flight spread in a hemispherical electron energy analyzer // Rev. sci. instrum. – 2003. – Vol. 74, № 9. - pp.3955-3961.
115 Kurnayev V.A., Urusov V.A. Vliyaniye apparatnykh funktsiy elektrostaticheskikh i magnitnykh analizatorov na obrabotku eksperimental'nykh rezul'tatov [Influence of hardware functions of electrostatic and magnetic analyzers on the processing of experimental results] // Zhurnal tekhnicheskoy fiziki. – 1997. - V.67, № 6. - pp. 86-91. [in Russian]
116 Kurnayev V.A., Urusov V.A. Vliyaniye fluktuatsiy potentsialov na apparatnyye funktsii elektrostaticheskikh analizatorov [Influence of potential fluctuations on the instrumental functions of electrostatic analyzers] // Zhurnal tekhnicheskoy fiziki. – 1997. - V.67, № 6. - pp. 92-95. [in Russian]
117 Shevchenko S.I. Nekotoryye aspekty raboty energoanalizatora tipa tsilindricheskoye zerkalo. Ch. I. [Some aspects of the operation of an energy analyzer of the cylindrical mirror type. Part I] // Nauchnoye priborostroyeniye. – 2011. - V.21, № 1. - pp. 76-86. [in Russian]
118 Shevchenko S.I. Ob osobennostyakh nakhozhdeniya aksial'nykh elektrostaticheskikh poley vblizi osi. II. Metod analiticheskoy zameny [On the features of finding axial electrostatic fields near the axis. II. Method of analytical replacement] // Nauchnoye priborostroyeniye. – 2009. - V.19, № 1. - pp. 58-66. [in Russian]
119 Shevchenko S.I. Metod vychisleniya apparatnoy funktsii aksial'nykh elektrostaticheskikh energoanalizatorov [Method for calculating the instrumental function of axial electrostatic energy analyzers] // Nauchnoye priborostroyeniye. – 2010. - V.20, № 2. - pp. 73-81. [in Russian]
120 Grinfel'd D.E., Monastyrskiy M.A., Tarasov V.A. Metody vozmushcheniy v zadachakh [Perturbation methods in problems] // Prikladnaya fizika. – 2006. - № 3. - pp.64-74. [in Russian]

121 Protopopov O.D., Trubitsyn A.A. Quasi-conical energy analyzers for electron spectroscopy // J. Electron Spectrosc. Relat. Phenom. – 1994. – Vol. 69. - pp.159-163.
122 Trubitsyn A.A. Korrelyatsionnyy metod poiska uglovoy fokusirovki vysshikh poryadkov [Correlation method for searching for higher-order angular focusing] // Zhurnal tekhnicheskoy fiziki. – 2001. - V. 71, No. 5. - pp. 126-127. [in Russian]
123 Trubitsyn A.A. Programma "Focus" modelirovaniya aksial'no-simmetrichnykh elektronno-opticheskikh sistem: algoritmy i kharakteristiki ["Focus" program for modeling axially-symmetric electron-optical systems: algorithms and characteristics] // Prikladnaya fizika. – 2008. - №2. - pp.56-61. [in Russian]
124 Astakhov V.I., Dyagilev A.A., Trubitsyn A.A. Programmnyy kompleks "Focus Planar System" dlya modelirovaniya planarnykh elektronno- i ionno-opticheskikh sistem [Software package "Focus Planar System" for modeling planar electron- and ion-optical systems] // Prikladnaya fizika. – 2010. - №5. - pp.66-72. [in Russian]
125 Gurov V.S., Trubitsyn A.A., Mamontov Ye.V., Dyagilev A.A. Resheniye ploskoy vneshney zadachi Dirikhle metodom granichnykh elementov [Solving the Plane External Dirichlet Problem by the Boundary Element Method] // Vestnik RGRTU. - 2008. - № 2, No. 24. - pp. 91-94. [in Russian]
126 Skuntsev A.A., Trubitsyn A.A. Chislennyy metod poiska usloviy prostranstvennoy fokusirovki vysshikh poryadkov [Numerical method of searching for conditions of spatial focusing of higher orders] // Vestnik RGRTU. - 2009. - V. 30, № 4, - pp. 40. [in Russian]
127 Pomozov T.V., Yavor M.I. Ustraneniye osevogo astigmatizma v krayevykh polyakh sfericheskogo sektornogo deflektora [Elimination of axial astigmatism in the marginal fields of a spherical sector deflector] // Nauchnoye priborostroyeniye. – 2008. - V.18, №4. - pp. 120-123. [in Russian]
128 Kholin N.A., Shorina T.A., Kubrik D. Ot kvazikonicheskikh energoanalizatorov k sferoidal'nym [From quasi-conical energy analyzers to spheroidal ones] // Nauchnoye priborostroyeniye. – 2009. - V.19, № 2. - pp. 25-33. [in Russian]
129 Baysanov O.A., Doskeyev G.A., Zaripova Z.G., Spivak-Lavrov I.F. Differentsial'nyye uravneniya, opredelyayushchiye otkloneniye

chastits ionnogo puchka ot osevoy trayektorii v elektricheskikh i magnitnykh polyakh [Differential Equations Determining the Deviation of Ion Beam Particles from the Axial Trajectory in Electric and Magnetic Fields] // Prikladnaya fizika. – 2010. - V.3. - pp.109-115. [in Russian]
130 Sise O., Ulu M., Dogan M., Martinez G., Zouros T.J.M. Fringing field optimization of hemispherical deflector analyzers using BEM and FDM // J. Electron Spectrosc. Relat. Phenom. – 2010. – Vol. 177. - pp. 42–51.
131 Semenov S.O. Nekotoryye osobennosti rascheta trayektoriy zaryazhennykh chastits na setke potentsialov metoda konechnykh elementov [Some features of the calculation of charged particle trajectories on the potential grid of the finite element method] // Prikladnaya fizika. - 2010. - V.3. - pp.96-102. [in Russian]
132 Krasnova N.K. Dvumernyye stepennyye elektronnyye spektrografy s ploskost'yu simmetrii [Two-dimensional power electronic spectrographs with a plane of symmetry] // Zhurnal tekhnicheskoy fiziki. – 2011. - V.81, No.6. - pp. 97-103. [in Russian]
133 Badalyan G.V. Polucheniye postoyannykh elektricheskikh poley zadannoy formy v neyavnoelektrodnoy sisteme [Obtaining constant electric fields of a given form in an implicit electrode system] // Zhurnal tekhnicheskoy fiziki. – 2011. – V.81, No.1. - pp.140-143. [in Russian]
134 Zashkvara V.V., Tyndyk N.N. Nelaplasovy krugovyye mul'tipoli [Non-Laplace circular multipoles] // Zhurnal tekhnicheskoy fiziki - Journal of technical physics. – 1995. – Vol.65, № 7. – pp.154-166. [in Russian]
135 Zashkvara V.V., Tyndyk N.N. Electrostatic axially symmetric multipole in deflector-type analyzers // Nuclear Instruments & Methods in Physics Research. – 1992. – № A313. – P. 315-327.
136 Zashkvara V.V., Tyndyk N.N. Axially symmetric multipole in magnetic analyzers // Nuclear Instruments & Methods in Physics Research. – 1992. – № A321. – P. 439-446.
137 Saulebekov A.O., Trubitsyn A.A., Kambarova Zh.T. Calculation of electron-optical characteristics of a quadrupole-cylindrical field // Bulletin of the Karaganda University. «Physics» series. - 2019. - № 1 (93). – P. 87-93.

138 Saulebekov A.O., Kambarova Zh.T. Analyzer of charged particles based on the electrostatic quadrupole-cylindrical field in the «axis-ring» focusing regime // Proceedings - 2020 7th International Congress on Energy Fluxes and Radiation Effects. 2020. – P. 1031-1033.
139 Utility model patent № 4237. Axially symmetric electrostatic energy analyzer, Kazakhstan, 05/20/2019; publ.16.08.2019, Bull. No. 33. Kambarova Zh.T., Saulebekov A.O.
140 Assylbekova S.N., Kambarova Zh.T., Saulebekov A.O. Numerical modeling of the electrostatic energy analyzer based on hexapole-cylindrical field with a concave outer electrode// Eurasian Physical Technical Journal. – 2015. - V.12, No 1 (23). – P.25-29.
141 Ashimbayeva B.U., Chokin K.SH., Saulebekov A.O., Kambarova Zh.T. Modelirovaniye elektronno-opticheskoy skhemy analizatora s geksapol'no-tsilindricheskim polem [Modeling of the electron-optical scheme of an analyzer with a hexapole-cylindrical field] // Prikladnaya fizika - Applied Physics. - 2012. - № 2. – pp. 45-48. [in Russian]
142 Innovative patent of the Republic of Kazakhstan №30885, registered 08.01.2016, bulletin №1, 15.01.2016. Author's certificate №91534 «Electrostatic energy analyzer of charged particles» / Saulebekov A.O., Ashimbayeva B.U., Kambarova Zh.T.
143 Kambarova Zh.T., Saulebekov A.O., Kopbalina K.B. Calculation of the electron-optical scheme of a new type mirror energy analyzer of charged particles // Bulletin of the Karaganda University. «Physics» series. – 2022. – №2 (106). – pp.49-57. doi: 10.31489/2022PH2/49-57.
144 Saulebekov A.O., Kambarova Zh.T., Saulebekova D.A. Modeling of electrostatic decapole-cylindrical mirror analyzer// IOP Conf. Series: Materials Science and Engineering. - 2017. – V. 168. – 012078. doi:10.1088/1757-899X/168/1/012078
145 Kambarova Zh.T. Trubitsyn A.A., Saulebekov A.O.Axially symmetric energy analyzer based on the electrostatic decapole-cylindrical field Technical Physics. –2018. - V.63. - No.11. - P.1667–1671. https://doi.org/10.1134/S106378421811014
146 Innovative patent of the Republic of Kazakhstan №30476, зарегистрировано 23.09.2015, bulletin №10, 15.10.2015. Author's

certificate №90020. Electrostatic particle energy analyzer / Saulebekov A.O., Ashimbayeva B.U., Kambarova Zh.T.
147 Kambarova Zh.T. Modelirovaniye elektrostaticheskikh analizatorov energiy zaryazhennykh chastits [Modeling of electrostatic energy analyzers of charged particles]. Monograph. Karaganda: Publishing house of KSU, 2019. - 141 p. [in Russian]
148 Kambarova Zh. T. Design and calculation of high-luminosity corpuscular-optical systems based on electrostatic fields. Monograph. Karaganda: LLP "Typography Arko", 2020. -131 p. [in Kazakh]
149 Gurov V.S., Saulebekov A.O., Trubitsyn A.A. Advances in imaging and electron physics. Analytical, Approximate-Analytical and Numerical Methods in the Design of Energy Analyzers / Editor-in-chief Peter W. Hawkes CEMES-CNRS Toulouse, France. - Academic Press is an imprint of Elsevier, 2015. – V.192. - 224 p. (Монография).
150 Saulebekov A.O., Venos D., Kambarova Zh.T. The high resolution electrostatic energy analyzer for space research. Eurasian Physical Technical Journal, 2020, V.17(33). – pp.163-168.
151 Kambarova Zh.T., Saulebekov A.O., Kopbalina K.B., Tussupbekova A.K., Saulebekova D.A. About the possibility of creating an efficient energy analyzer of charged particle beams based on axially-symmetrical octupole-cylindrical field // Eurasian Physical Technical Journal. – 2021. – Vol.18, No.2 (36). - pp. 96-102.
152 Kambarova Zh.T., Saulebekov A.O., Kopbalina K.B. Calculation of the electron-optical scheme of a new type mirror energy analyzer of charged particles // Bulletin of the Karaganda University. «Physics» series. – 2022. – №2 (106). – pp.49-57. doi: 10.31489/2022PH2/49-57.
153 Trubitsyn A., Grachev E., Gurov V., Bochkov I., Bochkov V., Proceedings of SPIE., 10250, 0V-1, 2017; doi: 10.1117/12.2256570
154 Kambarova Zh.T., Saulebekov A.O., Kopbalina K.B. The electron-optical scheme of the energy analyzer of small-sized electron spectrometer // Abstracts of 20th International Conference on Radiation Physics and Chemistry of Condensed Matter Methods, instruments and equipment for physicochemical studies (EFRE 2022), October 2 - 8, 2022, Tomsk, Russia. - R5-P-003102.

155 Utility model patent “Electrostatic mirror type energy analyzer” № 7085, Kazakhstan, 28.02.2022, Registration number 2022/0163.2 Kambarova Zh.T., Saulebekov A.O.
156 Neugebauer M., Snyder C.W. The Mission of Mariner II: Preliminary Observations, Solar Plasma Experiment // Science. 1962. - Vol. 138, No. 3545. - pp. 1095-1097.
157 O'Brien B.J., Abney F., Burch J., Harrison J. et al. SPECS, a Versalite Space - Qualified Detector of Charged Particles // Rev. Sci. Instrum. - 1967. - Vol.38, N 8. -pp. 1058-1063.
158 Wolfe, John H., et al. The compositional, anisotropic, and nonradial flow characteristics of the solar wind // Journal of Geophysical Research.- 1966. – Vol.71. – pp. 3329-3335.
159 Paschmann G. et al. The Plasma Instrument for AMPTE IRM. // IEEE Transactions on Geoscience and Remote Sensing GE-23. – 1985. – pp. 262-266.
160 Machida Shinobu, et al. Instrumental characteristics of the Electron Spectrum Analyzer (ESA) onboard the Planet-B mission and observational perspectives of the electron measurements // Earth, Planets and Space. - 1998. – Vol.50. - pp 207-211.
161 Kazama Y. 2013. Designing a toroidal top-hat energy analyzer for low-energy electron measurement, An Introduction to Space Instrumentation, Ed. K. Oyama & C.Z. Cheng, 181–192.
162 Li C., Wang Y., Zhang H., Li S., Liu Z., Zhao C. The analyzer constant of top hat electrostatic analyzer: Comparison between theory and simulations // Journal of Instrumentation. – 2018. –Vol.13(12) P12027-P12027. doi: 10.1088/1748-0221/13/12/P12027.
163 Allegrini, Frédéric et al. The entrance system laboratory prototype for an advanced mass and ionic charge composition experiment // The Review of scientific instruments. 2009. – Vol. 80 (10). – pp. 104502.
164 Victor, Allen L. et al. Top hat electrostatic analyzer for far-field electric propulsion plume diagnostics // Review of Scientific Instruments. - 2006. – Vol. 77. – p. 013505.
165 Fernandes, Philip A and Kristina A. Lynch. Electrostatic analyzer measurements of ionospheric thermal ion populations // Journal of Geophysical Research: Space Physics.- 2016. – Vol.121. - pp. 7316 - 7325.

166 Collinson Glyn A., et al. “A hybrid electrostatic retarding potential analyzer for the measurement of plasmas at extremely high energy resolution // The Review of scientific instruments. – 2018. – Vol.89, № 11. – pp.113306.
167 Andrews G.B., et al. The Energetic Particle and Plasma Spectrometer Instrument on the MESSENGER Spacecraft //Space Sci. Rev. - 2007. – Vol. 131. - pp. 523-556.
168 Vaisberg O.L. Advanced method for exploration of plasma velocity distribution funtions: All-sky camera for very fast plasma measurements // Adv. Space Res. - 2003. – Vol. 32. – pp. 385-388.
169 Vaisberg O.L. et al. Imaging mass-spectrometer of ions for studying near-planetary plasma // Cosmic Research. – 2006. – Vol. 44. – pp. 202-208.
170 Vaisberg O.L., et al. Imaging mass-spectrometer of ions for studying near-planetary plasma // Cosmic Research. - 2006. – Vol.44. – pp.202-208.
171 Becker J. Etude et développement d’un spectrometer de masse et énergie, modélisation et optimization de l’optique, realisation du prototype, PhD thesis, UPMC, Paris. - 2013.
172 Vaisberg O.L., et al. The 2π charged particles analyzer: All-sky camera concept and development for space missions // Journal of Geophysical Research: Space Physics. - 2016. – Vol.121. – pp. 11,750 - 11,765.
173 Trubitsyn, A., Grachev, E., Gurov, V., et al. CAE “FOCUS” for modelling and simulating electron optics systems: development and application // Proc. SPIE, 2017. - 102500V.
174 Gurov, V.S., Saulebekov, A.O., & Trubitsyn, A.A. 2015, Analytical, Approximate-Analytical and Numerical Methods in the Design of Energy Analyzers, ed. P.W. Hawkes, Adv. Imag. Electron Phys., Academic Press, UK, 209 p.
175 Wrobel, L.C., & Aliabadi, M.H. The boundary element method, John Wiley & Sons, New York. 2002.
176 Cheng A.H.-D., Cheng, D.T. Engineering Analysis with Boundary Elements // Engineering Analysis with Boundary Elements. – 2005. - 29, 268-302.

177 Trubitsyn A. A. Calculation of the singular integrals arising in the boundary-element method for the Dirichlet problem // Comput. Math. Math. Phys. – 1995. – Vol. 35:4. – pp. 421–428.
178 Bimurzaev, Seitkerim Bimurzaevich et al. “Boundary and Current Elements for Simulation of Electromagnetic Fields.” 2021 IEEE International Conference on Smart Information Systems and Technologies (SIST). – 2017. – pp. 1-5.
179 Trubitsyn, Andrey. A correlation method of search for higher-order angular focusing // Technical Physics. - 2001. – Vol. 46. – pp. 630-631.
180 Trubitsyn, A., V. Astakhov and E. Grachev. The numerical techniques of conditions search of high order time-of-flight focusing // Eighth International Conference on Charged Particle Optics (CPO-8). Singapore (12-16 July 2010). – pp.186-187.
181 Trubitsyn A. A correlation method of search for higher-order angular focusing // Technical Physics. 2001. – Vol.46. – pp. 630-631.
182 Wolfe John H. et al. The compositional, anisotropic, and nonradial flow characteristics of the solar wind // Journal of Geophysical Research. – 1966. – Vol. 71. – pp. 3329-3335.
183 Zashkvara, V.V., Tyndyk N.N. Potential fields based on circular multipole series // Nuclear Instruments & Methods in Physics Research Section A-accelerators Spectrometers Detectors and Associated Equipment. - 1996. – 370. - pp. 452-460.
184 Zashkvara V.V., Tyndyk N.N. The method for the calculation of multipole-cylindrical fields // Nuclear Instruments & Methods in Physics Research. Section A. – 1999. – A370. – P. 223-231.
185 Zashkvara V.V., Tyndyk N.N. Electrostatic axially symmetric multipole in deflector-type analyzers // Nuclear Instruments & Methods in Physics Research. Section A. – 1992. – A313. – P. 315-327.
186 Ashimbaeva B.U., Masyagin B.E., Saulebekov A.O., Tyndyk N.N., Chokin K.Sh. Electron optical parameters of a mirror analyzer with hexapole cylinder field // Eurasian Physical Technical Journal.- 2006.- V3., No.2(6).- P.51-55.

Scientific edition

Kambarova Zhanar Tursynovna

DESIGN OF ELECTROSTATIC ENERGY ANALYZERS

Monograph

Printed from the author's original

Signed for printing 13.10.2023. Format 60×84 1/16. Offset paper. Volume 7,68 printed sheet. Print run 100 copies. Ordering № 15.

Printed in the printing center "Polygraphist"
100024, Karaganda., Yazeva str, 2.